

ScholarWorks@GSU

Biomimicry of Volatile-Based Microbial Control for Mitigating Fungal Pathogenicity

Authors	Gabriel, Kyle T
Citation	Gabriel, Kyle T. 2017. "Biomimicry of Volatile-Based Microbial Control for Mitigating Fungal Pathogenicity." Georgia State University. https://doi.org/10.57709/10060088
DOI	https://doi.org/10.57709/10060088
Download date	2026-03-09 03:37:25
Link to Item	https://hdl.handle.net/20.500.14694/1988

BIOMIMICRY OF VOLATILE-BASED MICROBIAL CONTROL FOR MITIGATING FUNGAL
PATHOGENICITY

by

KYLE T GABRIEL

Under the Direction of Sidney A. Crow, Jr., PhD

ABSTRACT

Volatile organic compounds (VOCs) are organic chemicals typically characterized as having low molecular weight, low solubility in water, and high vapor pressure. Consequently, they readily evaporate from liquid to the gaseous phase at standard temperature and pressure. VOCs are produced by many microorganisms as a result of both uninduced and induced metabolic pathways. Volatile-based microbial inhibition in environments such as soil is well founded, with numerous antimicrobial VOCs and formulations having been identified. Inhibitory VOCs are of particular interest as microbial control agents, as low concentrations of gaseous VOCs have been observed to elicit significant antimicrobial effects. It is believed that this contact-independent antagonism may present unique advantages over traditional microbial control methods, particularly where contact-dependent treatment methods are either impractical or inconvenient. This method may be of particular benefit for managing infections where disease may become pervasive in the population, such as with white-nose syndrome (WNS) among bats.

A list of potential antifungal compounds and formulations was compiled by referencing the scientific literature. Screening of compounds and formulations was conducted through toxicity analyses and antimicrobial susceptibility testing for the *in vitro* ability of VOCs and formulations to inhibit growth of select pathogenic fungi. A dispersal system was developed that entailed electrical circuit and software engineering as well as quantitative analysis to validate consistent and accurate dispersal of potential treatment compounds and formulations. Successful completion of these goals culminated in exposure trials involving live bats to determine any significant toxicological effects. *Ex* and *in situ* treatment trials were conducted to determine efficacy of promoting the reduction of disease severity and increasing survivorship of infected bat populations. The identification of volatile-based inhibitory compounds, in conjunction with a novel method for accurate and automated delivery, could prove a promising treatment and prophylactic in combatting microbial pathogenesis and contamination.

INDEX WORDS: White-nose syndrome, conidia, mycelia, volatile organic compound, VOC, antifungal, fungistasis, biocontrol, microbial control

BIOMIMICRY OF VOLATILE-BASED MICROBIAL CONTROL FOR MITIGATING FUNGAL
PATHOGENICITY

by

KYLE T GABRIEL

A Dissertation Submitted in Partial Fulfillment of the Requirements for the Degree of

Doctor of Philosophy

in the College of Arts and Sciences

Georgia State University

2017

Copyright by
Kyle T. Gabriel
2017

BIOMIMICRY OF VOLATILE-BASED MICROBIAL CONTROL FOR MITIGATING FUNGAL
PATHOGENICITY

by

KYLE T GABRIEL

Committee Chair: Sidney A. Crow, Jr.

Committee: George E. Pierce

Eric S. Gilbert

Electronic Version Approved:

Office of Graduate Studies

College of Arts and Sciences

Georgia State University

May 2017

DEDICATION

This dissertation is dedicated to my mother, Christine D. Ingram, my father, Gary T. Gabriel, and my brother, Gregory M. Gabriel, for whom I have much love and admiration for, and were crucial in nurturing my curiosity, determination, integrity, scholarship, and skepticism- virtues that have prepared me for a lifetime of fascination and inquisitiveness about the world.

ACKNOWLEDGEMENTS

I would like to express my sincerest gratitude to my advisor, Dr. Sidney A. Crow, Jr., who guided me throughout this process and expanded my knowledge and understanding of biology, and who swore if I learned nothing else over the past several years, I should at least emerge with an enhanced appreciation and palate for fine wine, whiskey, and tobacco.

I would also like to thank the rest of my dissertation committee, Dr. George E. Pierce and Dr. Eric S. Gilbert, and my colleague, Dr. Christopher T. Cornelison, for their encouragement and excellent mentorship. I would like to thank my fellow lab mates for the stimulating discussions, alternative hypotheses, and the variety of foods and fermented beverages they brought to our potluck lab socials. I would also like to thank the many professors and staff who assisted, advised, and enhanced my research and writing efforts over the years.

TABLE OF CONTENTS

ACKNOWLEDGEMENTS	v
LIST OF TABLES	ix
LIST OF FIGURES	x
LIST OF ABBREVIATIONS	xii
1 INTRODUCTION	1
1.1 Background.....	1
1.2 Microbial Antagonism	1
1.3 White-Nose Syndrome	3
1.4 Antifungal Volatile Organic Compounds	6
1.5 Synergistic Inhibitory Activity.....	8
1.6 Mechanisms of Inhibition	9
1.7 Collateral Impacts	11
1.8 Dispersal Development	11
1.9 White-Nose Syndrome Treatment	13
1.10 Hypotheses	13
2 DISPERSAL SYSTEM RESEARCH AND DEVELOPMENT.....	15
2.1 Hardware and Manufacturing.....	15
2.2 Circuit Development	18
2.3 Software Development	23
2.4 Power Efficiency	25
2.5 Air Chamber Development	26
2.6 Headspace Sampling	27
3 EXPERIMENTS.....	28

3.1	Spore Harvesting and Culture Maintenance	28
3.2	Antimicrobial Susceptibility	29
3.2.1	<i>Quantification of Filamentous Fungi Growth</i>	29
3.2.2	<i>In Vitro Evaluation of Antifungal VOCs</i>	32
3.3	Dispersal System Development	35
3.3.1	<i>Dispersal Characterization</i>	35
3.3.2	<i>High-Frequency Acoustic Output</i>	38
3.4	Standard Gaseous Curve Development.....	38
3.5	Bat Toxicological Histopathological Evaluation.....	41
3.6	Treatment at Black Diamond Tunnel	42
4	RESULTS.....	45
4.1	Antimicrobial Susceptibility	45
4.1.1	<i>Quantification of Filamentous Fungi Growth</i>	45
4.1.2	<i>Exposure Assays with Six Previously-Described VOCs</i>	47
4.1.3	<i>Exposure Assays with VOC Formulations</i>	51
4.2	Dispersal System Development	57
4.2.1	<i>Dispersal Characterization</i>	58
4.2.2	<i>High-Frequency Acoustic Output</i>	61
4.3	Standard Gaseous Concentration Curves.....	63
4.4	Bat Toxicological and Histological Evaluation.....	68
4.5	Treatment at Black Diamond Tunnel	72
5	CONCLUSIONS.....	78
5.1	Post-harvest Loss Due to Fungal Decay	78
5.2	Antifungal Volatile Organic Compounds	79

5.3	Novel Fungal Management Strategies.....	81
5.4	Wildlife Disease Management.....	82
5.5	Treatment at Black Diamond Tunnel	83
5.6	Beyond White-Nose Syndrome	84
	REFERENCES.....	86
	APPENDICES.....	93
	APPENDIX A	93
	APPENDIX B.....	94
	APPENDIX C	95
	APPENDIX D	96

LIST OF TABLES

Table 1.1 The chemical composition of the B-23 formulation.....	8
Table 2.1 Bill of materials used to construct one dispersal controller (version 1.4)	20
Table 4.1 Comparison of ruler and digital measurements of mycelial growth area	46
Table 4.2 Summary of the differences between the jet nebulizer and rotary atomizer	58
Table 4.3 Tissues examined from each bat.....	70
Table 4.4 Summary of tissues from bats 1 through 37 that tested positive	71
Table 4.5 Area calculation of Black Diamond Tunnel using three calculation methods	76
Table 5.1 Combinations of several compounds in formulations of two and three compounds....	81

LIST OF FIGURES

Figure 1.1 US and Canadian counties/districts positive for the presence of WNS, since 2006	5
Figure 2.1 Hardware diagram of the dispersal controller and a jet nebulizer	17
Figure 2.2 Hardware diagram of the dispersal controller and the L30 rotary atomizer.....	18
Figure 2.3 Circuit schematic of the dispersal controller	21
Figure 2.4 Circuit board layout of the dispersal controller	22
Figure 2.5 Flowchart of the version 1.4.4 software of the dispersal controller	24
Figure 2.6 Example program diagram of version 1.4.4 of the dispersal controller	25
Figure 3.1 Radial growth of <i>Pseudogymnoascus destructans</i> under various growth conditions..	30
Figure 3.2 Equation for calculating mycelial area from pixels of a digital photograph	32
Figure 3.3 Equations for converting a desired gaseous concentration to a liquid volume	34
Figure 3.4 Operational diagram of a jet nebulizer (Vecellio, 2006).....	36
Figure 3.5 Tri-colored bat population counts at Black Diamond Tunnel from 2010 to 2016	43
Figure 3.6 Diagram of the infrastructure at Black Diamond Tunnel	44
Figure 4.1 Growth of <i>Pseudogymnoascus destructans</i> exposed to single VOCs at 15°C	49
Figure 4.2 Growth of <i>Pseudogymnoascus destructans</i> exposed to single VOCs at 4°C	50
Figure 4.3 <i>Pseudogymnoascus destructans</i> area growth when exposed to 2 VOCs	52
Figure 4.4 <i>Pseudogymnoascus destructans</i> inhibition when exposed to 2 VOCs	53
Figure 4.5 <i>Pseudogymnoascus destructans</i> area growth when exposed to 3 VOCs.....	54
Figure 4.6 <i>Pseudogymnoascus destructans</i> inhibition when exposed to 3 VOCs	55
Figure 4.7 <i>Pseudogymnoascus destructans</i> growth area following exposure to B-23.....	56
Figure 4.8 <i>Pseudogymnoascus destructans</i> inhibition following exposure to B-23	57
Figure 4.9 Dispersal rates of two compounds using a jet nebulizer	60
Figure 4.10 Spectrograms of audio samples acquired from several aerosolization technologies	62
Figure 4.11 Standard curve of toluene using gas-tight syringe headspace sampling	64
Figure 4.12 Standard curve of toluene using SPME headspace sampling.....	65
Figure 4.13 Chromatogram of the B-23 formulation.....	66
Figure 4.14 Standard curves of the primary and secondary peaks of the B-23 formulation	67
Figure 4.15 Two sets of the dimensional measurements of Black Diamond Tunnel	73
Figure 4.16 Linear trend of the dimensional measurements of Black Diamond Tunnel	74

Figure 4.17 Polynomial trend of the dimensional measurements of Black Diamond Tunnel 75

Figure 4.18 Chromatograms of a gaseous standard (black) and post-treatment at BDT (red) 77

Figure 4.19 Tri-colored bat population counts at Black Diamond Tunnel from 2010 to 2017 78

LIST OF ABBREVIATIONS

AC	Alternating current
B-23/Flavorzon	A synthetic formulation of VOCs produced by <i>Muscodor crispans</i> strain B-23
DC	Direct current
DPI	Days post-inoculation
EFD	Emerging Fungal Disease
FDA	Food and Drug Administration
GCMS	Gas chromatography-mass spectroscopy
GRAS	Generally recognized as safe
Hz	Hertz, the SI unit of frequency
mol	Mole, the SI unit of the amount of a substance
PBS	Phosphate-buffered saline
PCB	Printed circuit board
PDMS	SPME fiber material; Polydimethylsiloxane
PDMS-CAR	SPME fiber material; Polydimethylsiloxane-Carboxen
PDMS-DVB	SPME fiber material; Polydimethylsiloxane-Divinylbenzene
ppmv	Parts per million by volume
PSI	Pounds per square inch
SA-V	Surface area to volume ratio
SDA	Sabouraud dextrose agar
SFD	Snake fungal disease
SPME	Solid-phase micro-extraction
v	Volt, the SI unit of electrical potential
VOC	Volatile organic compound
WNS	White-nose syndrome

1 INTRODUCTION

1.1 Background

Biomimicry is an approach to developing solutions to problems by emulating the successful survival strategies found throughout nature. Microorganisms have invested billions of years of combined research and development via evolution. If failure has resulted in extinction, then those that thrive hold not just the key to their survival, but also to our prosperity. In the pursuit of developing novel microbial control methods, we need look no further than the arena these organisms compete in for survival to discover effective tools for controlling undesired microbial growth.

The fitness of an organism or species is influenced by numerous factors. Competition is one such interaction that often promotes the fitness of one species, to the detriment of another. The competitive exclusion principle is the theory that different species in competition for the same resources cannot maintain coexistence if they share the same ecological niche (Gause, 1934). Although additional factors have been identified that continue to shape our understanding of coexistence (Rastetter and Gren, 2002), the ability of a species to thrive largely hinges on the competitive advantages its members have over others. Among the many adaptive mechanisms microorganisms have evolved to compete is the production and dissemination of antimicrobial compounds.

1.2 Microbial Antagonism

Antibiotics are one class of antimicrobial compounds produced by microorganisms, which may be further classified by mechanism of action, molecular structure, and spectrum of activity, among other characteristics. While some of the first antibiotics to be discovered were

the products of eukaryotic fungi (Fleming, 1929), it has been revealed a great number are also produced by prokaryotes, such as *Streptomyces* spp. (Watve et al., 2001).

Another novel class of antimicrobials was discovered following observations of fungal spore germination being inhibited when exposed to certain soil substrates, termed fungistatic soils (Dobbs and Hinson, 1953). The inhibitory properties of these suppressive soils were later found to be a result of exposure to microbially-produced volatile organic compounds (VOCs) (Balis and Kouyeas, 1968). VOCs are chemical compounds typically characterized by their low molecular weight, low boiling point, low solubility in water, and high vapor pressure. These characteristics often facilitate evaporation to the gaseous phase at standard temperature and pressure (STP). The dissemination of these compounds into the surrounding airspace has enabled microorganisms to interact and elicit antagonistic effects from a greater distance than could be achieved by direct contact. The ability of a microorganism to utilize antifungal VOCs to negatively impact another microorganism without requiring direct contact has been termed contact-independent antagonism.

The volatile-based fungistatic properties of suppressive soils has been widely observed across terrestrial environments (Zou et al., 2011). The inhibitory activities of VOCs are of particular interest due to the ability of these compounds to inhibit microbial growth in dense and diverse ecosystems, from a gaseous, contact-independent exposure (Balis and Kouyeas, 1968; Voisard et al., 1989; Kerr et al., 1999; Ezra et al., 2003; Chuankun et al., 2004; Garbeva et al., 2011). Recent research has begun investigating microbially-produced VOCs for their potential agricultural benefits, by preventing infection through controlling phytopathogenic fungi as well as stimulating crop growth (Weisskopf, 2013). Additionally, investigations have demonstrated the ability of a ubiquitous soil-dwelling bacterium, *Rhodococcus Rhodochrous* strain DAP

96253, to inhibit the growth of several fungal pathogens and spoilage organisms, including *Pseudogymnoascus destructans*, when induced for antifungal activity and placed in a shared airspace with the target organism (Pierce et al., 2011; Cornelison et al., 2014). The low inhibitory concentrations observed with select VOCs suggest a potential to utilize these compounds in novel ways to combat undesired microbial growth and infection.

1.3 White-Nose Syndrome

Emerging fungal diseases (EFDs) have become a growing concern for wildlife and food security, with several plant and animal pathogens posing direct threats to biodiversity and food production in the US and around the world (Fisher et al., 2012). One particular fungus has recently been exposed to naive species of bats in North America, and left unchecked, threatens certain bat species with population decline and extinction.

Pseudogymnoascus destructans, a psychrophilic ascomycete, has been identified as the etiological agent responsible for a deadly EFD among North American bats, known as white-nose syndrome (WNS) (Blehert et al., 2009; Lorch et al., 2011). WNS is typified by an invasion of the host tissue by *P. destructans* during torpor, which typically takes place through the winter season. During this period, the host's body temperature and metabolic activity, including immune function, is greatly reduced. When bats enter torpor, their body temperature falls within the growth range of *P. destructans* (1°C to 15°C), and coupled with an inability of the immune system to effectively combat the infection, clinical WNS can quickly develop. The resulting tissue damage from fungal invasion is known to cause the disruption of thermoregulation, water regulation, and electrolyte balance, as well as increase the rate of torpor arousal, leading to premature expenditure of fat stores (Cryan et al., 2010; Verant et al., 2014). These insults have

led to severe population declines for several species, with up to 99% mortality in just a few years following the pathogen's introduction to some hibernacula (Frick et al., 2010).

Since its identification near Albany, New York in 2006, WNS has spread to 31 US states and 5 Canadian provinces (White-Nose Syndrome Map, 2017; Figure 1.1). A 2011 population study estimated at least 5.7 to 6.7 million bats have died from this disease (Froschauer et al., 2012). Although ecological impacts are still being thoroughly assessed, initial analyses have suggested US agricultural impacts from the loss of bats may range from \$3.7 to \$53 billion per year, which is predominantly impacted by the loss of the insect-control bats provide (Boyles et al., 2011). However, this estimate only accounts for the cost of pesticides used to compensate for the amount of insects consumed by bats. There may very well be other negative effects that emerge from the loss of bats, such as potential downstream effects from increased pesticide use, an increase in insect-borne diseases, or disruptions to ecological systems and predator-prey dynamics.

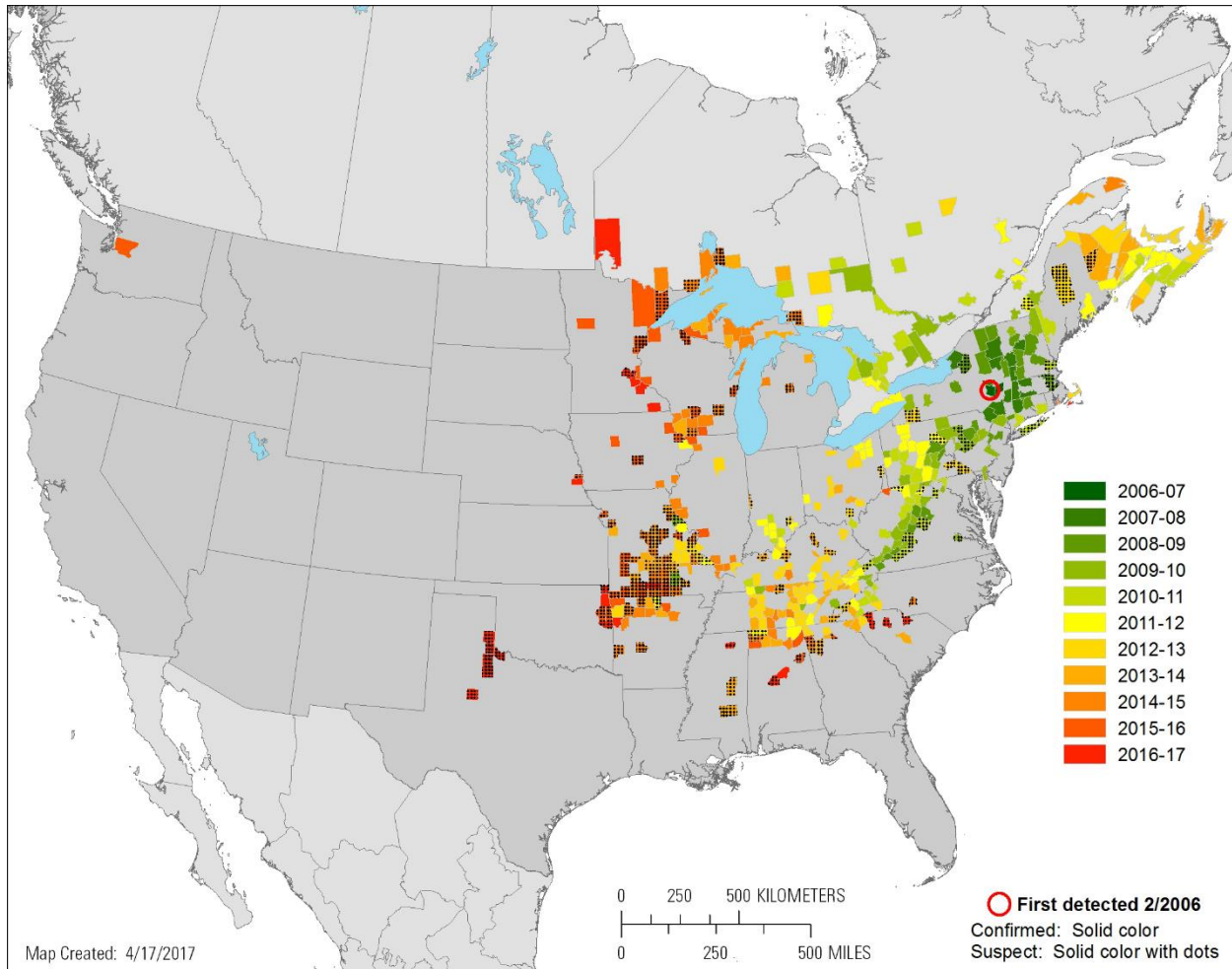


Figure 1.1 US and Canadian counties/districts positive for the presence of WNS, since 2006

The map depicts the first time WNS was reported to be suspect or confirmed in a county or district. Each time period spans a winter bat hibernation period. Last updated April 17, 2017.

The rapid spread and high mortality associated with WNS has made development of methods for treating and preventing *P. destructans* infections an important objective for wildlife management agencies. Accordingly, the development of methods for biological and chemical treatment has become a significant priority for State and Federal agencies, as outlined in the 2011 National WNS Management Plan established by the United States Fish and Wildlife Service (Ballman et al., 2011).

Analyses of population declines have suggested that regional extinction of the hardest hit species, the little brown bat (*Myotis lucifugus*), could occur as soon as 2022, 16 years from the pathogen's initial emergence in the US (Frick et al., 2010). *In silico* modeling has indicated a critical decision interval for evolutionary rescue (DIER) favors early treatment (within 11 years of the initial WNS emergence), and deployment of successful treatment during this time period may yield the greatest potential benefit to promote population stability for the little brown bat (Maslo and Fefferman, 2015). Furthermore, Maslo et al. suggest that a moderate 13% reduction in mortality could lead to stability of little brown bat populations (unpublished, 2014 WNS Workshop presentation). This population stability may provide the greatest benefit by encouraging an increased birth rate that promotes a naturally evolved resistance to develop in the offspring.

1.4 Antifungal Volatile Organic Compounds

When a gaseous VOC enters an airspace, it has a propensity to permeate and envelop the objects in the vicinity. Pathogenic spores and mycelia exposed to the airspace, either on a host or in the environment, are at risk of being affected by potential fungistatic or fungicidal activities of the VOC. This contact-independent antagonism has the potential to be utilized to reduce growth, pathogenicity, viability, or the environmental load of the target microorganism. Several microbially-produced antifungal VOCs have been identified from the scientific literature for their potential to be used for microbial control and disease management (Appendix A). Initial testing demonstrated the ability of single VOCs to inhibit fungal growth and conidia viability as well as several VOC formulations to elicit significant inhibitory synergism, when tested in the gaseous phase.

Several antimicrobial susceptibility assays with synthetic formulations were conducted with previously discovered formulations in order to discover novel antimicrobial effects. These formulations were developed from analyses of the gaseous headspace constituents of cultures of microorganisms that have demonstrated microbial antagonism. *Muscodor crispans* strain B-23 is a novel endophytic fungus isolated from Bolivian wild pineapple (*Ananas ananassoides*). The fungus has demonstrated an ability to inhibit several plant and human pathogens by contact-independent antagonism (Mitchell et al., 2008; Mitchell et al., 2010). A synthetic formulation of the gaseous compounds produced by *Muscodor crispans* strain B-23 has been produced synthetically, which only includes compounds listed by the food and drug administration (FDA) as generally regarded as safe (GRAS), and has been patented (Strobel et al., 2012; Table 1.1) and marketed under the commercial name Flavorzon 185B (Jeneil Biotech, Inc., Saukville, WI, USA). This synthetic formulation, further referred to as B-23, has been demonstrated to be safe and of low toxicity to mammals, and has been incorporated into several commercial products, for use with multiple mammal species, agriculture, and food storage. Several qualities of the synthetic B-23 formulation make it appealing to use as a control agent, including its ability to inhibit growth of *P. destructans*, preliminary studies with bats demonstrating a non-aversion to B-23-soaked sachets (Last and Morris, unpublished 2014 WNS Workshop presentation), and the compounds appearing on the FDA list of GRAS compounds.

Table 1.1 The chemical composition of the B-23 formulation

Compound	Molecular Weight (g/mol)	Percentage of Formulation
Acetaldehyde	44.03	0.34%
2-Butanone	72.06	0.69%
Propanoic acid, 2-methyl-, methyl ester	102.07	7.47%
Acetic acid, 2-methylpropyl ester	116.08	0.56%
Propanoic acid, 2-methyl-, 2-methylpropyl ester	144.12	0.27%
1-Propanol, 2-methyl-	74.07	0.44%
2-Butenal, 2-methyl-, (E)-	84.06	0.37%
1-Butanol, 3-methyl-, acetate	130.1	1.17%
Propanoic acid, 2-methyl-, 2-methylbutyl ester	158.13	1.17%
1-Butanol, 3-methyl-	88.09	1.32%
Propanoic acid, 2-methyl-	88.05	85.89%
Acetic acid, 2-phenylethyl ester	164.08	0.32%

The names, molecular weights, and percentages of the most abundant constituents produced by *Muscodor crispans* strain B-23, detected using GCMS (Mitchell et al., 2010). Non-GRAS compounds have been excluded from the formulation.

1.5 Synergistic Inhibitory Activity

Synergistic inhibition is said to have occurred when the inhibitory effects observed from a formulation of VOCs is greater than the additive inhibitions of the same VOCs exposed singly, when each exposure is at the same concentration. By enhancing the antagonism of a formulation through synergism, the benefits have the potential to be two-fold: in addition to the formulation producing a greater degree of inhibition at the same concentration, there may also be reduced toxicity to the host by any single VOC because the concentration of each is reduced in the

formulation. However, it may also be possible that an increased toxicity toward the pathogen will also increase toxicity toward the host.

The presence, absence, and ratio of constituents of a formulation may also be manipulated to elicit target-specific effects, potentially enhancing antagonistic effects toward germination, mycelial growth, virulence, and sporulation, and potentially improving the host's response to the pathogen. This suggests there may be an optimum period for utilizing certain treatment formulations based on seasonality, disease progression, and host metabolic activity, among other factors, in order to elicit optimum effects.

1.6 Mechanisms of Inhibition

Although the determination of specific mechanisms related to pathogen inhibition or host survivorship is beyond the scope of this investigation, it is nonetheless an important aspect to consider. Inhibitory mechanisms will often exploit a particular characteristic shared by a clade of organisms. As such, it should be recognized that a consequence of both the host and pathogen being members of the eukaryotic domain, many physiological characteristics are shared, and therefore the potential exists for collateral impacts to the host when targeting the pathogen.

In the 16th century, Paracelsus, heralded as the father of toxicology, expressed in his *Dritte Defensio* (1538) that “all things are poison and nothing is without poison; only the dose makes a thing not a poison.” Indeed, modern toxicology recognizes that virtually all substances display dose-dependent effects. However, there are numerous compounds known to stimulate a positive response, either because of a genuine promotion of health or because of exposure to a low concentration of a toxin. This phenomenon of a generally favorable response due to exposure to a low concentration of a toxin or stressor is known in toxicology as hormesis, and is

often the opposite response than what is observed with higher doses (Southam and Ehrlich, 1943). Although not well-understood, there have been numerous observations of the hormesis phenomenon, suggesting the potential to change how toxicology is understood in relation to risk assessment, study design, and dose-response modeling, among others (Calabrese and Baldwin, 2003).

The body of literature comprising known microbially-produced volatile organic compounds is numerous and contains a large number of chemical analogues that may also be potentially effective at eliciting microbial inhibition. The analyses required for determining inhibitory mechanisms often require in-depth metabolic and genomic study. Therefore, mechanisms by which many of these volatiles elicit their inhibition is not thoroughly understood. Prior to the initial investigation to discover the potential of several VOCs to inhibit *P. destructans* (Cornelison et al., 2014), these compounds have been observed in other studies to elicit inhibition of germ-tube growth (nonanal), inhibition of mycelial growth (2-ethyl-1-hexanol, benzaldehyde, benzothiazole, and nonanal), inhibition of pigment production (benzothiazole), and inhibition of spore germination (2-ethyl-1-hexanol, benzothiazole, nonanal) (Weisskopf, 2013). Inhibition of pigment production may be of particular interest, as pigments are known virulence factors of several pathogenic fungi, for their ability to inactivate reactive oxygen species produced by the host-defense response (Taborda et al., 2008).

In lieu of direct analysis, possible inhibitory mechanisms may be inferred from the study of the analogues of particular compounds. For instance, benzaldehyde derivatives are known to cause cytoplasmic coagulation or lysis through the disruption of the cellular membrane (Alamri et al., 2012). Certain azoles have been observed targeting heme-containing proteins, interfering

with the production of sterols and leading to the disruption of the plasma membrane, while others inhibited membrane-bound enzymes or lipid biosynthesis (Ghannoum et al., 1999).

1.7 Collateral Impacts

Disturbance to an environmental system, such as with the application of disease treatments and prophylactics, have the potential to cause non-target collateral impacts. This may result from the construction of infrastructure, environmental release of VOCs, the propagation of a transitory agent such as a microorganism, among other actions. Collateral impact assessments are commonly performed in the course of developing treatments for animals and their habitats to ensure environmentally-safe application and minimal harm to the natural environment. Since the focus of this work is to isolate the antimicrobial effects and separate them from the biological agent, thereby excluding the use of living cells, collateral impacts from the use of VOCs will be the primary concern with these treatments. Therefore, environmental monitoring of substrates for contamination as well as assessments of non-target organism effects will be conducted.

1.8 Dispersal Development

The existence of antimicrobial VOCs has been known for quite some time. However, development of their use with target-specific, contact-independent antagonism of microbial growth, coupled with a cost-effective, scientifically validated distribution system, has been lacking. A distribution system provides the ability to autonomously attain and maintain a precise target concentration. Potential benefits include fewer collateral impacts and greater treatment efficacy by accurately maintaining the target concentration, as well as lowering the risk of developing negative health effects associated with VOC exposure to researchers and clinicians,

by automating distribution. Understanding how microorganisms deploy antagonistic VOCs may help guide future developments in this area.

Microorganisms have evolved over millions of years in direct competition and have developed complex mechanisms for effectively producing and disseminating antimicrobial compounds. There are several advantages to abstracting the process of disseminating these compounds from the biological agent (the cell). These include eliminating the time and cost of culturing large quantities of an organism or biological catalyst, eliminating the variability of any potential microbial induction processes, and eliminating the possibility of releasing a self-propagating microorganism into the environment. Other benefits include the ability to modify VOC formulations and compound ratios to enhance effects, the ability to regulate the exact concentration being dispersed, and the ability to regulate the quality of the VOC or formulation constituents.

Evaporation is often heavily influenced by surface area, with evaporation time decreasing as surface area increases. Therefore, by reducing the size of aerosol droplets, the surface-area-to-volume (SA-V) ratio increases, thereby increasing the total surface area of the liquid volume. For a defined volume of liquid comprised of an aerosol of 3-dimensional spheres, if the radii of the aerosol droplets decrease by half, the number of droplets will increase 800% and the total surface area will increase 100%. By reducing the droplet sizes to increase the SA-V ratio, the total surface area of the liquid increases, decreasing the evaporation time. Several commercial aerosolizers currently exist on the market that produce a microscopic liquid aerosol with a high SA-V ratio. The properties that facilitate evaporation may be utilized by these aerosolizers to efficiently produce a gaseous concentration in an air space, and may be manipulated to facilitate accurate dispersal for volatile compounds.

1.9 White-Nose Syndrome Treatment

Developing effective methodologies for treating bats is not without its challenges. From a logistical standpoint, several issues must be considered in order to develop a safe and efficacious treatment. During hibernation, when symptoms of WNS develop, many species congregate together, forming a “fused” colony of numerous individuals. In addition to promoting the spread of disease, these colonies may also roost in areas that make physical access to individuals difficult or impossible. Furthermore, handling of bats for individualized treatment is often costly and laborious. Handling also has the potential to cause undue stress and disturbance that may injure the animal or interrupt torpor, causing premature arousal and expenditure of adipose tissue that is vital for surviving winter hibernation.

It is believed that antimicrobial VOCs may be utilized with a dispersal system to limit growth and reduce the pathogenicity of *P. destructans*, serving as a potential treatment and prophylactic for bats afflicted with WNS or at risk for developing WNS from *P. destructans* infection. Gaseous exposure to antifungal VOCs enables the possibility of eliciting contact-independent antagonism and may overcome many of the aforementioned challenges associated with treating bats by providing a cost-effective means to treat bats *in situ*, both at the colony-level and with minimal disturbance.

1.10 Hypotheses

Several theories for developing effective disease management strategies were developed and tested during the course of this investigation. Although not all results were conclusive, the following hypotheses and resulting investigations laid a solid foundation for future studies to continue developing effective tools for microbial control and mitigating pathogenicity.

It has been hypothesized that VOCs and formulations identified from the scientific literature to demonstrate antimicrobial effects may be utilized to inhibit the growth and pathogenicity of select fungal pathogens. These VOCs may be acquired as pure, synthetically-produced compounds from a chemical supplier and may be selected and screened for an *in vitro* ability to inhibit germination, mycelial growth, sporulation, or virulence of pathogenic fungi. Additionally, certain VOCs, when combined in a formulation, have the potential to yield synergistic inhibition. As a result, a synergistic formulation would contain a lower concentration of each individual VOC, suggesting potential benefits of reducing toxicity of each VOC as well as increasing efficacy. If effective at inhibiting select fungi, these VOCs have the potential to be utilized to control microbial growth, reduce symptoms of disease in an afflicted host, and reduce environmental load.

It has been hypothesized that a VOC distribution system can be developed from inexpensive, off-the-shelf components, and can consistently and reliably distribute liquid VOCs and their formulations to produce an accurate gaseous concentration in an airspace of a known volume. A distribution system coupled with target-specific antimicrobial VOCs has the potential to reduce or abolish fungal growth or pathogenicity after contact-independent application. This entails the system may be used to disseminate antifungal VOCs or VOC formulations to elicit bio-static or -cidal activities against organisms exposed to the airspace. It is believed that this contact-independent application may be used alone or synergistically with current microbial control practices to enhance effectiveness and may present unique advantages over traditional microbial control methods where contact-dependent treatment methods are either ineffective or impractical.

It has been hypothesized that, if utilized for disease management, this distribution system may be able to limit pathogenic fungal growth on or in a host organism, slow or prevent the progression of disease, reduce the symptoms of infection, or promote increased fitness and survivorship of affected populations. This entails that the VOCs or formulations developed from *in vitro* studies be efficacious with *ex* and *in situ* inhibition of spore germination and mycelial growth, or promoting health among individuals of the host population. As chemical treatments often only elicit temporary effects, it has been hypothesized these methods will reduce or abolish disease symptoms instead of conferring life-long resistance. Therefore, the proposed studies will be carried out with intent to promote an increase of survivorship among individuals afflicted by WNS, and thus promoting a naturally-evolved resistance with their progeny.

2 DISPERSAL SYSTEM RESEARCH AND DEVELOPMENT

Development of a dispersal system was carried out to enable accurate and consistent dispersal of VOCs to attain a target gaseous concentration in a known airspace. Electrical circuits and software source code were engineered and utilized to enable automated control of a dispersal device, using known thermodynamic principles, such as the ideal gas law, to effectively modulate dispersal. Design focused heavily on dispersal consistency, accuracy, autonomy, and extending battery life.

2.1 Hardware and Manufacturing

The main components of the dispersal system include an enclosure, a controlling circuit, a power supply, and a dispersal device. The controller was designed to accept any unregulated 12-volt direct current (DC) power source, permitting the use of a DC battery or an adapter that

converts a standard 120- or 240-volt alternating current (AC) power source to 12 DC volts. The controller circuit board is housed in a custom 3D-printed case to protect against short-circuits and provide adequate airflow surrounding the circuit board to reduce the risk of component failure or fire from heat build-up. All circuitry is further encased in a weatherproof enclosure to protect against shock and to ensure the controller and battery are not exposed to conditions that may jeopardize the ability of the system to operate, such as a high humidity or corrosive environment.

The controller has the capability to utilize a number of different dispersal devices. In one iteration of the system, a Trek S pneumatic nebulizer (Pari Respiratory Equipment, Inc., Virginia, USA) was utilized. The pneumatic pump was powered from the controller's power source and a pressure sensor was incorporated for feedback to detect low power situations and to permit modulating the output to maintain accurate dispersal. A diagram was developed to visualize the interaction of the various hardware of this system (Figure 2.1).

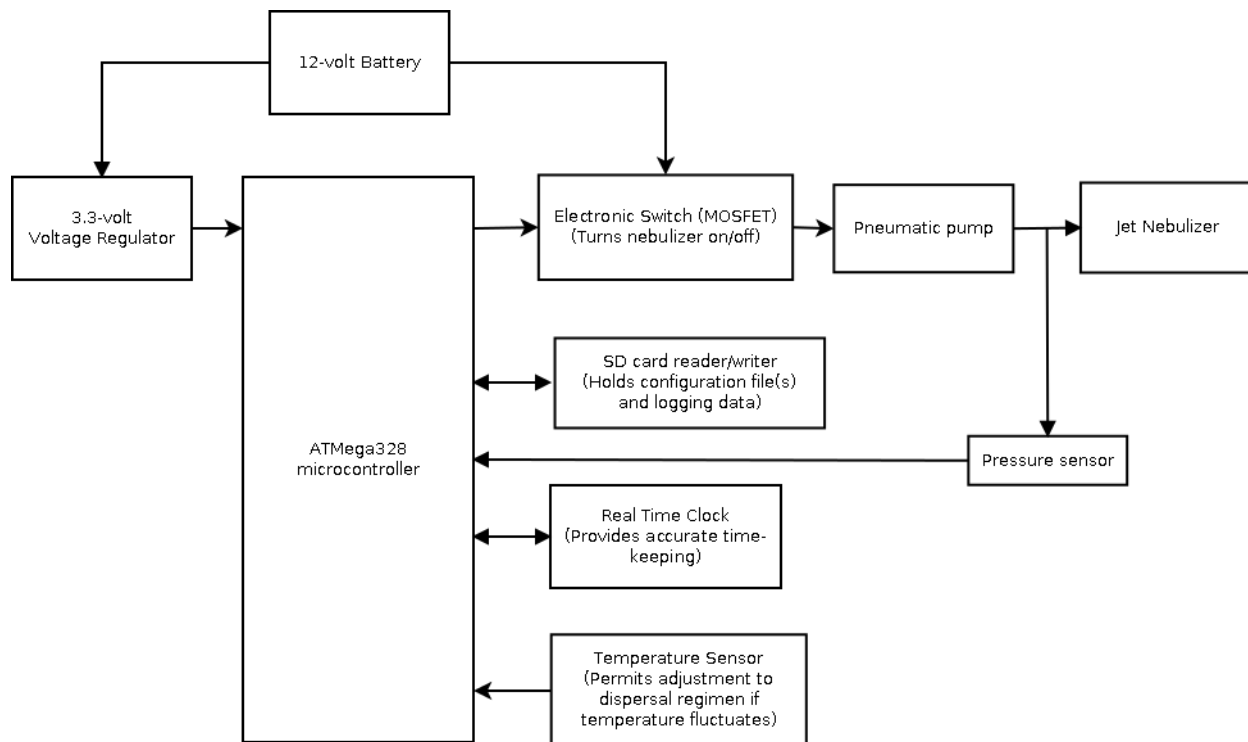


Figure 2.1 Hardware diagram of the dispersal controller and a jet nebulizer

In another iteration of the system, a Dyna-Jet L-30 rotary atomizer (Curtis Dyna-Fog, Indiana, USA) was powered by a solid state relay from its own high-current battery power supply (Figure 2.2). Both systems utilized the same controller but relied on different dispersal devices, each uniquely-suited to treating different volume airspaces. The jet nebulizer has been ideal for developing methodologies and performing experiments in a laboratory setting, however the increased airspace when moving to field application has necessitated the use of a dispersal device that was better-suited to large-volume dispersal, such as the L-30.

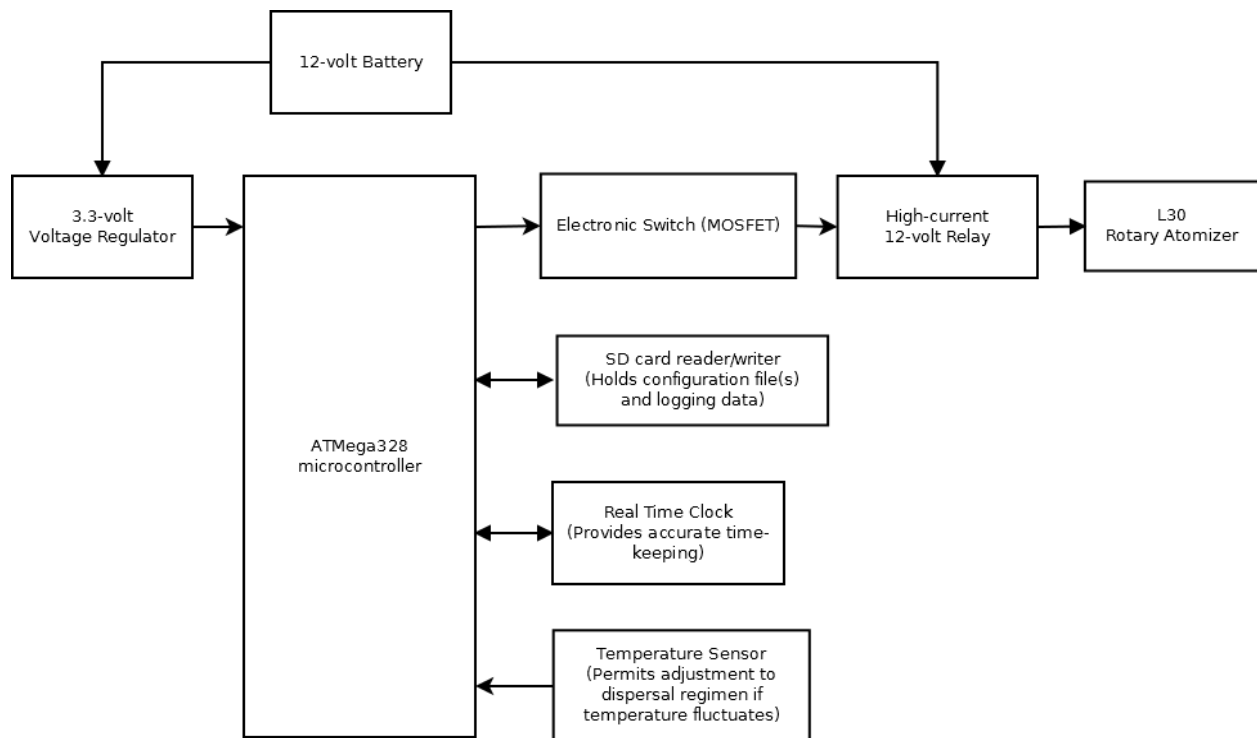


Figure 2.2 Hardware diagram of the dispersal controller and the L30 rotary atomizer

2.2 Circuit Development

Theorized controller circuits were developed from the hardware diagrams, utilizing several electrical components (Table 2.1). The controller circuit was developed on a prototyping breadboard to assess the operability of theorized circuit and program designs. A MAX16910 ultra-low quiescent current voltage regulator (Maxim Integrated, California, USA) was selected to convert and regulate a steady 3.3-volt DC power supply to the controller components and peripherals, from an unregulated 12-volt DC power input. The ATmega328p AVR microcontroller unit (MCU; Atmel, California, USA) was selected as the main integrated circuit, which combines a processor core, memory, and programmable input/output peripherals onto one chip. It features a low operating and standby power usage, memory for program and variable

storage, and several analog-to-digital converters for sensor integration. A solid state relay (SSR) or n-channel metal–oxide–semiconductor field-effect transistor (MOSFET) was selected to allow the MCU to modulate the high-power output to the distribution device. The DS1337 real time clock (RTC; Maxim Integrated, California, USA) chip is a precision low-power clock/calendar with alarm functions and was selected to perform all critical time-keeping operations. An SD card socket breakout board (Sparkfun Electronics, Colorado, USA) was selected to enable reading of configuration settings as well as data logging.

Circuit prototypes were tested under various conditions likely to be experienced under normal operation in order to develop a robust circuit schematic (Figure 2.3). Design of the printed circuit board (PCB) was developed with CadSoft’s EAGLE PCB design software before being printed (OSH Park, Oregon, USA) and hand-assembled (Figure 2.4).

Table 2.1 Bill of materials used to construct one dispersal controller (version 1.4)

Part Number (DigiKey)	Quantity	Description
DS1337+-ND	1	DS1337 Real Time Clock IC
728-1000-ND	1	32kHz Crystal
887-2015-ND	1	16MHz Crystal
CP3-1003-ND	1	Barrel Power Jack (male, 1.35mm ID, 3.5mm OD)
CP3-1000-ND	1	Barrel Power Jack (male, 2.1mm ID, 5.5mm OD)
CP-035D-ND	1	Barrel Power Jack (female, 1.35mm ID, 3.5mm OD)
CP-002A-ND	1	Barrel Power Jack (female, 2.1mm ID, 5.5mm OD)
BC2301-ND	1	Thermistor 10k ohm (500mW, 5%, 40C-125C)
RNV14FAL330KCT-ND	1	Resistor 330k ohm (1/4W, 1%)
S16KCACT-ND	1	Resistor 16k ohm (1/4W, 1%)
A105947CT-ND	7	Resistor 10k ohm (0.6W, 1%)
5.62KXBK-ND	1	Resistor 5.6k ohm (1/4W, 1%)
CF14JT150RCT-ND	2	Resistor 150 ohm (1/4W, 5%)
CF14JT100RCT-ND	1	Resistor 100 ohm (1/4W, 5%)
516-1779-1-ND	1	LED (30mA)
S1011EC-40-ND	1	Unshrouded Header (1x40, breakable)
S7006-ND	2	Header - 1x8 Female
490-7508-1-ND	1	Capacitor 4.7 μ F
399-4266-ND	1	Capacitor 0.1 μ F
490-7322-1-ND	2	Capacitor 1.0 nF 50V 5%
1N5817-TPCT-ND	2	Diode, Schottky (20V, 1A)
1N4001-TPMSCT-ND	1	Diode, Schottky (50V, 1A)
A100210-ND	1	DIP Socket (2x14, 28-Pin, 0.3")
3M5473-ND	1	DIP Socket (2x4, 8-Pin, 0.3")
NDP6020P-ND	1	P-MOSFET (20V, 24A, Vgs(th)=1V@250uA)
497-12703-5-ND	2	N-MOSFET (25V, 80A, Vgs(th)=1V@250uA)
ATMEGA328P-PU-ND	1	ATMEGA328P-PU (1.8-5.5v, 20Mhz, 32KB)
	1	Toggle switch
	1	Toggle Switch Waterproof Cover
MAX16910CASA9/V+-ND	1	Voltage Regulator
522-1035-ND	1	12 volt rechargeable VRLA Battery
MPX4250AP-ND	1	0-36 PSI analog sensor
	1	SD-card breakout board

The bill of materials, including DigiKey part number, quantity, and description of each part, to construct one controller circuit. The cost to manufacture the circuit board is not included.

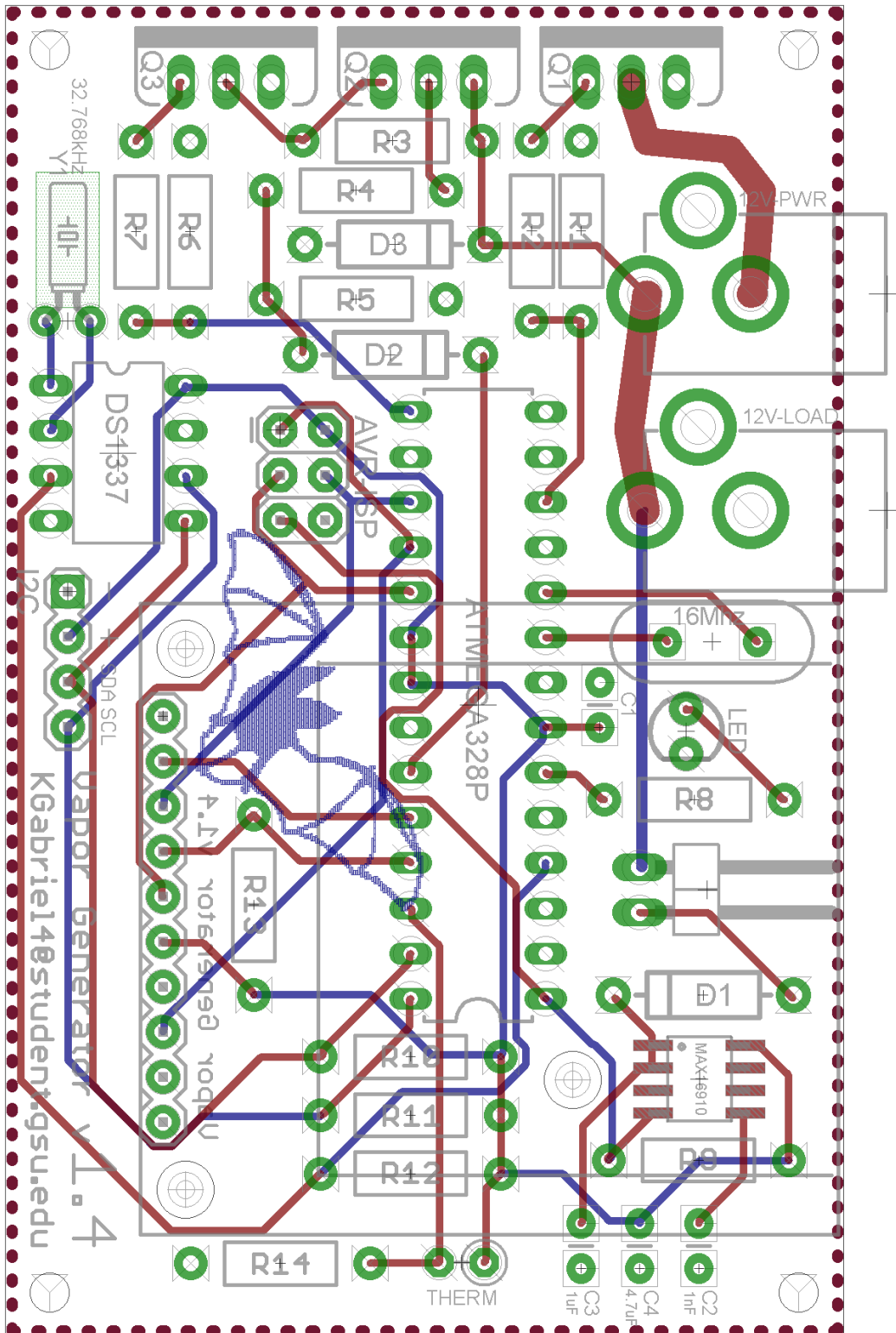


Figure 2.4 Circuit board layout of the dispersal controller

A double-sided printed circuit board (PCB) with red traces (top) and blue traces (bottom) denoting circuit connections. The PCB dimensions are approximately 75 mm by 47 mm.

2.3 Software Development

Software development was performed with an emphasis on customizability, to enable creating a wide variety of custom treatment regimens. The durations the aerosolizer is powered and depowered may be defined by the user or automatically calculated based on user input of environmental conditions, treatment compound characteristics, and desired gaseous concentration in the airspace. Figure 2.5 demonstrates the logical flow of software operation and Figure 2.6 demonstrates the variability of several custom treatment regimens that may be employed to attain a desired effect.

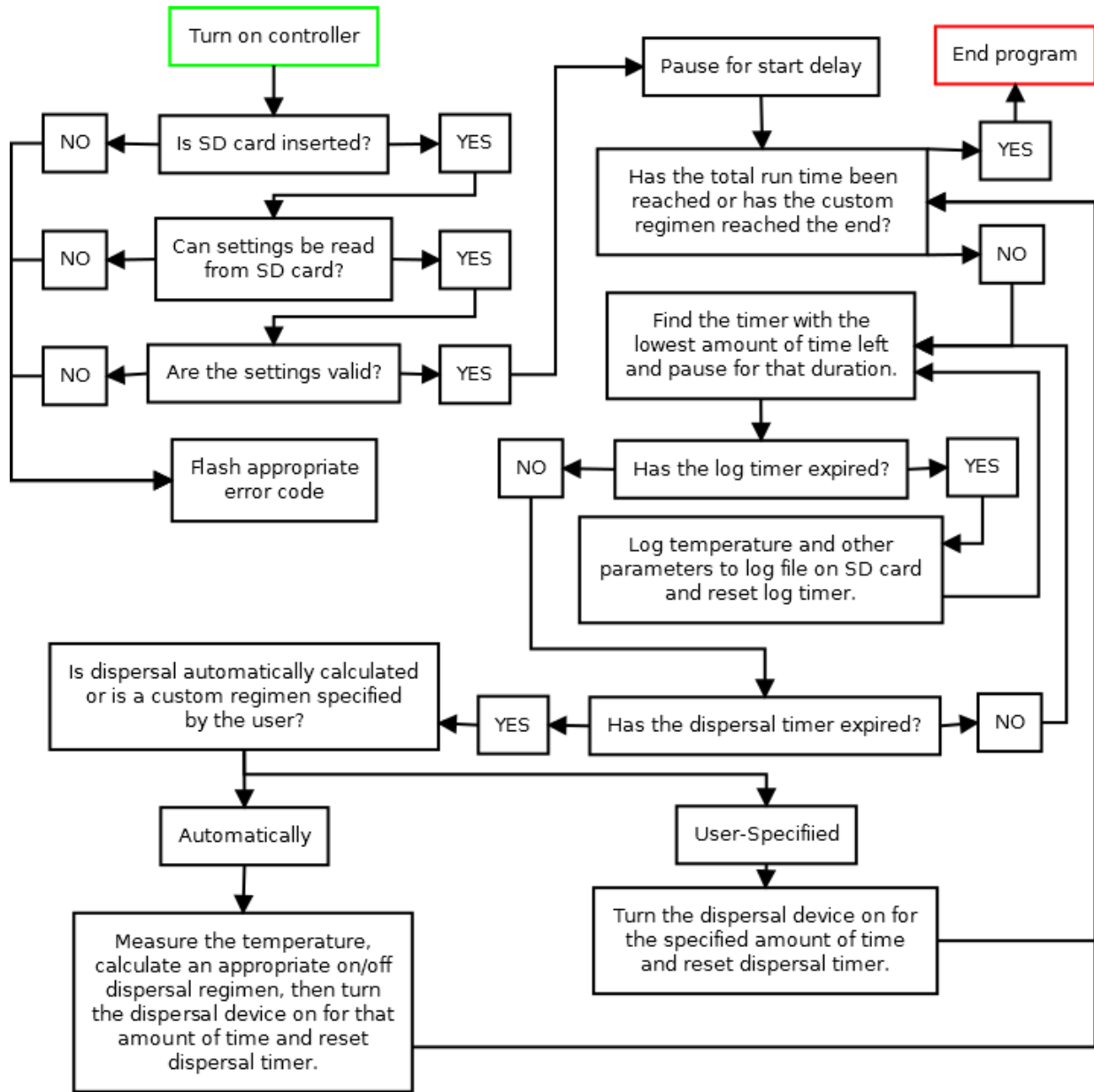


Figure 2.5 Flowchart of the version 1.4.4 software of the dispersal controller

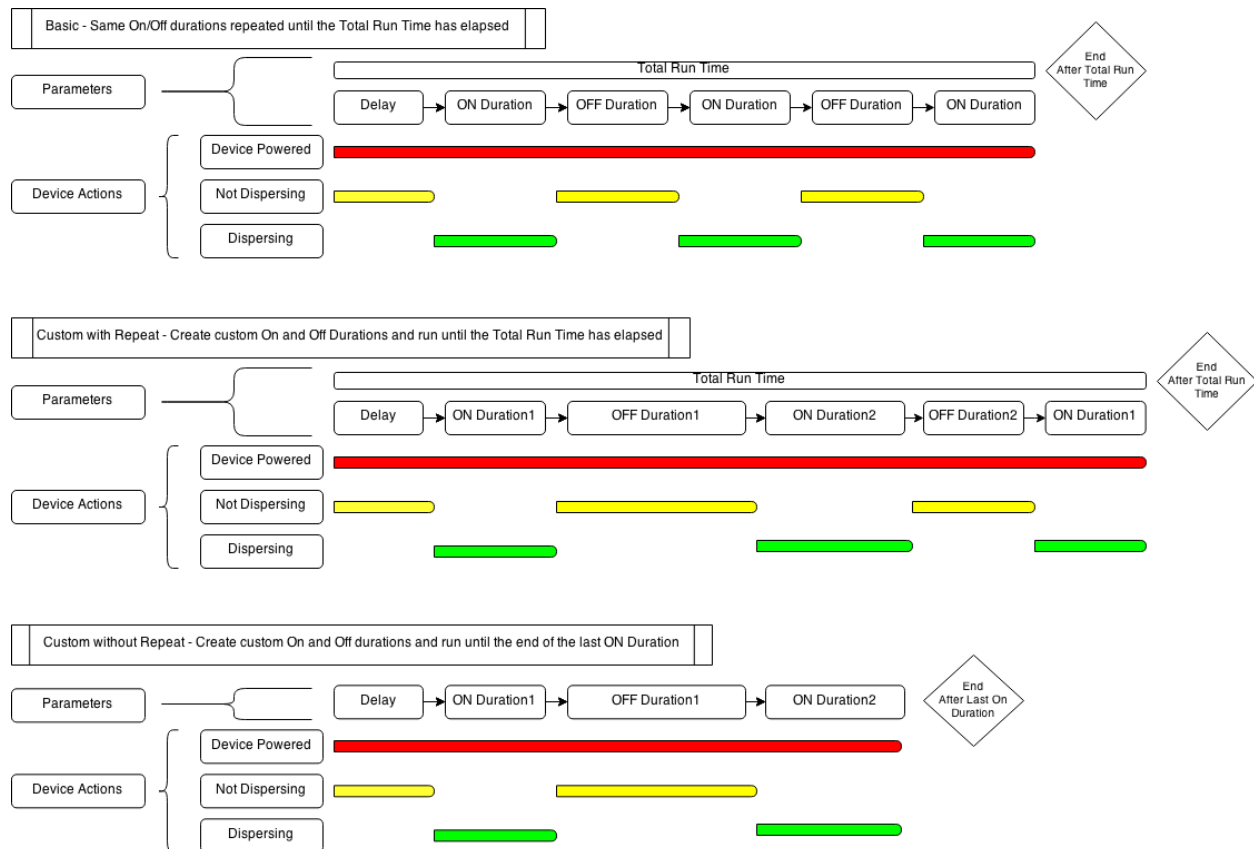


Figure 2.6 Example program diagram of version 1.4.4 of the dispersal controller

2.4 Power Efficiency

Due to the remote and widely disseminated locations of many bat hibernacula, the ability of the dispersal system to run autonomously and on battery power are fundamental requirements for field deployment for the management of WNS. Battery operation greatly expands the range of the dispersal system outside of the built environment and facilitates *in situ* management of WNS. However, as a battery drains, both voltage and current diminish, potentially causing negative effects on the circuitry and/or the output of the dispersal device, which both rely on constant power to operate consistently. These effects can be mitigated or abolished if feedback systems are developed that allow real-time correction during diminishing power situations. By

analyzing battery drain characteristics and system energy usage or output, consistent operation during battery-powered use can be achieved as well as permitting a more efficient battery selection.

Evaluation of the dispersal system operational characteristics was performed under various battery drain scenarios. These results were used to test feedback systems that sought to mitigate the negative effects of battery drain. Modulation of power from a benchtop regulated power supply (Extech, New Hampshire, USA) was used to simulate battery drain and evaluate system performance during battery drain scenarios. Feedback monitoring was performed with a MPX4250AP pressure sensor (Freescale Semiconductor, Texas, USA), with output monitored with an AutoSystem XL gas chromatograph (GC; PerkinElmer, Massachusetts, USA) and a quantitative gas analysis mass spectrometer (QGA-MS; Hiden, United Kingdom), in order to determine aberrant jet nebulizer output during battery drain. The results of these tests allowed software functions to be produced that modulated output of the jet nebulizer to rectify issues due to battery drain.

2.5 Air Chamber Development

A polypropylene glove box (Cleatech, California, USA) was used to conduct airspace studies involving the jet nebulizer and conduct inhibition assays. The glove box was sealed from the outside environment to ensure there was no airflow in or out of the box. The inner dimensions were measured and the total internal volume was calculated to be $2.923 \times 10^{-1} \text{ m}^3$. Bulkhead electrical ports were outfitted to transmit power to an internal circulatory fan and a Peltier thermoelectric device. The thermoelectric device was used to heat a watch glass containing aliquots of VOCs and formulations to evaporation temperatures.

2.6 Headspace Sampling

Direct headspace sampling and analysis by GCMS was conducted for quantifying gaseous concentrations of compounds. Both syringe and solid-phase micro-extraction (SPME) fiber sampling techniques were explored for accuracy, reproducibility, and ease of use. Samples were extracted with either a gas-tight syringe or SPME fiber, through a bulkhead fitting with a septum, then injected or thermally desorbed in a heated injector port of an Agilent 7890A gas chromatograph connected to an Agilent 5977A mass spectrometer (GCMS, Agilent, California, USA).

Several SPME fiber materials were evaluated for both the affinity and degree of adsorption of target compounds. Three fiber materials were selected that are commonly used to detect low molecular weight or volatile compounds- polydimethylsiloxane (PDMS), polydimethylsiloxane/carboxen (PDMS-CAR), and polydimethylsiloxane/divinylbenzene (PDMS-DVB). Each fiber material was exposed to a known concentration of each analyte, then analyzed with the GCMS.

Programming was performed in the Arduino programming language with a combination of original source code and open-source libraries (Appendix D). Source code was compiled with the Arduino Integrated Development Environment (IDE; version 1.0.6) to produce a hex file containing machine code. The machine code was uploaded to the MCU with either the Arduino IDE or AVRDUde software, using the Pocket AVR hardware programmer (Sparkfun Electronics, Colorado, USA).

3 EXPERIMENTS

3.1 Spore Harvesting and Culture Maintenance

P. destructans isolates were obtained from Kevin Keel and his WNS diagnostic work at the University of Georgia's Southeastern Cooperative Wildlife Disease Study. Conidia were stored at -20°C in a phosphate-buffered saline solution (PBS, Appendix B) for short-term storage. To prepare conidia for long-term storage, glycerol was added to the conidia-PBS solution to produce a solution comprised of 30% glycerol and 70% PBS. This solution was aliquoted into cryogenic vials (Nalgene, New York, USA) and stored at -80°C until use. Mycelial growth of *P. destructans* was propagated on Sabouraud Dextrose Agar (SDA, BD, New Jersey, USA) at 15°C .

To produce confluent lawns of *P. destructans*, 100 μl aliquots of conidia solution (10^6 conidia ml^{-1}) were evenly spread on the surface of SDA in 90 mm Petri dishes. Each dish was sealed with a paraffin film (Parafilm M, Bemis, Wisconsin, USA) and incubated at 15°C for approximately 3 or 6 weeks to produce confluent lawns for inhibition assays or conidia harvesting, respectively.

To harvest conidia, a 10 ml aliquot of conidia harvesting solution (Appendix C) was dispensed onto the mycelial lawn in each Petri dish. The mycelia surface was agitated with a sterile loop to dislodge conidia into the harvesting solution. A serological pipette was used to transfer the conidia harvesting solution from the Petri dish to a conical Falcon tube (BD, New Jersey, USA). The solution was centrifuged at 3,000 revolutions per minute (RPM) for 10 minutes, then the supernatant was removed and the pellet resuspended in 10 ml PBS by vortexing. Centrifugation and resuspension was repeated 3 times or until the supernatant became clear (whichever occurred first). The pellet was resuspended in 10 ml PBS by vortexing, then

filtered through a sterile glass wool-packed funnel to remove residual mycelial fragments. The glass wool was rinsed with an additional 5 ml PBS to recover remaining conidia. Spore solutions were either placed in short-term storage at -20°C or prepared for long-term storage at -80°C .

3.2 Antimicrobial Susceptibility

3.2.1 *Quantification of Filamentous Fungi Growth*

Filamentous fungi grow by hyphae elongation instead of distinct cellular division that is typical of bacteria and yeast. Therefore, quantification of filamentous fungi inhibition requires alternative methods than the classic disc diffusion assay utilized to quantify bacteria or yeast inhibition, which relies on the ability of the organism to produce a zone of inhibition. Comparing the radial growth area of mycelia over a flat agar surface to unexposed control growth has been the accepted method for assessing mycelial inhibition.

However, a ruler commonly used to measure the area of mycelial growth of filamentous fungi presents its own challenges. Mycelial core plugs will often grow asymmetrically, either naturally or as a response to exposure to control agents (Figure 3.1). To attain a greater accuracy in measuring mycelial growth, a technique was developed that utilized digital photography and computer analysis.

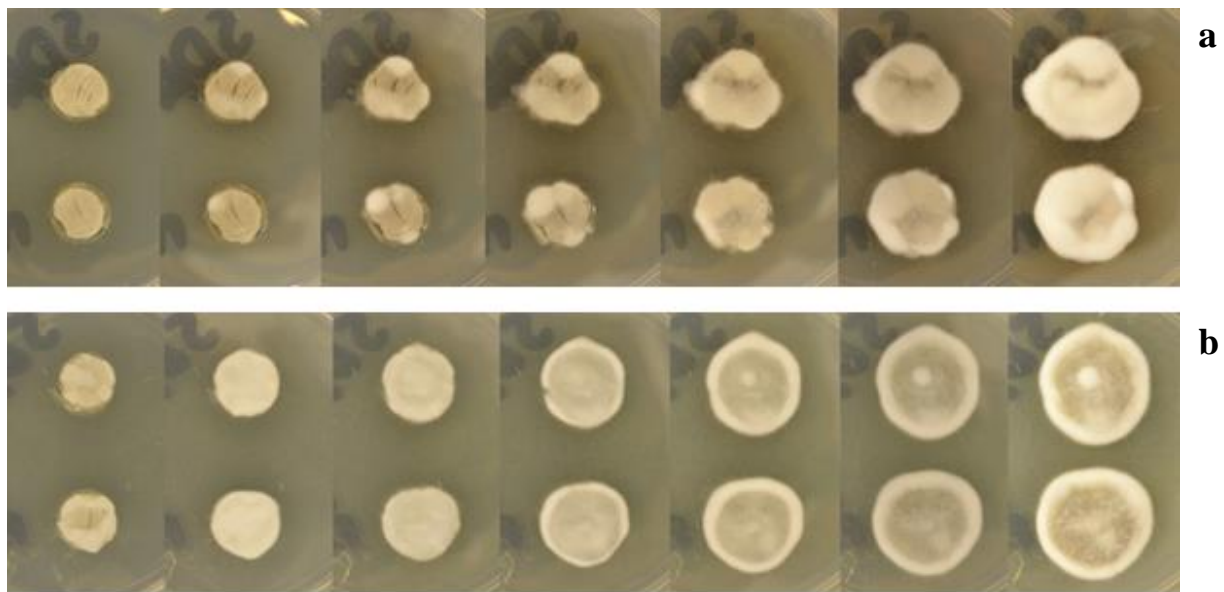


Figure 3.1 Radial growth of Pseudogymnoascus destructans under various growth conditions

Growth morphologies of *Pseudogymnoascus destructans* following a 14-day exposure to a control agent (a) and unexposed controls (b).

The GIMP (GNU Image Manipulation Program) is open-source, freely distributed software for image editing. This software allows for the direct measurement between two points or the area selection of a digital photograph. The quantity of pixels measured, which are the smallest units of a digital photograph, can be converted to meters after measuring the length, in pixels, between demarcations of a ruler in a photograph and deriving a conversion ratio between pixels and meters.

A Nikon D3100 digital single lens reflex (DSLR) camera with an 18 - 55 mm lens and a tripod was used to capture images. The camera was attached to the tripod and aimed down to a horizontal surface in order to provide a consistent distance from the lens to the object being photographed, ensuring the same pixel-to-meter ratio was retained for all acquired images of a set. If the height changed, a new calibration image of the ruler would be required to derive the

new pixel-to-meter ratio. Subsequent images of mycelial plugs had their corresponding image numbers catalogued for later identification. Manual focus was required to retain the same focal point throughout all image captures and a remote shutter release device was used to ensure stable images acquisition. Contrast was required between the growth medium and mycelia to produce an accurate margin selection for area measurement as well as to be able to discern the margin of the ruler demarcations using GIMP. Therefore, the location of the photos as well as the camera's white balance, exposure, f-stop, and ISO, among other parameters, may need to be manually adjusted in order to attain consistent contrast between photo acquisitions.

A photo of a ruler was used to set the initial focal point for the photo set as well as serving as a calibration device for determining the conversion factor during image analysis. The ruler was placed at the same height as the agar surfaces to be photographed, either by supporting it or by cutting the edges of a Petri dish to allow the ruler to be set into the Petri dish at the height of the agar. The image of the ruler was analyzed by measuring the number of pixels between two demarcations on the ruler that equaled a distance of one centimeter.

To measure the area of radial mycelial growth, an area selection tool was used. The Fuzzy Selection tool is designed to select areas based on color similarity. The threshold was adjusted to change the degree to which similarly colored areas were selected. By increasing the threshold, a broader range of similar colors was selected, and conversely, by decreasing the threshold, the narrower range of similar colors was reduced. A Threshold of 10 to 20 worked well for the majority of image analyses. Selection of mycelial area produced an output of the number of pixels that comprised the selected area. Percent difference between test and control growth area could be calculated without a conversion to meters, however if a comparison was

desired in SI units, then a conversion was necessary. Using the conversion equation (Figure 3.2), the area in pixels² was converted to mm².

$$\left(\frac{\text{Number of pixels in area}}{\text{Number of pixels per mm}}\right)^2 = \text{Area of mycelia in mm}^2$$

Figure 3.2 Equation for calculating mycelial area from pixels of a digital photograph

3.2.2 *In Vitro Evaluation of Antifungal VOCs*

In vitro inhibition assays were conducted to evaluate the anti-*P. destructans* activity of VOCs with known antifungal activity. Select formulations were created and modified by the addition and subtraction of compounds, and manipulation of compound ratios, with the intent to enhance antifungal activity. *In vitro* testing was conducted with a broad range of VOCs and VOC formulations, and at different concentrations, to evaluate the degree of inhibition to mycelial growth and conidial germination of *P. destructans*, as per the methods of Cornelison et al. (2014). These results have facilitated development of effective treatment regimens for *in vivo* testing.

Two exposure methods were used to assess the degree of inhibition caused by gaseous VOC exposure, with preparation similar between the methods. Each method required a 30 mm Petri dish containing SDA to have either 25 µl of conidia solution (10⁶ conidia ml⁻¹) spread on the surface or a mycelial plug inserted. To produce the mycelial plug, a 5 mm diameter agar core was removed from the fresh agar with a transfer tube (Spectrum Medical, SC, USA) and discarded. Then, a 5 mm diameter mycelial core was cut from a confluent mycelial lawn and placed into the empty core of each 30 mm Petri dish.

The first exposure method required each 30 mm Petri dish to be placed, without a lid, inside a larger 150 mm Petri dish, in addition to a watch glass containing an absorbent disc. Each disc had a specific amount of liquid VOC or VOC formulation dispensed into it. Each 150 mm Petri dish was then sealed with Parafilm and incubated at 15°C.

The second exposure method required a sealed glove box of a known volume and a hot plate with a watch glass placed inside to evaporate a known quantity of VOC or VOC formulation. The amount of VOC or formulation required to produce a specific gaseous concentration was determined using equations derived from the ideal gas law (Figure 3.3). Glass jars containing the 30 mm Petri dishes were opened inside the glove box after evaporation and homogenization of the VOC or formulation, then sealed with Parafilm and incubated at 15°C.

Controls were sealed and incubated without exposure to VOCs. All exposures and controls were performed in triplicate and examined several days post-inoculation to qualify spore germination and quantify growth area of exposed and unexposed mycelial plugs, to determine any significant differences in the quantity and rate of growths.

$$V_I = R \times \frac{T}{P} \quad A_P = \frac{M}{V_I} \times V_G \quad A_T = A_P \times C$$

R = Gas Constant 8.2057338×10^{-2} (L atm K⁻¹ mol⁻¹)

T = temperature (Kelvin)

P = pressure (atm)

M = molecular weight of the compound (g/mol)

V_I = volume of an ideal gas (m³)

V_G = volume of headspace (m³)

A_P = Amount to raise 1 ppmv (g)

C = Desired concentration (ppmv)

A_T = Total amount (g) to attain desired concentration (C) in a known volume (V_G)

Figure 3.3 Equations for converting a desired gaseous concentration to a liquid volume

Modification of VOCs and VOC formulations that demonstrated inhibition focused on incorporating other previously identified anti-*P. destructans* VOCs to enhance inhibitory activity (Cornelison et al. 2014). The discovery of highly effective and synergistic anti-*P. destructans* VOC formulations permitted lowering the effective dose of each compound while maintaining or enhancing inhibitory effects. VOC formulations chosen for continued testing with the dispersal system were required to undergo dispersal rate analysis in order to be accurately dispersed with the dispersal system utilizing the jet nebulizer.

3.3 Dispersal System Development

3.3.1 Dispersal Characterization

Volatile organic compounds will evaporate at different rates when exposed to varied environmental conditions and when used with different dispersal technologies. Investigating the factors that affect dispersal and evaporative efficiency among different dispersal technologies enables determination of an appropriate use of each technology as well as aiding in developing corrective measures to ensure consistent and accurate dispersal under diverse environmental conditions. Two different aerosolization technologies were studied, the jet nebulizer and rotary atomizer.

3.3.1.1 Jet Nebulizer

The jet nebulizer is an aerosolization technology developed for the medical industry to dispense respiratory therapy medications to patients in the form of an aerosol inhaled into the lungs. It produces a microscopic aerosol that permits efficient drug delivery through respiration. Of the three most common nebulizer technologies on the market, jet, vibrating mesh, and ultrasonic, the jet nebulizer was chosen for initial study because of its lower cost, simpler design, and greater resilience to clogging. It operated by pressurized air that is passed through a small jet aperture to produce a high-pressure airflow that disrupts a thin layer of fluid (Figure 3.4). The aerosol produced contains both large- and small-diameter droplets. A baffle deflects and returns the larger droplets to the reservoir to be recycled but permits the smaller droplets to be carried out of the nebulizer by the airflow. The small size of nebulizers makes them well suited for portable, small- to medium-scale applications.

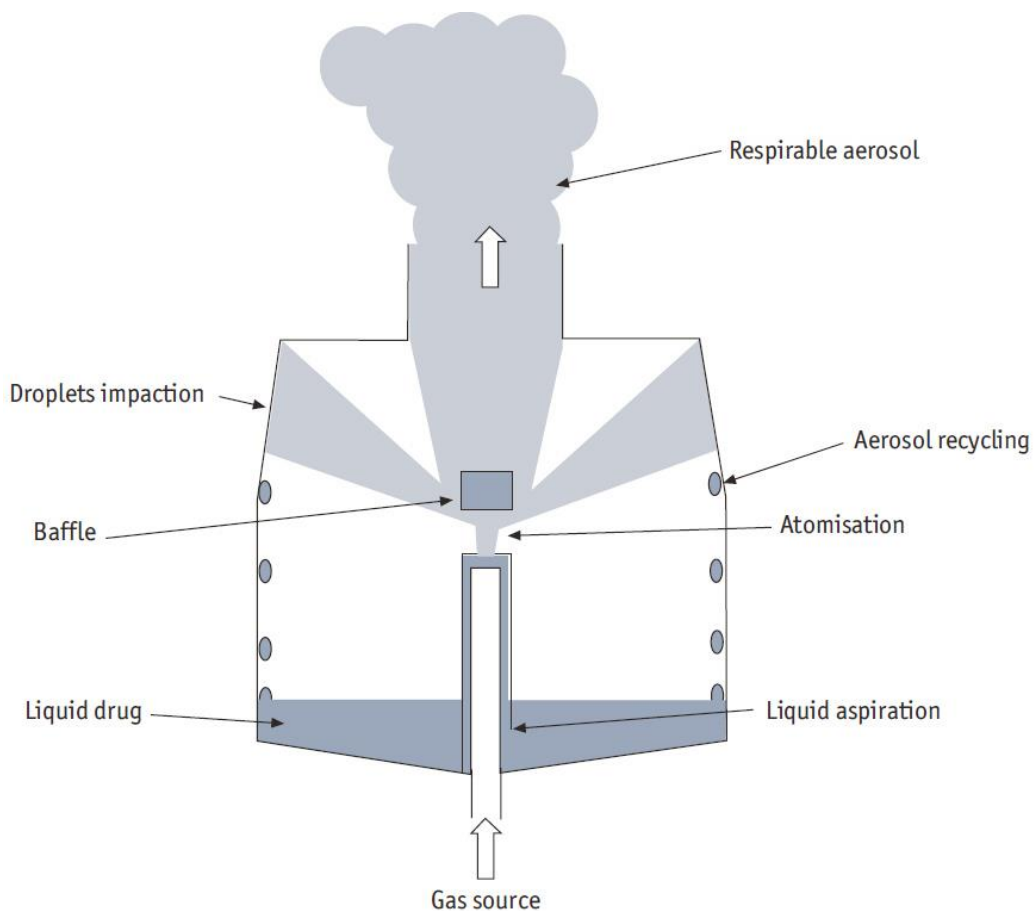


Figure 3.4 Operational diagram of a jet nebulizer (Vecellio, 2006)

Evaluation of the jet nebulizer was performed with an air chamber to analyze dispersal characteristics as well as investigate dispersal irregularities that may arise from conditions present in natural hibernacula. This evaluation required the development of a chamber that was both inert to gaseous VOC exposure and granted the ability to modify abiotic conditions. Direct headspace sampling from the chamber was conducted with a gas-tight syringe (Agilent, California, USA) and solid-phase micro-extraction (SPME) fibers (Supelco, Inc., Pennsylvania, USA). Analysis was carried out on an Agilent 7890A gas chromatograph connected to an

Agilent 5977A mass spectrometer (GCMS, Agilent, California, USA) to determine aerosolization rates, evaporative efficiency, and overall reproducibility.

As compounds with different physical characteristics aerosolize at different rates, testing required empirically determining the rate of dispersal for treatment compounds in order to ensure accurate dispersal. Dispersal analyses enabled determination of a specific aerosolization rate for a specific compound or formulation. The results from air chamber headspace analyses were used to determine the dispersal rates of treatment formulations as well as further advance the mathematical functions and feedback mechanisms used to modulate the jet nebulizer and produce more accurate VOC dispersal.

3.3.1.2 Rotary Atomizer

The Dyna-Jet L-30 rotary atomizer is an industrial-scale ultra-low volume (ULV) aerosolizer. The L-30 utilizes a rotary atomizer that produces aerosol from centrifugal force that propels liquid outward from the center of a high-speed rotating disc. As the liquid moves toward the edge of the disc, it spreads out and creates atomized droplets at the edge. The L-30 was chosen for analysis for its ability to operate fully on electric power, disperse large volumes, produce very low diameter aerosol droplets (90% below 24 μm median diameter), and operate quietly. The L-30 has several advantages over the jet nebulizer. In addition to being able to disperse larger volumes, it also utilizes a piston pump to dispense its fluid. This enables an absolute dispersal rate to be maintained, precluding the need to conduct a dispersal rate analysis for each VOC or formulation.

3.3.2 High-Frequency Acoustic Output

Due to their nocturnal activity, bats have evolved the ability to navigate in darkness, which includes the ability to hear and echolocate in the ultrasonic range. The most sensitive range is between 15 kHz to 90 kHz, however some species have an extended range up to 200 kHz (Adams and Pedersen, 2000).

Several different aerosolization technologies were powered to their respective operating specifications to have their acoustic output analyzed. An M500 ultrasonic microphone (Pettersson Elektronik, Sweden), with a parabolic cone to focus sound, was positioned approximately 5 feet from several dispersal devices during normal operation. Audio was sampled up to 500 kHz and recorded to a 16-bit raw WAV file. The frequency spectrum of the recording was analyzed with BatSound touch (Pettersson Elektronik, Sweden) to produce spectrograms from 0 – 250 kHz. The usable range for this microphone is 10 – 190 kHz, therefore all spectrograms were limited to 200 kHz.

3.4 Standard Gaseous Curve Development

There exist a number of confounding factors that may affect the gaseous concentration of VOCs when dispersed in their liquid form during treatment studies. As such, gaseous concentrations were validated with the creation of standard curves that enabled quantification of a headspace sample of an unknown gaseous concentration. In order to produce a standard curve, both a sealed air space of a known volume and the ability to create a known gaseous concentration were required.

Standards gaseous concentrations were prepared by evaporating a specific amount of pure VOC or formulation in a sealed glove box of a known volume. Amounts were calculated from the equations in Figure 3.3. An 80-watt direct current (DC) regulated power supply (Extech, New Hampshire, USA) was connected through the bulkhead port to a 12-volt DC Peltier device with a watch glass set on top of the heated surface. The heater was powered and limited to 12 volts and 1.5 amps, raising the temperature of the watch glass near 100°C. An 80 mm 12-volt DC fan was used to circulate the air to homogenize the headspace.

Several standard curves were produced from gaseous headspace samples, using two sampling methods: a gas-tight syringe (Agilent, California, USA) with direct-injection and solid-phase micro-extraction (SPME) fibers (Supelco, Inc., Pennsylvania, USA) and thermal desorption. Initial standard curve development focused on method development and analysis technique, and therefore a high-purity sample of toluene was used. Subsequent standard curve developments focused on analyzing the B-23 formulation. All liquid amounts that were evaporated to produce a known gaseous concentration were calculated from the equations in Figure 3.3. Calculating the amount required to produce specific gaseous concentrations of the B-23 formulation entailed calculating the required amount for each compound of the formulation, then adjusting each amount based on the percentage each contributed to the formulation.

The first gaseous toluene standard curve was produced with a direct headspace sampling and injection using a GC gas-tight syringe. The concentration range was from 50 to 250 ppmv, at 50 ppmv increments. An aliquot of toluene, in an amount calculated to produce a concentration of 50 ppmv, was pipetted onto a heated watch glass and allowed to evaporate and homogenize in a sealed glove box. A 100 µl headspace sample was extracted from the glove box through a bulkhead with a septum using a gas-tight GC syringe, and then manually injected into a GCMS

to analyze the sample. Separately, 50, 100, 150, 200, and 250 ppmv concentrations were produced in the glove box and analyzed with the GCMS, with each sample and analysis performed in triplicate. The GC method was programmed as follows: the injector port was held at 40°C in splitless mode, and the oven temperature was held at 30°C for 1 minute, then raised 50°C min⁻¹ to 150°C and held for 1 minute. The MS detector was programmed with a scan range of 37 - 94 m/z. Manual peak selection was performed on the resulting chromatograms and peak area was calculated for each trial of each concentration using MassHunter Qualitative Analysis (version B.07.00, Agilent, California, USA).

The second gaseous toluene standard curve was produced with a direct headspace sampling technique using a polydimethylsiloxane divinylbenzene (PDMS-DVB) SPME fiber. The concentration range was from 25 to 125 ppmv, at 25 ppmv increments. An aliquot of toluene, in an amount calculated to produce a concentration of 25 ppmv, was pipetted onto a heated watch glass and allowed to evaporate and homogenize in a sealed glove box. The SPME fiber was injected through the bulkhead with a septum and exposed to the headspace for 5 minutes, then thermally desorbed in the GC inlet for analysis. Separately, 50, 75, 100, and 125 ppmv concentrations were produced in the glove box and analyzed with the GCMS, with each sample and analysis performed in triplicate. The GC method was programmed as follows: the injector port was held at 40°C in splitless mode and the oven temperature was held at 30°C for 1 minute, then raised 50°C min⁻¹ to 150°C and held for 1 minute. The MS detector was programmed with a scan range of 37 - 94 m/z. Manual peak selection was performed and peak area was calculated for each trial of each concentration using MassHunter Qualitative Analysis.

A standard curve for the B-23 formulation was produced with a direct headspace sampling technique using a PDMS-DVB SPME fiber. The concentration range was from 100 to

500 ppmv, at 200 ppmv increments. An aliquot of the B-23 formulation, in an amount calculated to produce a concentration of 50 ppmv, was pipetted onto a heated watch glass and allowed to evaporate and homogenize in a sealed glove box. The SPME fiber was injected through the bulkhead with a septum and exposed to the headspace for 5 minutes, then thermally desorbed in the GC inlet for analysis. Separately, 100, 300, and 500 ppmv concentrations were produced in the glove box and analyzed with the GCMS, with each sample and analysis performed in triplicate. The GC method was programmed as follows: the injector port was held at 250°C with a 20:1 split and the oven temperature was held at 40°C for 1 minute, then raised 10°C min⁻¹ to 250°C and held for 1 minute. The MS detector was programmed with a scan range of 35 - 360 m/z. Manual peak selection was performed on the primary and secondary peaks and peak areas were calculated for each trial of each concentration using MassHunter Qualitative Analysis.

3.5 Bat Toxicological Histopathological Evaluation

To determine any negative toxicological effects from an effective anti-*P. destructans* formulation, a study was conducted in which uninfected tri-colored bats (*Perimyotis subflavus*) (n=37) were collected and housed at 8°C to induce hibernation, then exposed to a 10 ppmv gaseous VOC formulation with the treatment device. The VOC formulation consisted of 2-ethyl-1-hexanol, benzaldehyde, and decanal in a 1:1:1 molar ratio. This dispersal regimen was repeated every 24 hours, for 42 days. A random segment of both control and test groups were removed at days 10 (acute exposure, n=12), 42 (chronic exposure, n=12), and 42 with 8 days of euthermic temperatures (chronic exposure and post-euthermia, n=13), euthanized, and subject to a full necropsy with particular interest in the condition of respiratory tissues.

Thirty-seven formalin-fixed bats were stained with hematoxylin and eosin before being examined for lesions. All tissues were trimmed into histology cassettes. Bats numbered 1 through 12 were from the acute exposure group (10-day trial), with the first 6 exposed to VOCs and the last 6 controls. Bats numbered 13 through 24 were from the chronic exposure group (42-day trial), with the first 6 exposed to VOCs and the last 6 controls. Bats numbered 25 through 36 were from the post-hibernation group (42-day trial, followed by 8 days euthermia), with the first six exposed to VOCs and the last six controls. Bat numbered 37 was from the post-hibernation group exposed to VOCs.

3.6 Treatment at Black Diamond Tunnel

Black Diamond Tunnel is a railway tunnel in Clayton, Georgia that began construction in the 1850s. Construction was put on hold during the Civil War and was never resumed, leaving the tunnel uncompleted. The tunnel has one opening that is approximately 4.4 meters in width and 5.4 meters in height at the entrance. It extends 423 meters straight into the rock mountainside and at a 1° downward slope. As a consequence of no drainage, water has flooded the entire length of the tunnel, necessitating the use of a boat to safely gain access.

The tunnel has historically been the site of the largest tri-colored bat (*Perimyotis subflavus*) population known to Georgia, with population surveys consistently yielding approximately 5,000 each year, prior to 2014. However, since WNS was first detected in 2013, the population has undergone precipitous decline. Within 3 years of detecting WNS in 2013, the population has decreased 95%, with the latest pre-treatment survey yielding 220 tri-colored bats as of March, 2016 (Figure 3.5).

This is the site of an ongoing development of a VOC-based WNS mitigation effort using the L-30 to distribute doses of the B-23 formulation. Through The Conservation Fund and the Transcontinental Gas Pipeline Company, we have been awarded a \$200,000 grant to develop an integrated disease management (IDM) system over the next 4 years, with a goal of increasing survivorship of bat populations affected by WNS at Black Diamond Tunnel.

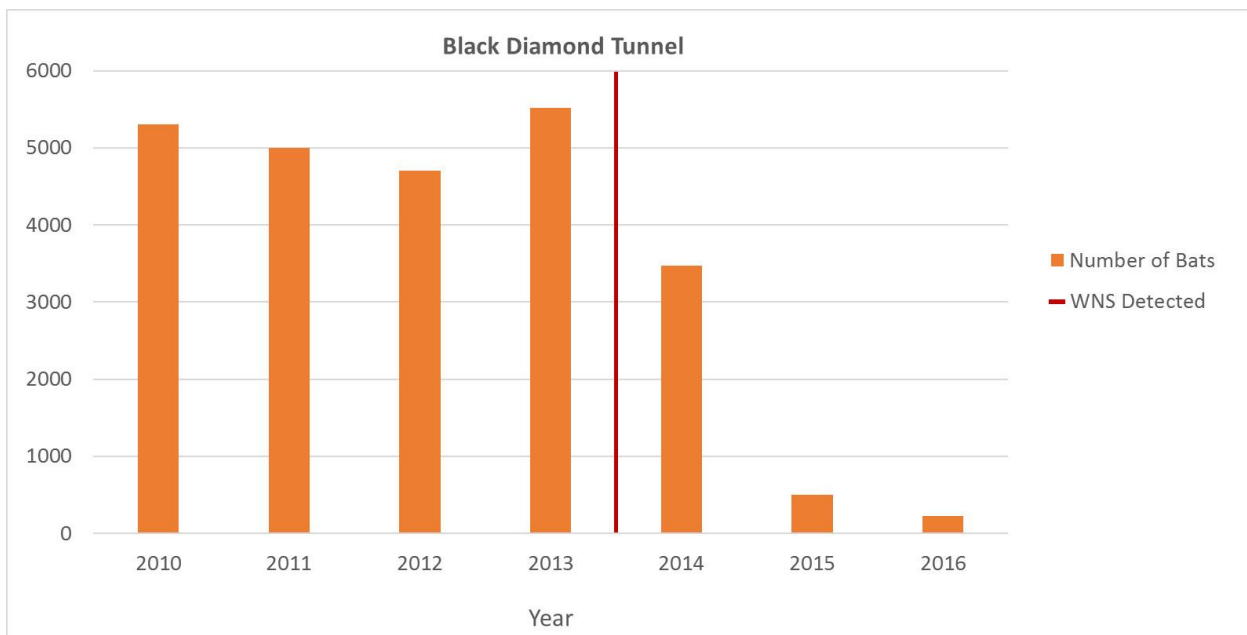


Figure 3.5 Tri-colored bat population counts at Black Diamond Tunnel from 2010 to 2016

To prepare the site for treatment, infrastructure was constructed inside and outside of the tunnel (Figure 3.6). A platform was constructed to secure a battery-powered capstan winch (Powerwinch 300; Powerwinch, Colorado, USA), to enable extension and retrieval of the L-30 that has been secured to a 10-foot flat-bottomed boat. A pulley was attached to a buoy and secured near the rear of the tunnel with 20 feet of 0.25-inch diameter polypropylene rope to 100 pounds of weight, acting as a mooring anchor. A length of 600 meters of 0.25-inch diameter

polypropylene rope was fed through the pulley and the free ends were attached to the bow and stern of the boat. With the open loop wrapped around the capstan winch drum, the vessel was able to be moved in and out of the tunnel at will by actuating the capstan winch at the entrance. Demarcations were produced along the rope every 12 meters, permitting accurate determination of the position of the boat inside the tunnel. This also allowed the speed of the boat and L-30 to be measured at $26 \text{ meters minute}^{-1}$, which verified the rated speed of the winch.

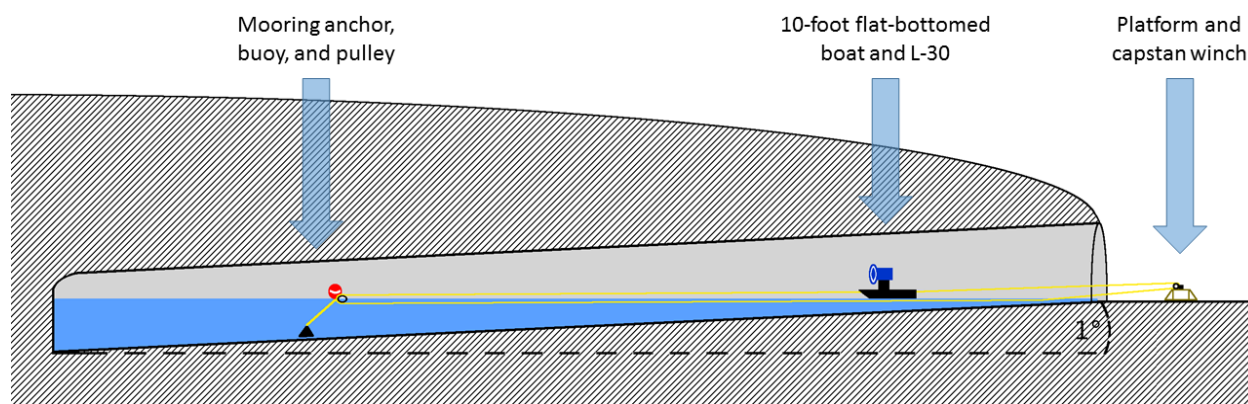


Figure 3.6 Diagram of the infrastructure at Black Diamond Tunnel

An initial target treatment concentration of 300 ppmv was chosen, as this was the minimal amount determined by *in vitro* studies to elicit significant *P. destructans* inhibition. Using the equations from Figure 3.3, and an estimated tunnel volume of $5,300 \text{ m}^3$, 6.772 liters of the B-23 formulation was calculated as the amount required to be dispersed to attain a 300 ppmv maximum homogeneous concentration, if 100% volatilization were to occur. The L-30 was calibrated to disperse at $200 \text{ ml minute}^{-1}$, rendering a total run time of 33.85 minutes to disperse 6.772 liters.

The vessel was sent into the tunnel 300 meters, the furthest point at which safe operation could be achieved without risk of the L-30 coming into contact with the ceiling, before beginning dispersal. With a boat movement speed of 26 meters minute⁻¹, traversing 300 meters would require 11.54 minutes. With the dispersal requiring a longer duration than the boat retrieval, 22.31 minutes would need to be accounted for. After dispersal began, the vessel was retrieved using the capstan winch, stopping at every 12-meter demarcation for approximately 56 seconds. The addition of these timed stops enabled the retrieval to match the dispersal duration, promoting an even dispersal throughout the tunnel length. The entrance of the tunnel was not sealed for any of the three treatments during the first winter treatment, in order to allow any bats to freely leave the tunnel and to permit a visual assessment of bat disturbance.

Water samples were obtained at the entrance of the tunnel, pre-treatment and up to 1 hour post-treatment. Air samples were obtained 150 meters into the tunnel, pre-treatment and up to 1 hour post-treatment. Air and water samples were also obtained 7 days post-treatment at the same locations, which underwent concentration analyses to determine the environmental fate of the B-23 formulation. The first winter treatments were conducted on November 4, 2016, December 2, 2016, and January 6, 2017. Bat population surveys were conducted prior to the first and second treatments, as well as post-winter, on February 28, 2017.

4 RESULTS

4.1 Antimicrobial Susceptibility

4.1.1 *Quantification of Filamentous Fungi Growth*

Area measurements derived from ruler and digital analyses were not shown to differ significantly when small areas (approximately 20 mm² or less) were measured. However, as

areas increased, the differences between them increased significantly. Ruler measurements consistently yielded smaller area calculations, resulting in larger calculated percent inhibitions (Table 4.1).

Table 4.1 Comparison of ruler and digital measurements of mycelial growth area

Comparison of area from ruler and digital measurements (measured in mm²)						
Method	Ruler	Digital	Ruler	Digital	Ruler	Digital
DPI	8	8	11	11	13	13
Plug 1	14.19	10.73	27.54	43.81	46.66	86.47
Plug 2	13.55	13.4	22.36	37.52	44.51	83.02
Plug 3	20.24	19.68	43.1	47.62	57.93	100.28
Plug 4	13.55	11.95	19.54	29.12	31.42	74.94
Plug 5	20.24	19.26	34.63	48.62	62.88	106.02

Comparison of percent reduction of growth from ruler and digital measurements (measured in mm²)						
Method	Ruler	Digital	Ruler	Digital	Ruler	Digital
DPI	8	8	11	11	13	13
Plug 1	66.40%	73.80%	59.50%	44.30%	45.30%	29.90%
Plug 2	67.90%	67.30%	67.10%	52.30%	47.90%	32.70%
Plug 3	52.10%	52.00%	36.60%	39.40%	32.10%	18.70%
Plug 4	67.90%	70.80%	71.30%	63.00%	63.20%	39.20%
Plug 5	52.10%	53.00%	49.10%	38.20%	26.30%	14.00%

This discrepancy between the accuracy of measurement methods is primarily due to two factors. First, as area increases, miscalculations produce a greater error. For instance, an error of 1 mm when measuring a radius of 5 mm produces a minimum area of 50.3 mm² and maximum of 113.1 mm², with a difference of 62.8 mm². An error of 1 mm when measuring a radius of 10 mm yields a minimum area of 254.5 mm² and maximum of 380.1 mm², with a difference of 125.6 mm².

Second, there is higher resolving power when measuring with digital photography than with the human eye. A resolution of a photograph is determined by how many pixels are present in the measured area, whereas the resolution of a ruler is determined by the number of delineations. For instance, it is not uncommon for the resolution of 1 mm of a digital photograph to be 200 pixels, or 200 discernable units per 1 mm. However, a ruler may have only 4 discernable units per mm. Using the same example above, a circle with a radius of 5 mm would yield an error of 15.7 mm² using a ruler with 4 units per mm, yet only 0.3 mm² from a digital photograph with 200 units per mm.

4.1.2 Exposure Assays with Six Previously-Described VOCs

The degree of inhibition each VOC induced was calculated by comparing the growth area from the exposed mycelial plugs to the unexposed control plugs, at both 15°C (Figure 4.1) and 4°C (Figure 4.2).

At 15°C, *P. destructans* displayed a range of susceptibility to the tested VOCs. With exposure to 30 µl of each VOC, partial inhibition of mycelial growth was observed in the presence of decanal, which exhibited 68% inhibition after 11 days post-inoculation (DPI), and complete inhibition with all others. With exposure to 3.0 µl of each VOC, partial inhibition of mycelial growth was observed in the presence of decanal and N-N-dimethyloctylamine, both exhibiting $\geq 20\%$ inhibition after day 7 DPI and $\geq 10\%$ inhibition after 11 DPI, and complete inhibition with all others. With exposure to 0.3 µl of each VOC, partial inhibition of mycelial growth was observed with 2-ethyl-1-hexanol, benzaldehyde, benzothiazole, decanal, and nonanal, and stimulated growth was observed with exposure to N-N-dimethyloctylamine. Decanal induced the least inhibition, from 0% after 7 DPI to 7% after 11 DPI. 2-ethyl-1-hexanol

induced the greatest inhibition, with 52% after 7 DPI to 60% after 11 DPI. N-N-dimethyloctylamine stimulated growth, from 24% after 7 DPI to 9% after 11 DPI. Growth plots can be seen in Figures 4.1a, 4.1b, and 4.1c.

At 4°C, exposure to 30 µl and 3.0 µl aliquots of each VOC resulted in complete inhibition of *P. destructans* mycelial growth. With exposure to 0.3 µl of each VOC, *P. destructans* displayed partial inhibition with all VOCs. Benzaldehyde induced the least inhibition, at 4% after 19 DPI and 8% after 36 DPI. Decanal induced the greatest inhibition, with 100% after 19 DPI to 99% after 36 DPI.

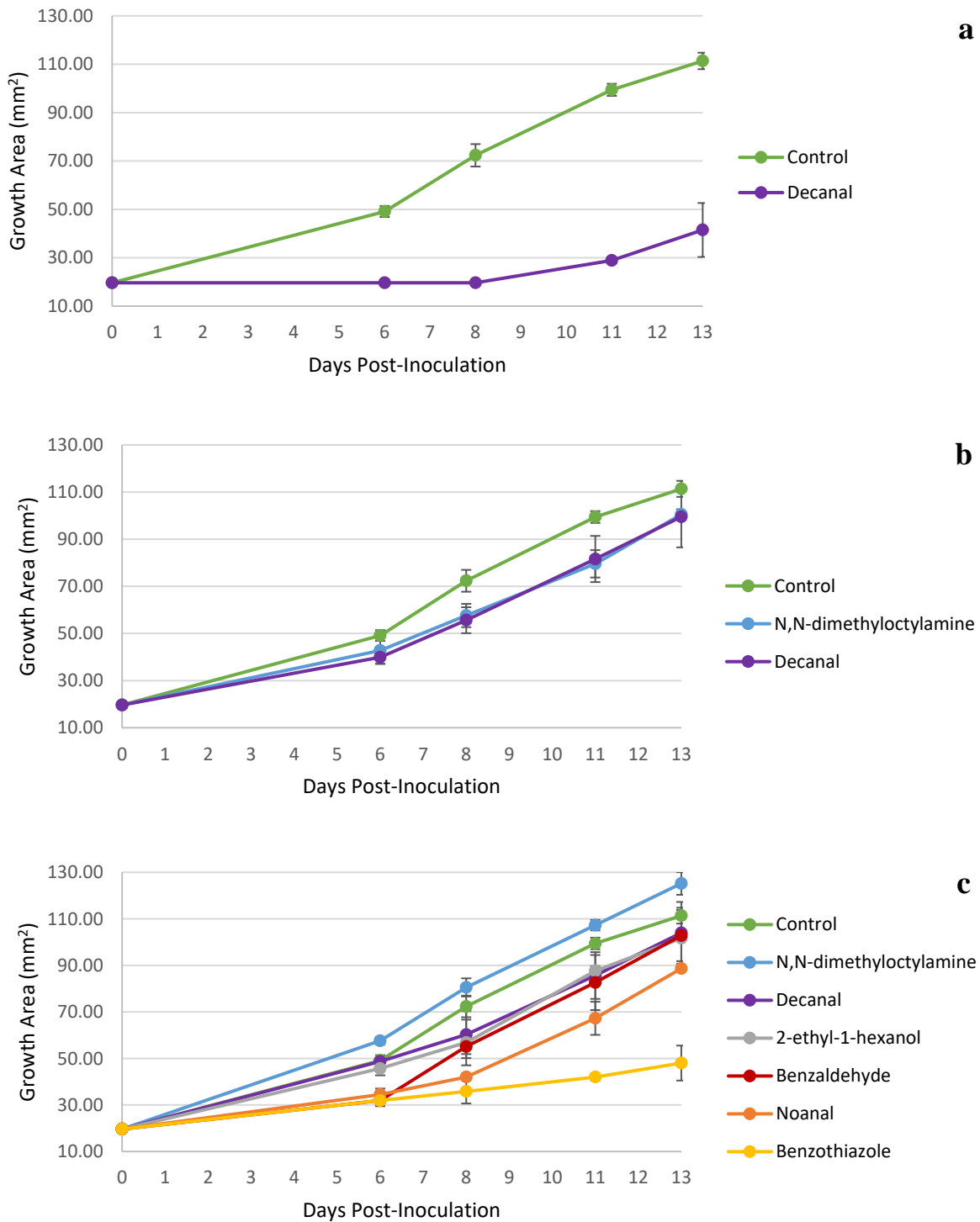


Figure 4.1 Growth of *Pseudogymnoascus destructans* exposed to single VOCs at 15°C

Inhibition assays with *Pseudogymnoascus destructans* exposed to 30.0 μ l (a), 3.0 μ l (b), and 0.3 μ l (c) of each of 6 VOCs and incubated at 15°C. Absence of any of the 6 VOCs from a graph indicates there was no growth when exposed to that VOC.

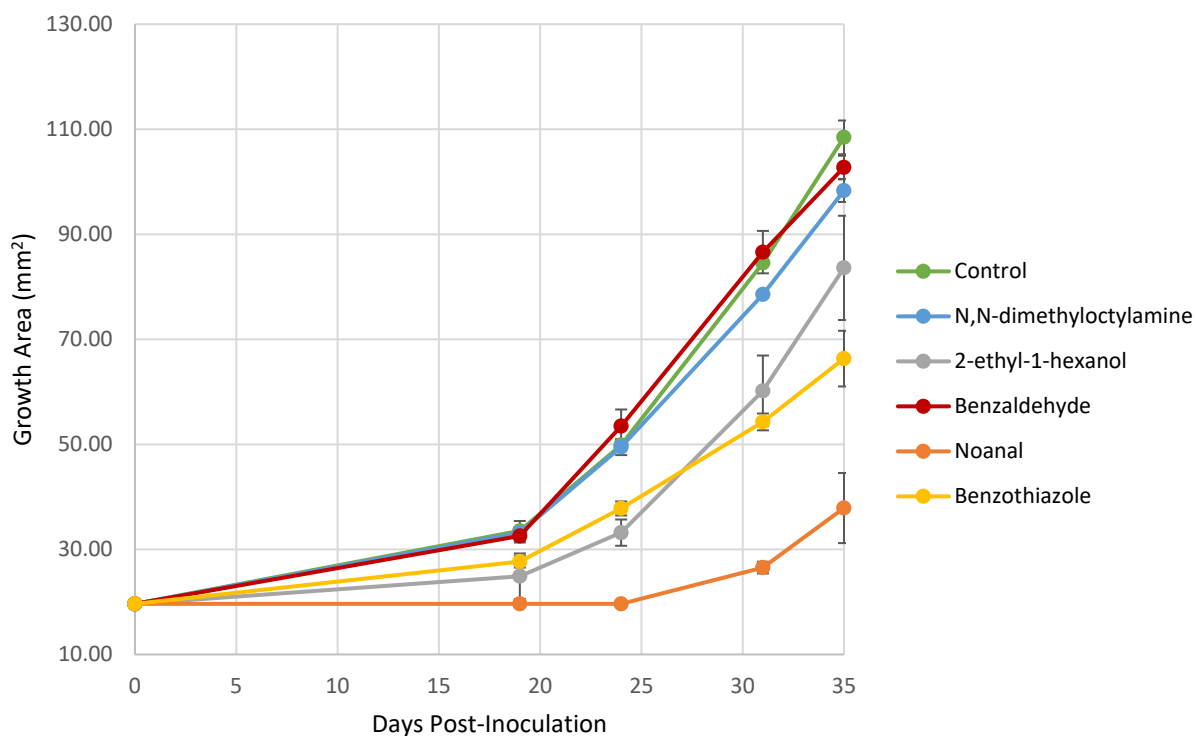


Figure 4.2 Growth of *Pseudogymnoascus destructans* exposed to single VOCs at 4°C

Inhibition assays with *Pseudogymnoascus destructans* exposed to 0.3 µl of each of 6 VOCs and incubated at 4°C. Absence of decanal from the graph indicates there was no growth when exposed to that VOC.

4.1.3 Exposure Assays with VOC Formulations

Three VOC formulations comprised of two VOCs were observed to promote significant synergistic inhibition of *P. destructans* mycelial growth (Figure 4.3). Those include 2-ethyl-1-hexanol and benzaldehyde, 2-ethyl-1-hexanol and nonanal, and 2-ethyl-1-hexanol and decanal. The greatest difference between the inhibitions elicited by the formulation vs. the combined inhibitions of each VOC occurred after 6 DPI with 2-ethyl-1-hexanol and benzaldehyde, 14 DPI with 2-ethyl-1-hexanol and nonanal, and 14 DPI with 2-ethyl-1-hexanol and decanal. Growth areas of *P. destructans* mycelial plugs exposed to each VOC and formulation are provided in Figure 4.3 and percent inhibition was calculated in Figure 4.4.

Two VOC formulations comprised of three VOCs were observed to promote significant synergistic inhibition of *P. destructans* mycelial growth. Those include a formulation of 2-ethyl-1-hexanol, benzaldehyde, and decanal, and a formulation of 2-ethyl-1-hexanol, nonanal, and decanal. Growth areas of *P. destructans* mycelial plugs exposed to each VOC and formulation are provided in Figure 4.5 and percent inhibition in Figure 4.6.

The B-23 formulation was observed to elicit significant inhibition of *P. destructans* mycelial growth area following a 24-hour gaseous exposure of 500 ppmv, after 7 DPI ($p=0.025$) and 11 DPI ($p=0.009$). Growth area of *P. destructans* mycelial plugs following a 24-hour exposure to various gaseous concentrations of the B-23 formulation are provided in Figure 4.7 and percent inhibition was calculated in Figure 4.8.

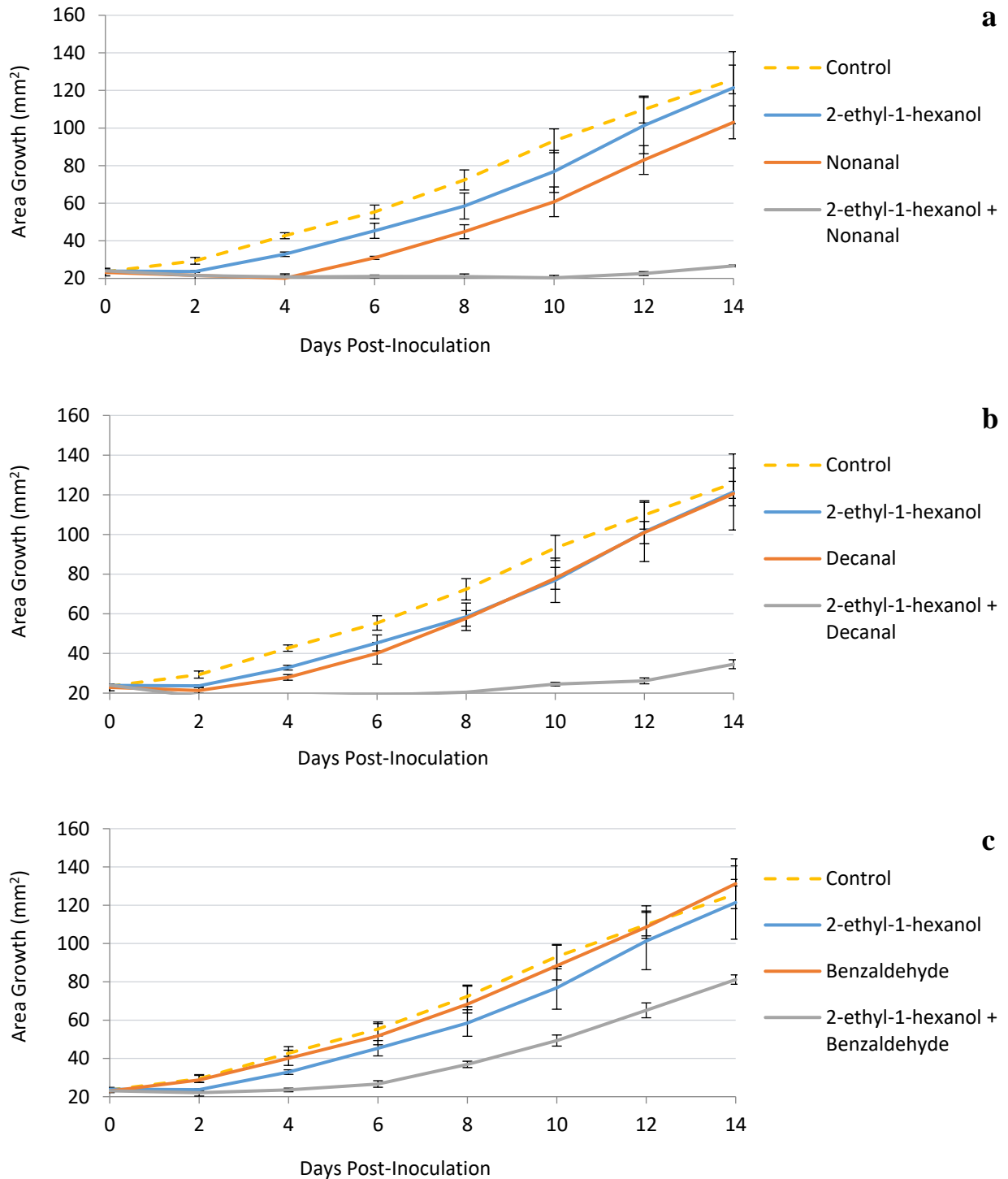


Figure 4.3 *Pseudogymnoascus destructans* area growth when exposed to 2 VOCs

A comparison of *Pseudogymnoascus destructans* mycelial growth while exposed to two pure VOCs and a formulation of those VOCs. All VOC and formulation exposures were 4 μmol (Cornelison et al., 2014).

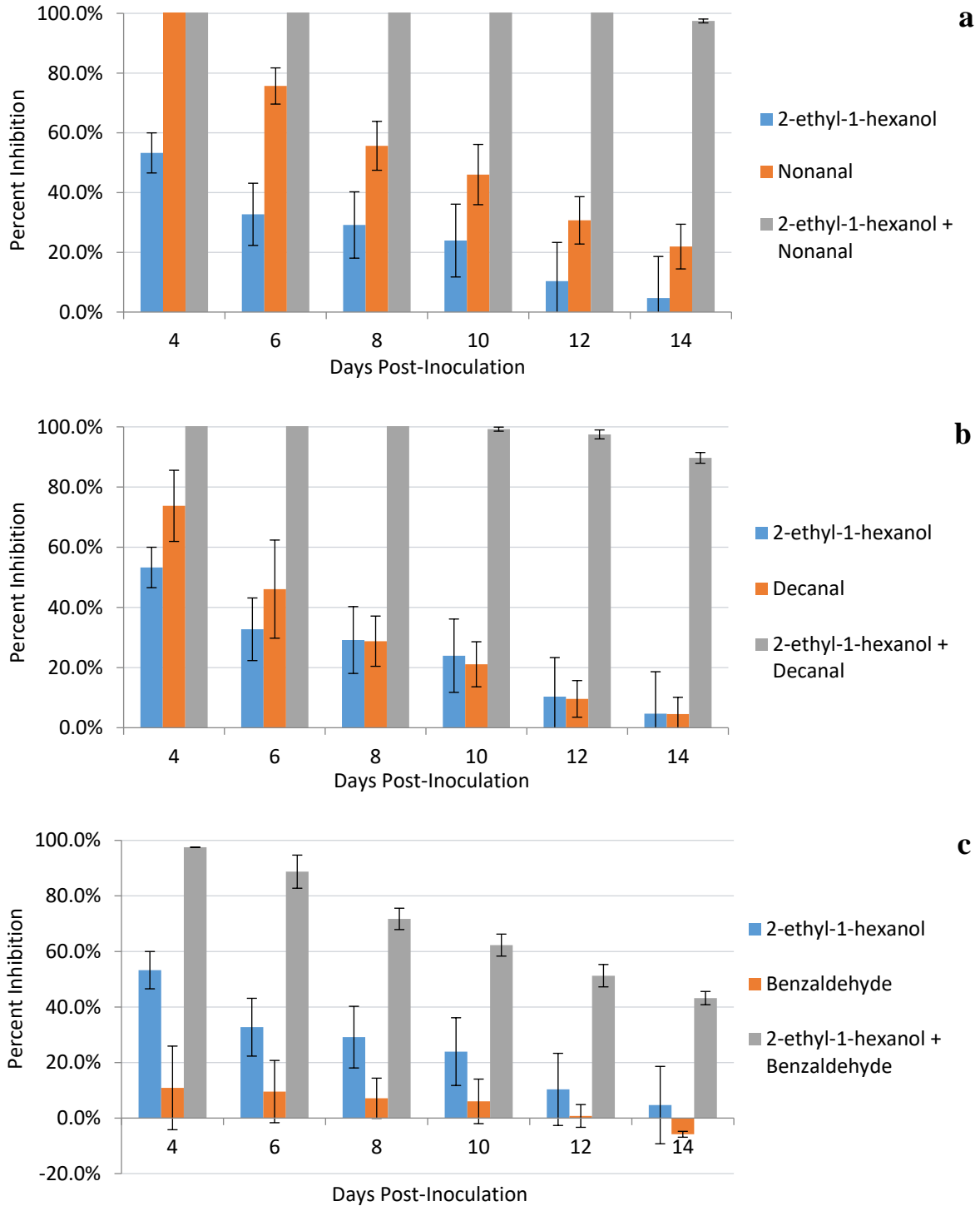


Figure 4.4 *Pseudogymnoascus destructans* inhibition when exposed to 2 VOCs

A comparison of *Pseudogymnoascus destructans* radial mycelial growth inhibition while exposed to two pure VOCs and a formulation of those VOCs. All VOC and formulation exposures were 4 μmol (Cornelison et al., 2014). Negative inhibition indicated stimulated growth.

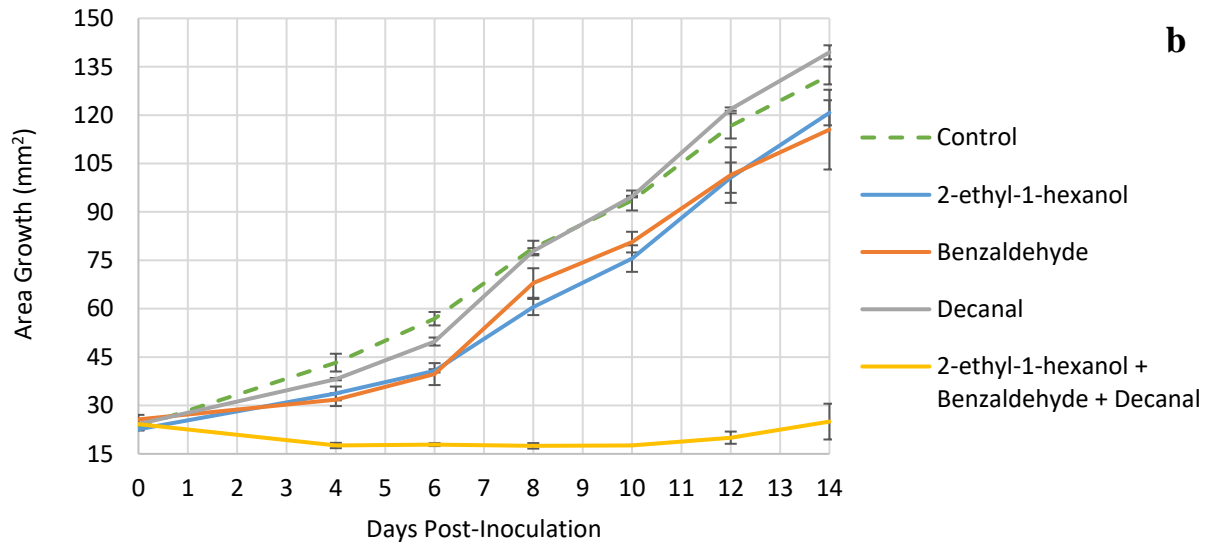
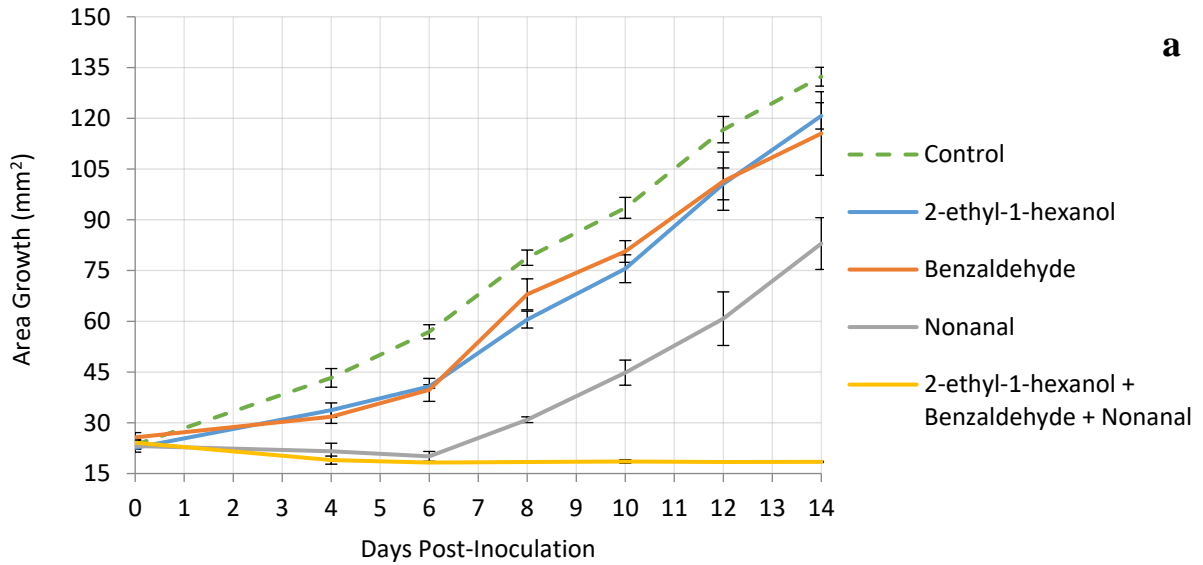


Figure 4.5 *Pseudogymnoascus destructans* area growth when exposed to 3 VOCs

A comparison of *Pseudogymnoascus destructans* mycelial growth while exposed to two pure VOCs and a formulation of those VOCs. All VOC and formulation exposures were 4 μmol (Cornelison et al., 2014).

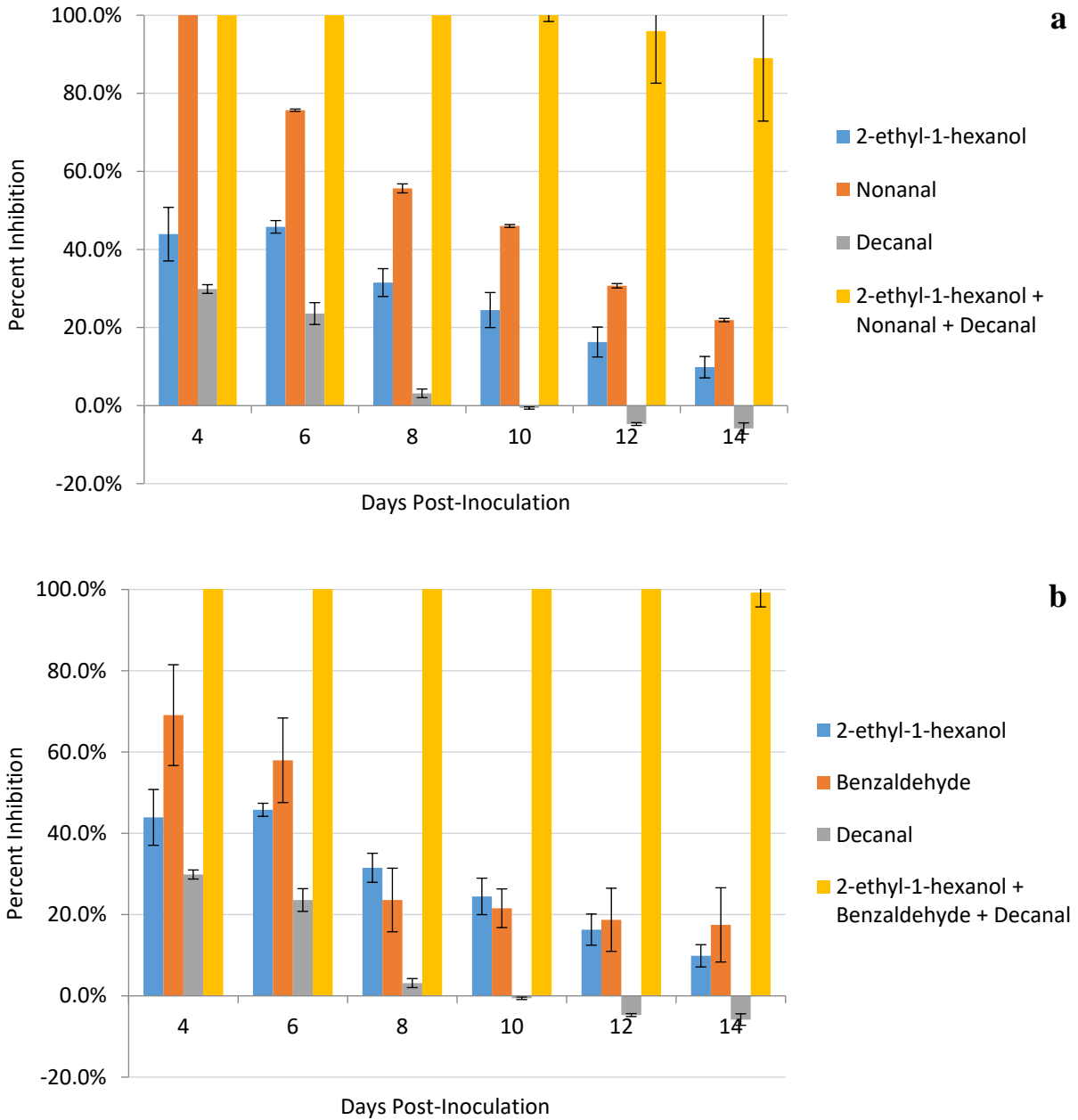


Figure 4.6 *Pseudogymnoascus destructans* inhibition when exposed to 3 VOCs

A comparison of *Pseudogymnoascus destructans* radial mycelial growth inhibition from exposure to three pure VOCs and a formulation of those VOCs. All VOC and formulation exposures were 4 μmol (Cornelison et al., 2014). Negative inhibition indicated stimulated growth.

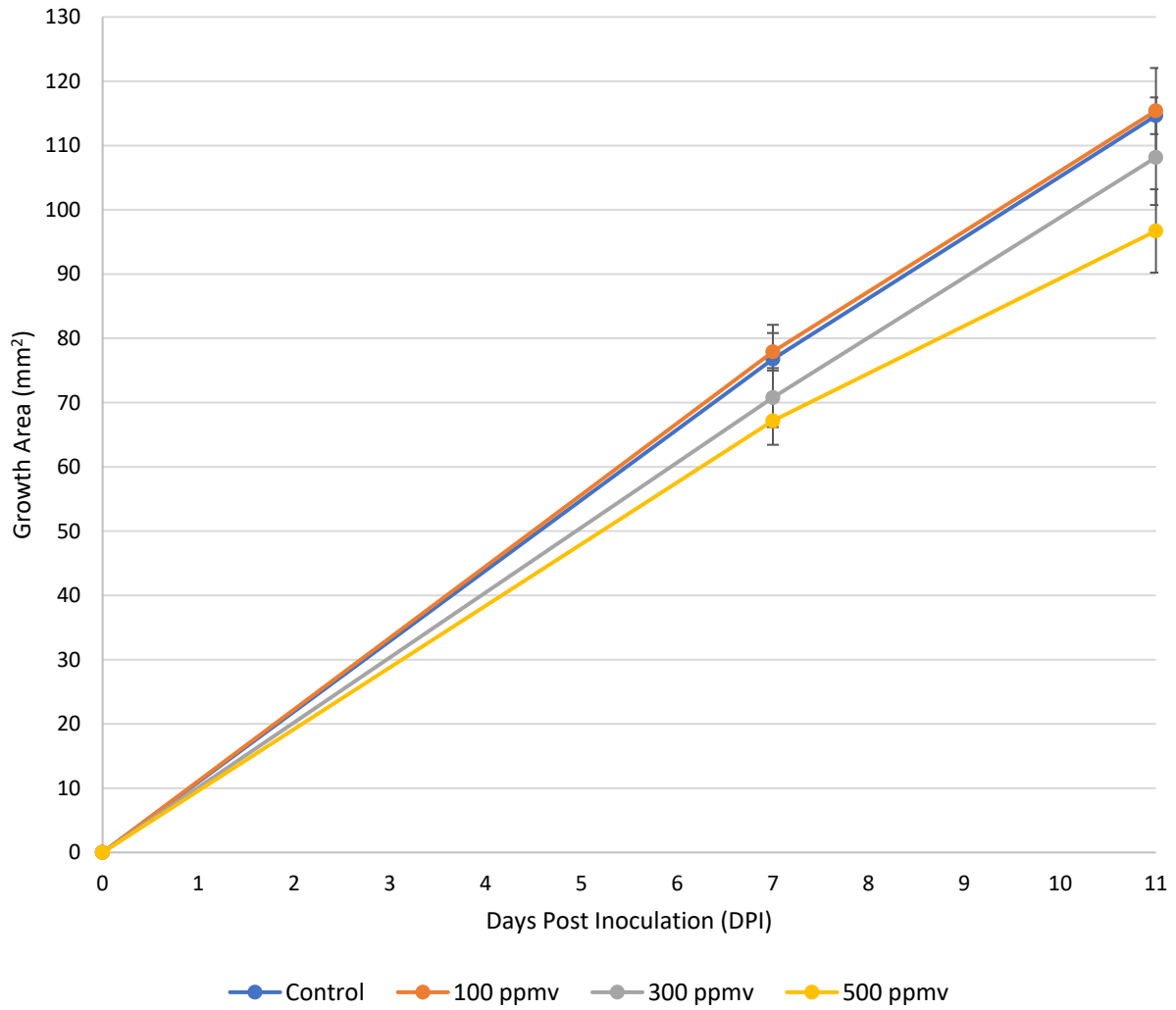


Figure 4.7 Pseudogymnoascus destructans growth area following exposure to B-23

A comparison of *Pseudogymnoascus destructans* mycelial growth following a 24-hour exposure to the B-23 formulation at different gaseous concentrations.

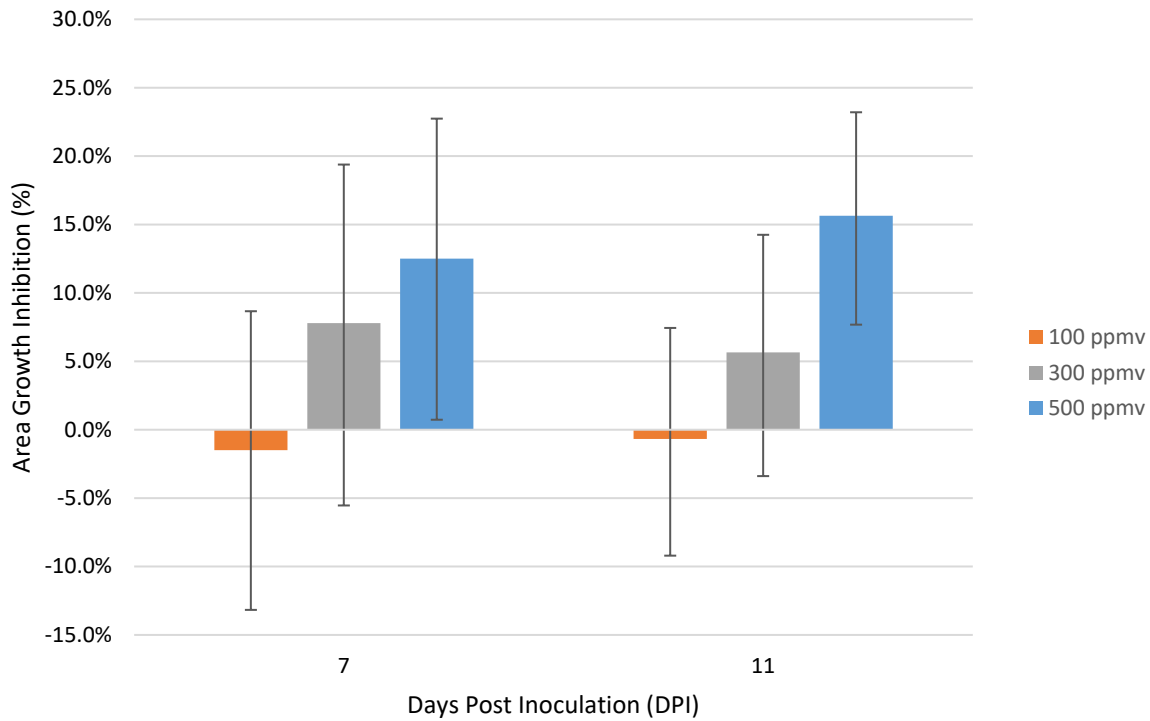


Figure 4.8 *Pseudogymnoascus destructans* inhibition following exposure to B-23

A comparison of *Pseudogymnoascus destructans* radial mycelial growth inhibition following a 24-hour exposure to the B-23 formulation at different gaseous concentrations.

4.2 Dispersal System Development

A summary of the key differences between each aerosolization technology can be found in Table 4.2. The size, cost, treatment area, and acoustic output differ greatly between these two technologies. As such, it is dependent upon the device technician, as well as any wildlife management officials, to determine which technology is most appropriate for use based on a number of factors, including the characteristics of formulation being used, the accessibility of the treatment location, the desired treatment area, the available budget, and the acceptable level of acoustic disturbance, among others.

Table 4.2 Summary of the differences between the jet nebulizer and rotary atomizer

	Jet Nebulizer	Rotary Atomizer
Droplet Size (diameter)	Extremely Small ($\leq 5 \mu\text{m}$)	Small ($\leq 20 \mu\text{m}$)
Dispersal Rate	Slow (20 ml hour^{-1})	Fast ($12,000 \text{ ml hour}^{-1}$)
Coverage Area	Small (2 kg)	Medium to Large (68 kg)
Acoustic Frequency Output	$\geq 200 \text{ kHz}$	$\leq 50 \text{ kHz}$
Physical Size	Small	Large
Cost	Inexpensive	Expensive

A summary of the major differences between the two different aerosolization technologies used in this study, a jet nebulizer and a rotary atomizer.

4.2.1 Dispersal Characterization

4.2.1.1 Jet Nebulizer

The Pari Trek S nebulizer relies on constant air pressure from a pneumatic pump to maintain a constant dispersal rate. Maintaining this pressure requires a constant voltage and current from the power supply. If power diminishes, the dispersal rate decreases, and if constant power cannot be supplied, such as during battery depletion, this needs to be compensated in some way to maintain accurate dispersal and reach the target concentration. This power compensation has been addressed in two ways.

The first method relies on providing an initial power duty cycle below 100%, and in the event of diminishing power, increasing the duty cycle to maintain output. Duty cycle is the percentage of time in which a signal or system is active. For instance, a 50% duty cycle would activate the nebulizer's pneumatic pump for an equal duration of time as it is off (50% of the time on, 50% of the time off). Typically, with electric motors, duty cycles are controlled by pulse

width modulation (PWM). PWM is a technique to rapidly switch the power on and off at a fast rate (typically hundreds of times per second). By controlling the duration of the on and off pulses by PWM, the amount of power output can be controlled without negatively affecting the performance of the motor. As a battery drains, the electrical voltage and current supplied to the pneumatic pump decrease, slowing the rotational speed of the motor shaft used to actuate the pump, resulting in a drop in output pressure. If the initial duty cycle of the pump is less than 100%, the duty cycle may be increased in order to compensate for diminished power and to maintain a constant output pressure. Because the initial duty cycle is less than 100%, this system will be required to run for a longer duration to attain the same dispersal amount as a system that begins with an initial duty cycle of 100%.

The second method relies on an initial power duty cycle of 100%, and the use of a sensor to measure the pump output pressure. With this method, the pump will experience an unavoidable but expected pressure drop as power diminishes, however, because the pneumatic pump's pressure is monitored with a sensor, the dispersal duration can be increased appropriately in order to attain the final target concentration.

Additionally, different compounds were discovered to disperse at different rates. Therefore, the dispersal rate for each compound used with the jet nebulizer was required to be empirically determined by performing a dispersal rate analysis. The results of two dispersal analyses are shown in Figure 4.9.

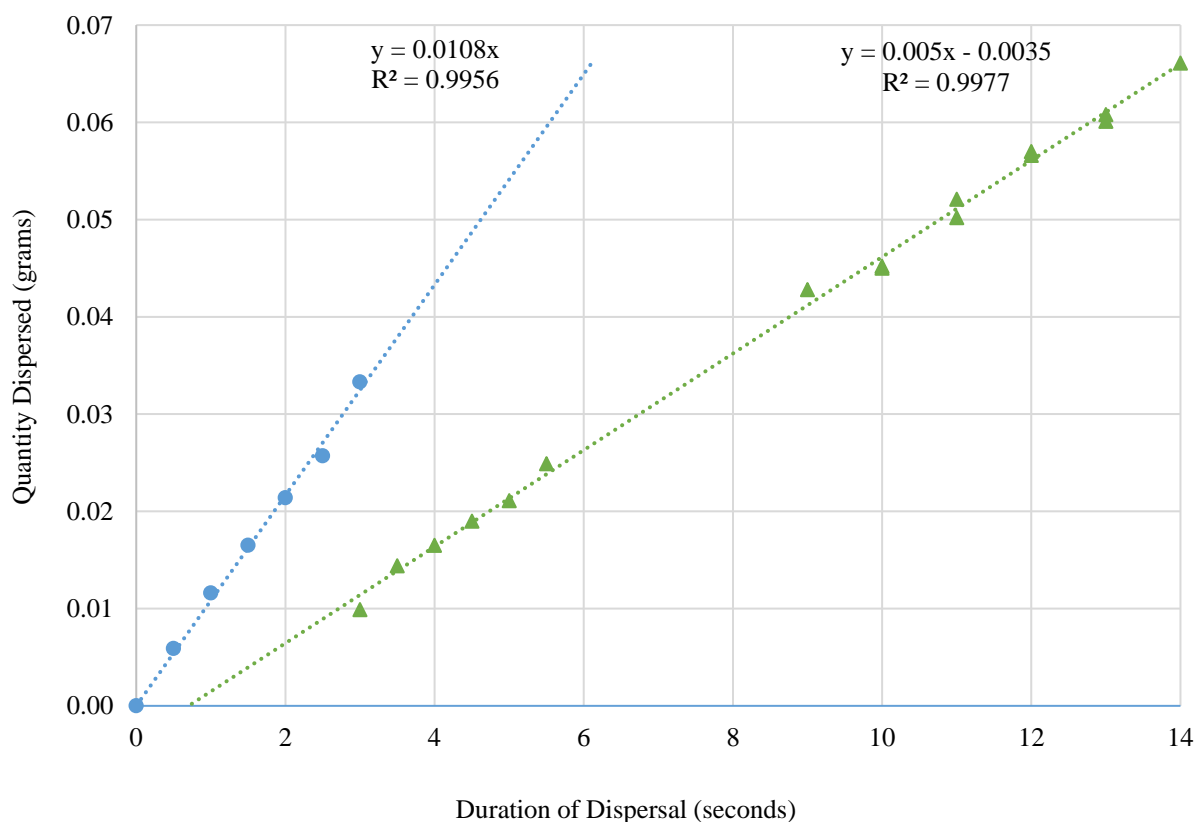


Figure 4.9 Dispersal rates of two compounds using a jet nebulizer

The dispersal rate of ethanol (blue) and a VOC formulation not containing ethanol (green).

4.2.1.2 Rotary Atomizer

The L-30 rotary atomizer utilizes a ceramic piston pump designed for precise fluid metering (flow rate). Flow rates were calibrated by adjusting the pump head position, changing the piston stroke length and, in turn, the fluid flow rate. Repeated analyses indicated a consistent flow rate, as verified by the manufacturer reproducible precision of 0.5% error (Fluid Metering Inc., New York, USA). Many of the difficulties encountered with attaining accurate dispersal rates with the nebulizer have been overcome by utilizing this technology, which maintains an accurate and consistent flow rate, despite differences in chemical composition or environmental

conditions. However, similar to the nebulizer, battery depletion may diminish the ability of the pump to maintain the target flow rate, necessitating compensation if an appropriate power source is not utilized.

4.2.2 High-Frequency Acoustic Output

Several distribution technologies were analyzed for their acoustic output. The three technologies tested include the Trek S pneumatic nebulizer, the Cyclone and Hurricane blower aerosolizers (Dyna-fog, Illinois, USA), and the L-30 rotary atomizer. There was considerable variance in both acoustic frequencies and amplitudes produced between each type (Figure 4.10). The Trek S produced considerably higher frequencies than any other device, due mainly to the design of the jet nozzle and high-pressure required to aerosolize the fluid. The Hurricane and Cyclone also produced high frequencies but were more consistent across the frequency spectrum and at a lower amplitude. The L-30 produced the smallest frequency range as well as the lowest amplitude of all devices tested.

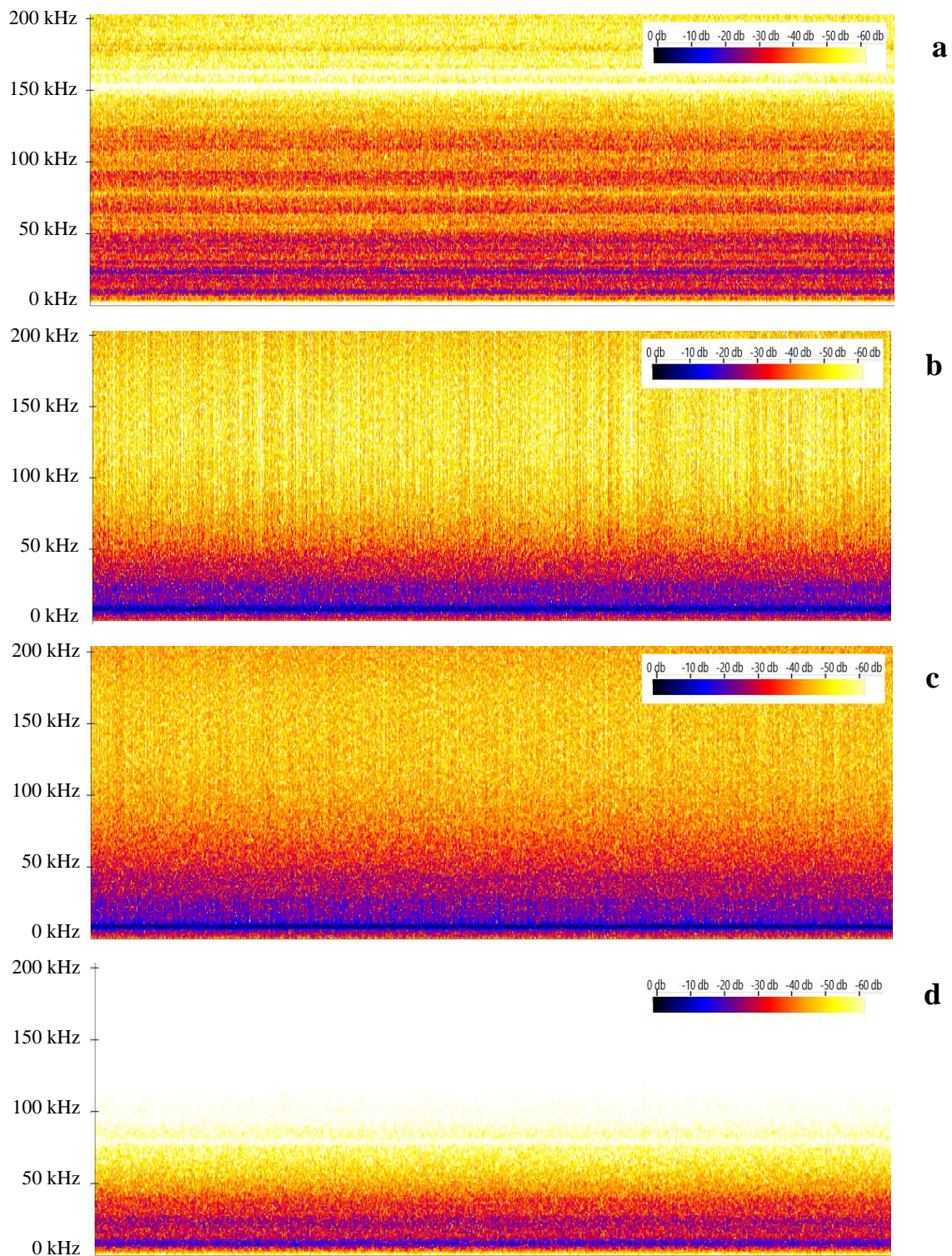


Figure 4.10 Spectrograms of audio samples acquired from several aerosolization technologies

Samples taken from the Pari Trek S (a), Dyna-fog Cyclone (b), Dyna-fog Hurricane (c), and Dyna-fog L-30 (d) aerosolizers, measuring 0 to 200 kHz, 0 to -65 db. Decibels scaled blue (0 db, loud) to yellow (-60 db, quiet), with white considered silent.

4.3 Standard Gaseous Concentration Curves

A standard curve was produced for a single, pure compound to become familiar with curve creation methodologies and GCMS method development, before developing a standard curve for the complex B-23 formulation. Toluene was selected to begin initial curve development, with two sampling methods used to compare the accuracy of each.

The curve produced using the gas-tight syringe sampling method produced high variability between successive measurements (Figure 4.11). The curve produced using the SPME fiber sampling method yielded less variability between successive measurements and produced a greater fit to a linear trend (Figure 4.12).

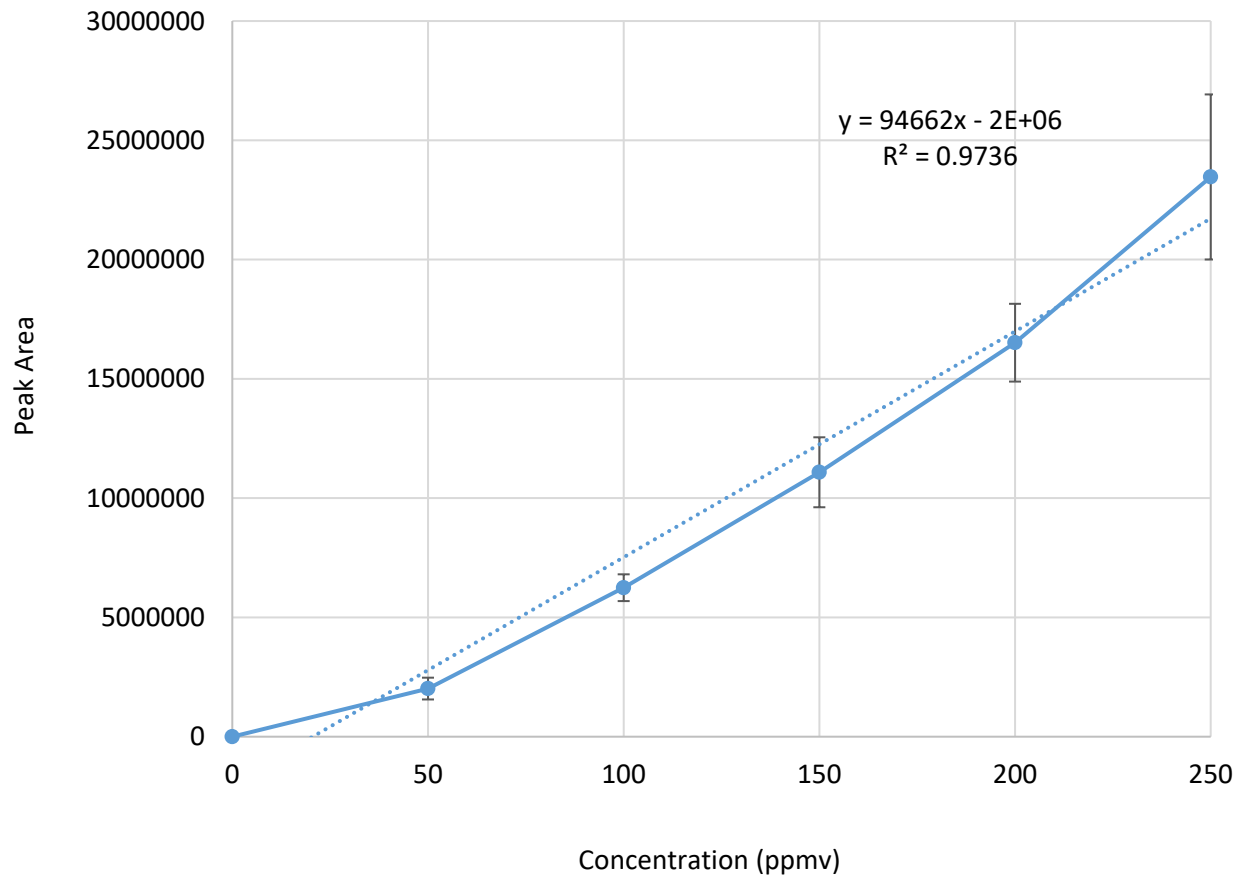


Figure 4.11 Standard curve of toluene using gas-tight syringe headspace sampling

A standard curve derived from the primary peak of a GC chromatogram of toluene, detected by GCMS-headspace analysis using gas-tight syringe headspace sampling and direct injection methods.

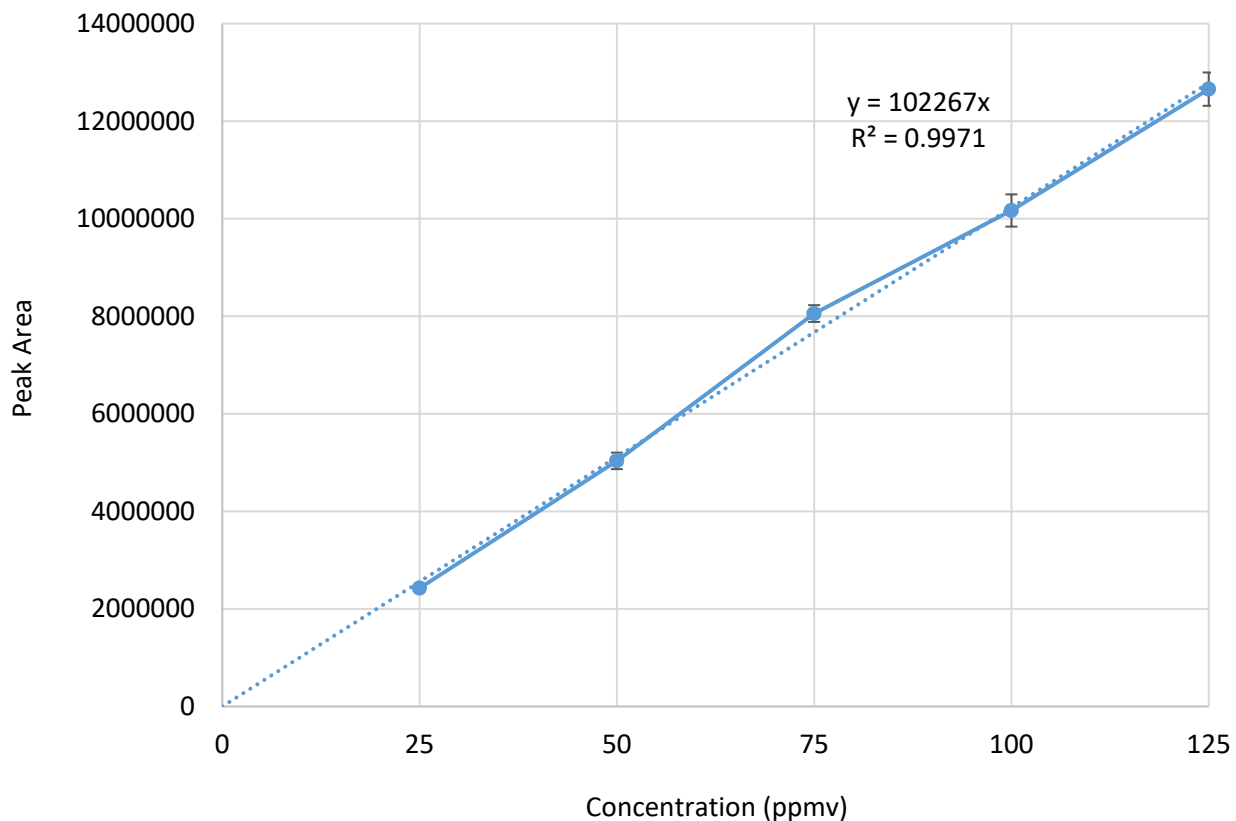


Figure 4.12 Standard curve of toluene using SPME headspace sampling

A standard curve derived from the primary peak of a GC chromatogram of toluene, detected by GCMS-headspace analysis using SPME headspace sampling and thermal desorption methods.

A standard curve of the B-23 formulation was produced from 100 ppmv to 500 ppmv, in 200 ppmv increments. Primary and secondary peaks of the chromatogram appeared at retention times of 8.3 minutes and 7.6 minutes, respectively (Figure 4.13). Manual peak selection was performed for the primary and secondary peaks of the formulation and the peak areas were calculated using MassHunter Qualitative Analysis. The average, standard deviation, and error was calculated for each set of trials and plotted to a graph (Figure 4.14).

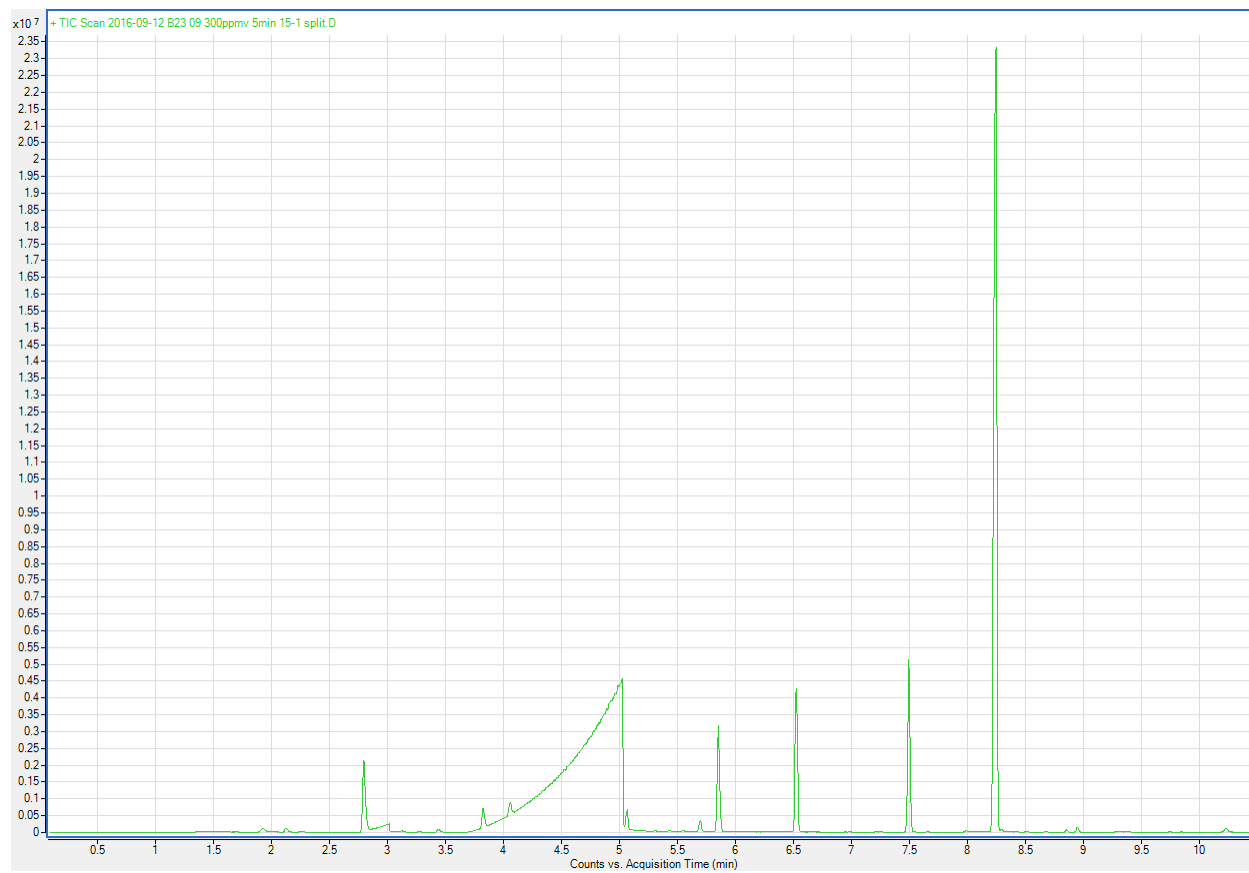


Figure 4.13 Chromatogram of the B-23 formulation

The first 10.5 minutes of the chromatogram produced by SPME desorption of the B-23 formulation. The primary peak had a retention time of 8.3 minutes and the secondary peak had a retention time of 7.6 minutes.

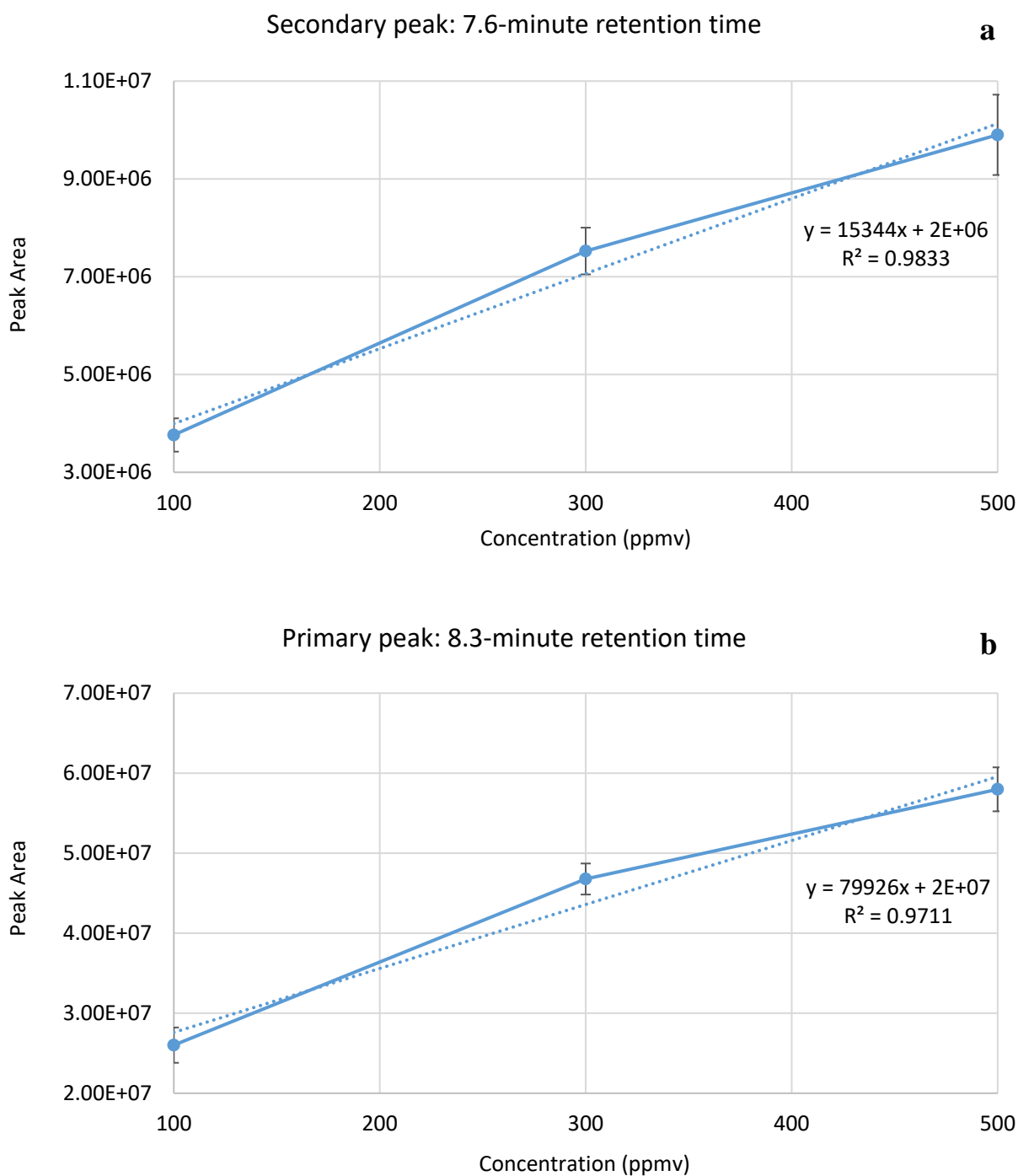


Figure 4.14 Standard curves of the primary and secondary peaks of the B-23 formulation

Standard curves derived from the primary (b) and secondary (a) peak areas of several incremental gaseous concentrations of B-23, detected by GCMS-headspace analysis.

4.4 Bat Toxicological and Histological Evaluation

A toxicological evaluation has been conducted with a prototype system utilizing the jet nebulizer, in which torpid tri-colored bats (*Perimyotis subflavus*) were exposed to an anti-*P. destructans* VOC formulation that demonstrated significant *in vitro* efficacy (Cornelison et al., 2014). Necropsies were conducted and described by Kevin Keel, DVM, and revealed neither acute nor chronic treatment groups exhibited significant negative toxicological effects when compared to controls (Tables 4.3 and 4.4). Ocular tissues, the respiratory tract, heart, liver, kidneys and skin were of particular interest for the toxicity assessment and were generally available for examination. Analysis of post-hibernation weight found that weight loss was greater within the test group than the control group.

Some degree of autolysis or putrefaction was evident in ten of the bats examined. Four of the samples (23, 25, 32 and 35) were affected severely enough to inhibit complete evaluation of the tissues. Two bats (5 and 32) had a mild conjunctivitis and surface bacteria were associated with the lesion of bat 32. Bat 27 had a mild acute keratitis in which neutrophils infiltrated the corneal stroma. The cause of the ocular inflammation was uncertain but was likely due to bacteria or a contact irritant. Two bats (13 and 17) had mild to moderate accumulations of neutrophils in the airway epithelium and in the lumen of bronchioles, bronchi, and/or trachea; however, microorganisms were not evident. This lesion could have been due to a respiratory irritant, but the absence of a visible pathogen is not enough to rule out a viral or bacterial etiology. Three bats (6, 9 and 34) had an acute interstitial pneumonia. As with the bronchitis/tracheitis, no bacteria were evident, therefore the etiology was uncertain.

The epithelium of the trachea and large airways, in nearly all samples, had some degree of cytoplasmic rarefaction or swelling. This could have been a postmortem artifact but it was not

clearly correlated with the degree of autolysis. The change was most significant in sample 9. Sample 33 had minimal cytoplasmic changes. If it was real, it could have been due to the excessive accumulation of fluid in the epithelial cells.

Many of the animals had peracute hemorrhage or edema of the lungs. This may have been due to euthanasia. One bat (18) had abundant blood within the GI tract and some of this appeared to have been digested. The source of the blood was not identified, but its appearance suggested swallowing of blood some time before death or hemorrhage into the anterior portion of the gastrointestinal tract.

The superficial keratinized layers of the skin on the patagium were generally elevated in the bats. This was not correlated with autolysis of other tissues and it may have been a normal postmortem change, or it may have occurred due to high humidity and softening of the tissue. One bat (14) had small fungal elements in hair follicles of the muzzle, which were most consistent with dermatophytosis.

Four bats had mild to moderate coccidiosis (possibly *Eimeria* sp.), but these were not associated with significant inflammation. One bat (17) had mild, acute, superficial, segmental enteritis with adherent bacteria. The etiology was uncertain, but the changes suggested bacterial enteritis. Three bats (16, 24 and 34) had mild acute colitis of unknown etiology. Two additional bats (18 and 29) had mild acute colitis, and the inflammatory infiltrates were intimately associated with large fungal hyphae or cystic structures in the mucosal epithelium or lamina propria. Some of the cystic structures directly gave rise to the fungal hyphae.

The pancreatitis in bat 30 was very unusual but was probably incidental to any of the treatments, as this was the only observed case. The other lesions listed were also considered

incidental. Most lesions (e.g. trematodiasis, coccidiosis) were probably reflective of the source population.

Table 4.3 Tissues examined from each bat

Group	Exposure	Bat	Brain	Heart	Eye	Trachea	Lung	Lymph n	Thymus	Spleen	Muzzle	Patagium	Liver	Pancreas	Stomach	Small intestine	Large intestine	White fat	Brown fat	Urinary bladder	Bone marrow	Sk muscle	Kidney	Esophagus	Adrenal gland	Testes	
Acute Group (8-day)	VOCs	1		y		y	y					y	y	y		y	y	y	y			y					
		2		y			y	y					y	y	y		y	y	y	y	y		y	y	y		
		3		y	y		y				y		y	y			y		y	y						y	
		4		y			y	y			y		y	y	y	y	y	y					y				
		5		y	y	y	y	y	y				y	y	y		y	y	y	y				y	y	y	y
		6		y			y	y	y				y	y	y		y	y	y	y	y	y		y	y	y	
	No VOCs	7		y			y	y					y	y	y		y		y	y	y		y	y	y		
		8		y			y	y					y	y	y	y			y	y	y		y	y	y		
		9		y			y	y					y	y	y	y			y	y	y		y	y	y		
		10					y	y	y				y	y	y			y	y	y				y			
		11			y		y	y	y				y	y	y	y	y	y	y	y	y		y	y	y	y	y
		12			y			y	y				y	y	y		y		y	y	y	y		y	y		
Chronic Group (40-day)	VOCs	13	y	y		y	y				y	y	y	y	y	y		y	y								
		14	y	y	y	y	y					y	y	y		y	y	y	y	y		y	y	y			
		15	y	y			y	y					y	y	y		y	y	y	y	y	y	y	y	y		
		16	y	y	y		y	y			y	y	y	y	y	y	y	y	y	y			y	y			
		17	y	y	y	y	y	y				y	y	y	y	y	y	y	y	y				y			
		18	y	y	y		y	y			y	y	y	y	y	y	y	y	y	y				y	y		
	No VOCs	19	y	y			y	y		y			y	y	y	y	y	y		y				y			
		20	y				y	y	y				y	y	y		y		y	y				y	y		
		21	y	y	y		y						y	y		y	y	y	y	y		y	y	y			
		22	y	y	y		y						y	y	y	y	y	y		y		y	y	y			
		23	y	y			y						y	y	y		y	y		y				y			
		24	y		y		y				y	y	y	y	y		y	y	y					y			
Chronic, Post-Hibernation Group	VOCs	25	y	y		y	y						y			y								y			
		26	y	y	y	y	y	y		y	y					y	y	y	y	y			y	y	y	y	
		27	y	y	y	y	y	y	y	y			y	y	y	y	y	y	y	y	y	y		y	y	y	y
		28		y	y	y	y	y	y	y	y	y	y	y	y	y	y	y	y	y				y	y	y	
		29	y	y	y			y					y	y	y		y	y						y			y
		30		y			y	y			y		y	y	y	y	y	y	y	y		y	y	y			
	No VOCs	31	y		y	y	y	y					y	y	y		y	y	y	y				y			
		32	y	y	y	y	y	y					y	y	y	y	y	y						y	y		
		33	y	y	y	y	y	y					y	y	y	y	y	y	y	y				y	y	y	
		34		y			y	y					y	y	y	y	y	y	y	y			y	y	y	y	y
		35	y	y	y	y	y						y	y	y	y	y	y	y	y		y		y	y	y	
		36	y		y			y	y		y	y	y	y	y		y		y	y				y			

This table identifies the test group each bat belonged to as well as the specific tissues examined for each bat. Produced by Kevin Keel, DVM.

4.5 Treatment at Black Diamond Tunnel

Laser measurements were obtained for the height and width of the tunnel at several points while traversing the length of Black Diamond Tunnel on a boat (Figure 4.15). Due to the variability of boat movement speed, distances between measurements were unable to be accurately determined, therefore volume calculations were conducted with the assumption that measurements were at evenly spaced intervals. Three methods were used to calculate the air volume in the tunnel: segments of the raw data (Figure 4.15), segments from linear trends of the raw data (Figure 4.16), and segments from 3^o polynomial trends of the raw data (Figure 4.17). The Airspace volumes calculated, including averages and standard deviations, are in Table 4.5.

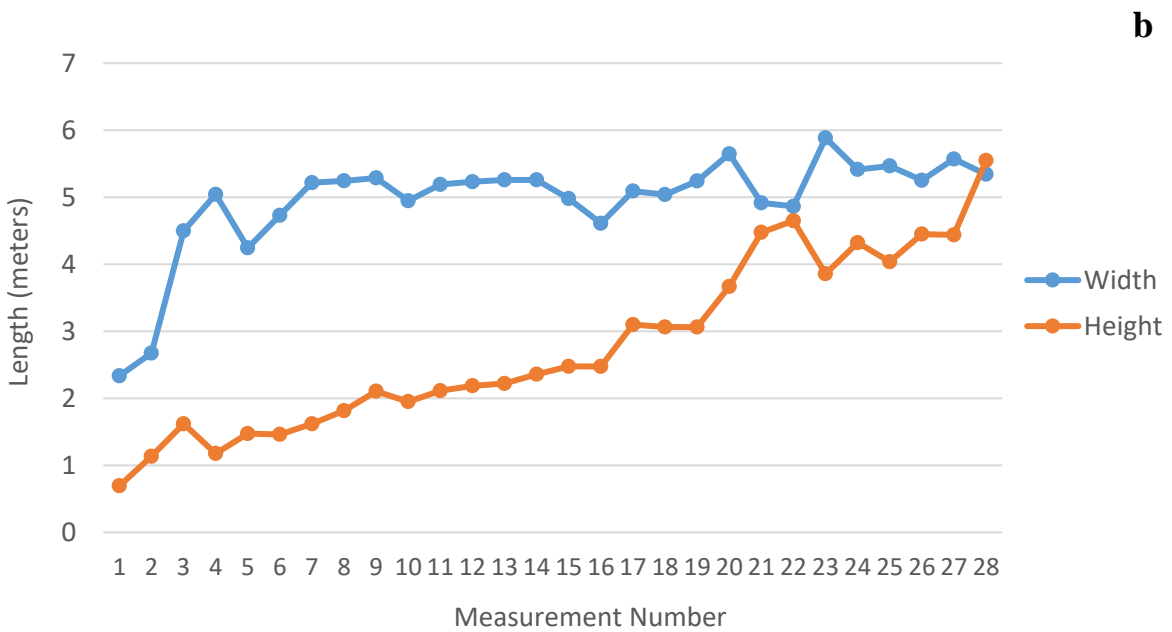
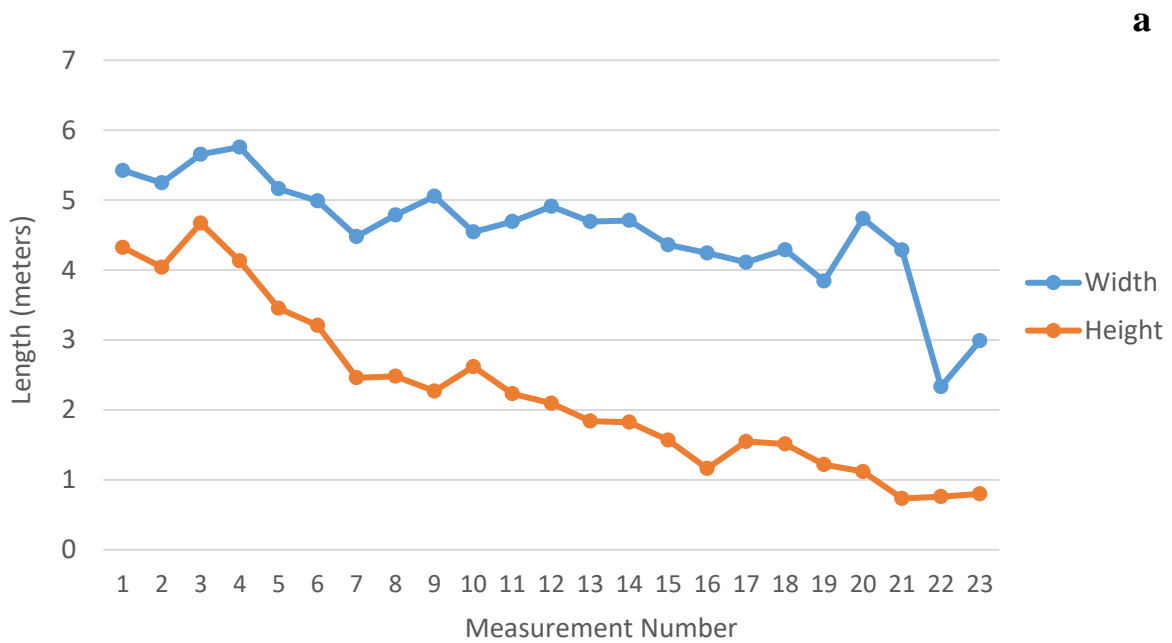


Figure 4.15 Two sets of the dimensional measurements of Black Diamond Tunnel

Two sets of measurements were obtained with a digital laser measurer of the height and width of Black Diamond Tunnel while traversing from the entrance to the end (a) and from the end to the entrance (b). Effort was made to take measurements at consistent intervals.

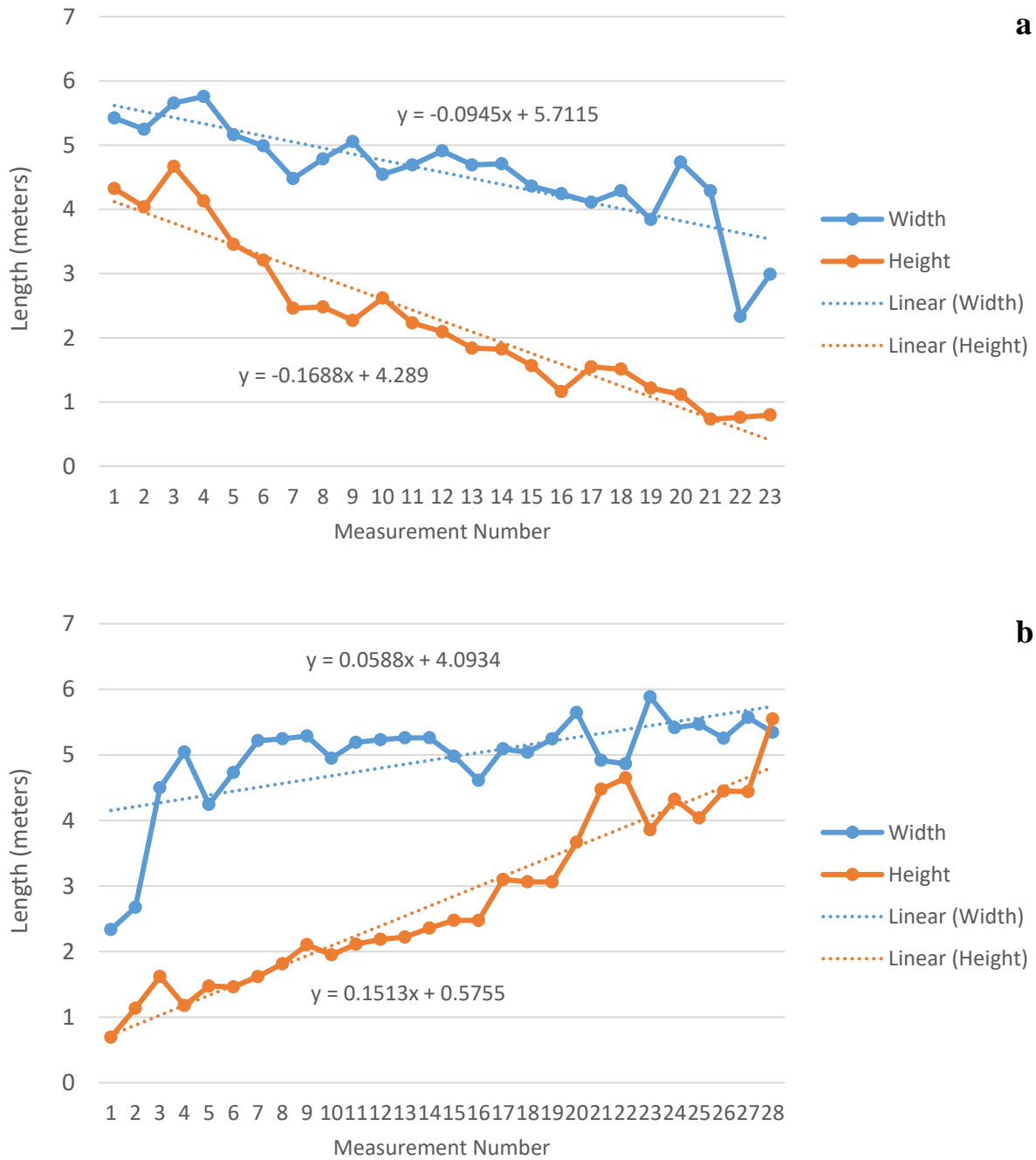


Figure 4.16 Linear trend of the dimensional measurements of Black Diamond Tunnel

A linear trend was calculated for the height and width measurements from the entrance to the end (a) and from the end to the entrance (b), to produce a best-fit line for calculating the estimated volume of the tunnel.

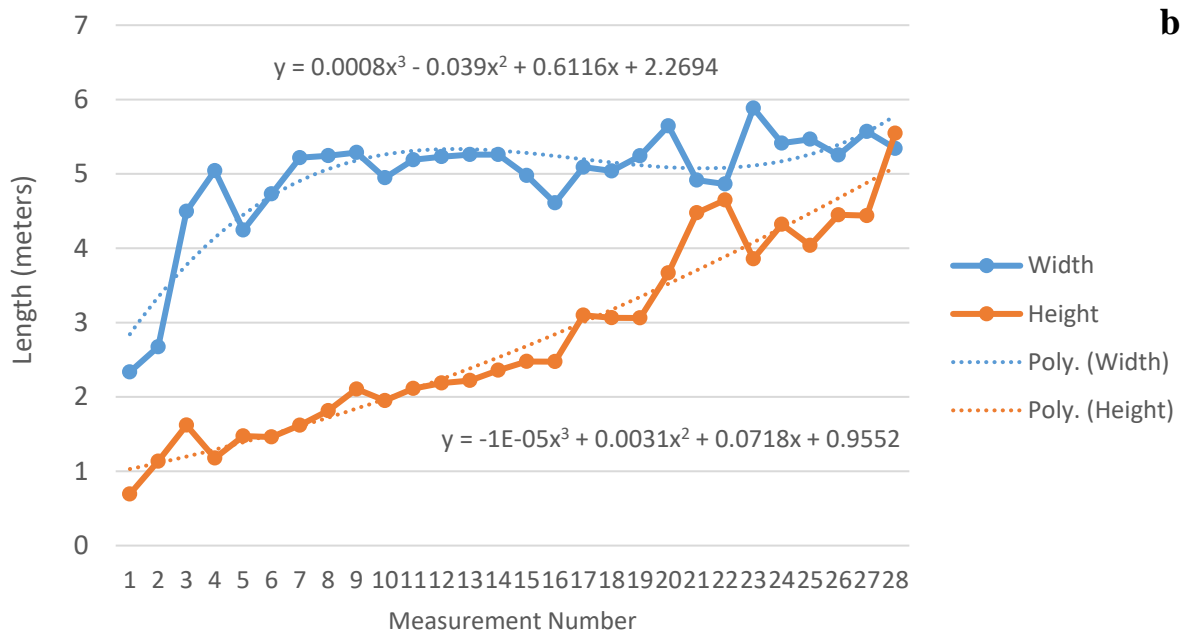
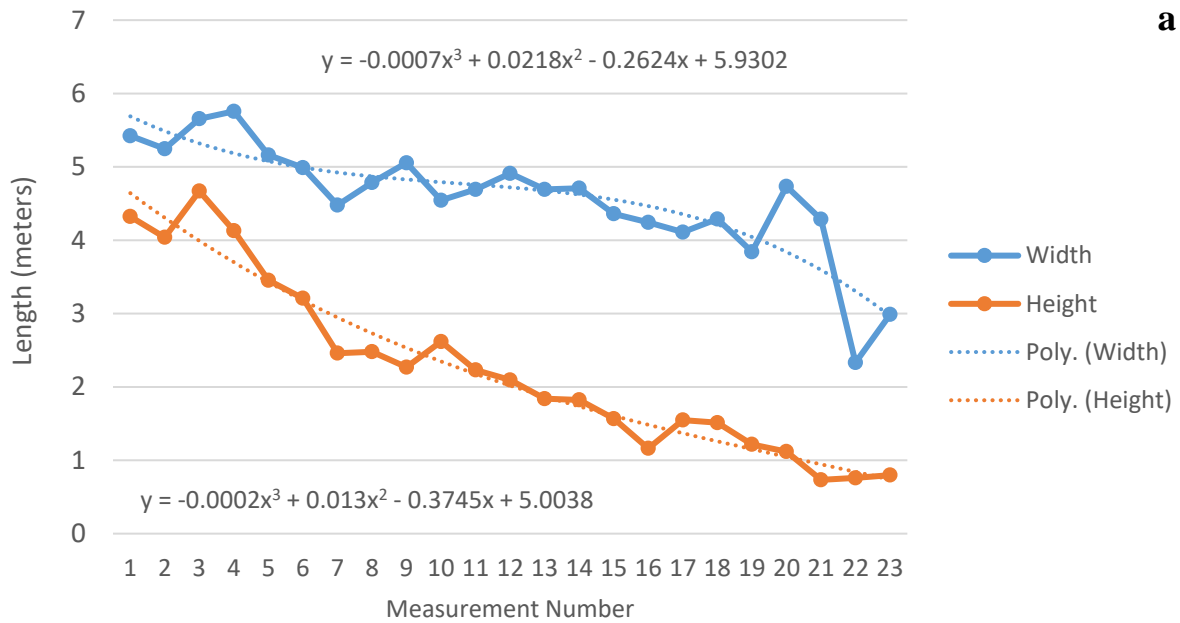


Figure 4.17 Polynomial trend of the dimensional measurements of Black Diamond Tunnel

A third degree polynomial trend was calculated for the height and width measurements from the entrance to the end (a) and from the end to the entrance (b), to produce a best-fit line for calculating the estimated volume of the tunnel.

Table 4.5 Area calculation of Black Diamond Tunnel using three calculation methods

Calculation Method	Entrance to End	End to Entrance	Average	Standard Deviation	Minimum	Maximum
Segments	4657	6007	5332	955	4377	6287
Linear Trend	5207	6490	5849	907	4942	6756
Polynomial Trend	4615	7361	5988	1942	4046	7930

Three calculation methods were employed to determine the volume of Black Diamond Tunnel, using two data sets (*Entrance to End* and *End to Entrance*). The average, standard deviation, minimum, and maximum volumes were calculated with each of these methods using both data sets. All values are volumes, represented in cubic meters (m³).

An initial bat population survey on November 4, 2016, prior to the first treatment, yielded 206 tri-colored bats. During the November 4 treatment, no bats were observed arousing or leaving the tunnel. B-23 was undetectable by GCMS in post-treatment water samples. Analysis of air samples obtained 1-hour post-treatment yielded several chromatographic peaks that were in agreement with the 300-ppmv gas standard (Figure 4.18); however, concentration varied. GCMS analysis of the 7-day post-treatment air samples did not detect any compound of the B-23 formulation.

Prior to the second treatment on December 2, 2016, a bat population survey was conducted that yielded a count of 216 tri-colored bats. Additionally, all bats appeared healthy, with no visual symptoms of WNS present at that time. It was also observed that many of the bats were roosting toward the rear of the tunnel. This second treatment was also conducted without observing any bat arousal or aversion, either during or after treatment. Air and water sample analyses were similar to the samples following the first treatment. A bat population count was not obtained prior to the January 6, 2017 treatment, but air and water samples were acquired, with GCMS analyses yielding similar results to prior treatments.

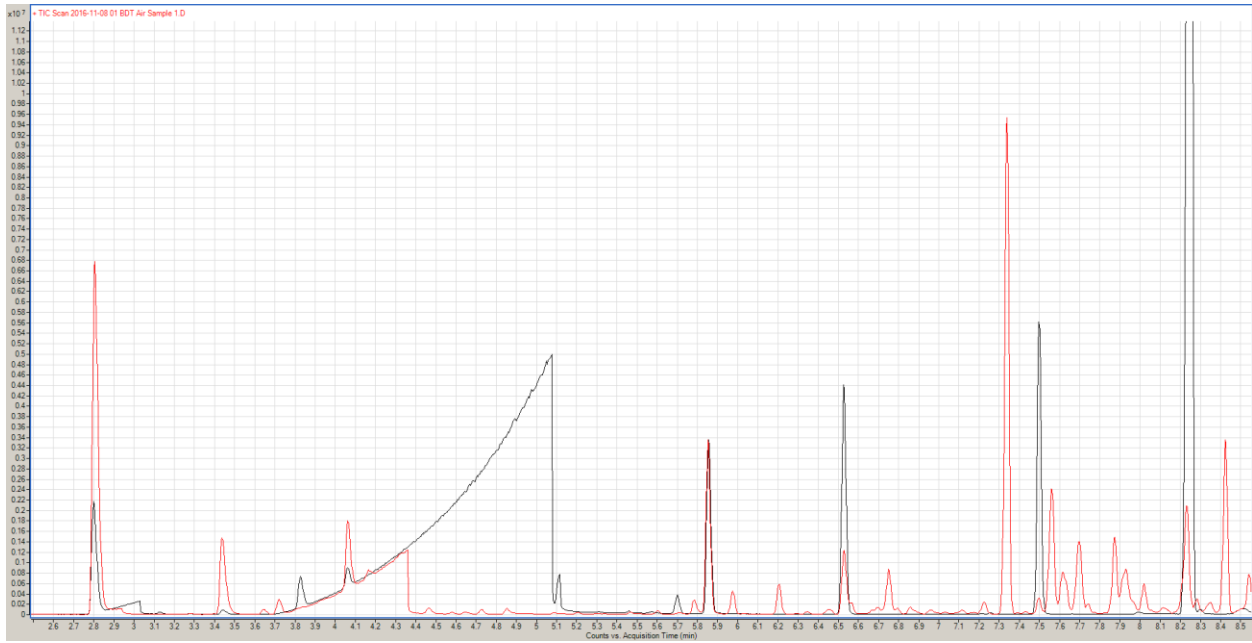


Figure 4.18 Chromatograms of a gaseous standard (black) and post-treatment at BDT (red)

Air samples following treatment at Black Diamond Tunnel were analyzed with a GCMS to yield a chromatogram (red) that was compared to the chromatogram of a 300-ppmv gaseous standard of B-23 (black).

A bat population survey was conducted February 28, 2017, which yielded a count of 152 bats. It was also noted that the majority of bats were roosting further back into the tunnel and, of the bats that were there, did not appear to present severe symptoms of infection. The most current population statistics for the past 8 years at Black Diamond Tunnel is illustrated in Figure 4.19.

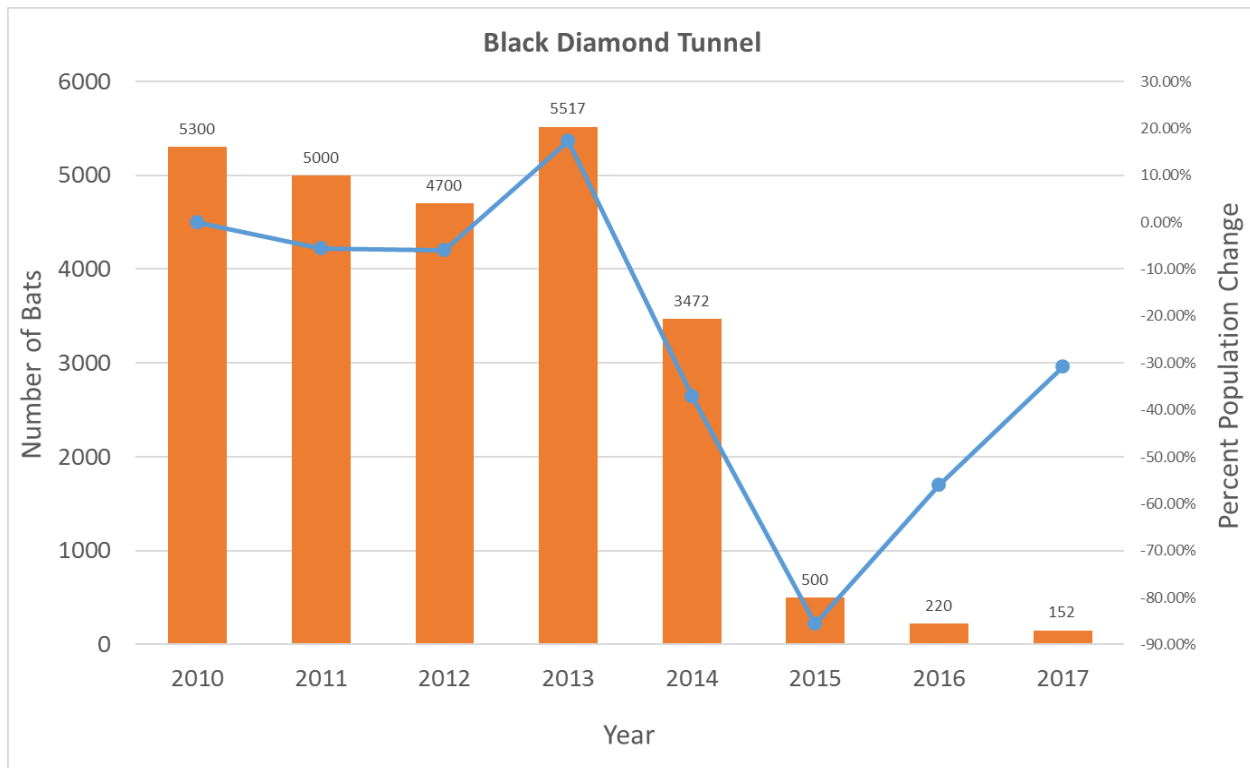


Figure 4.19 Tri-colored bat population counts at Black Diamond Tunnel from 2010 to 2017

Population change at Black Diamond Tunnel, with population counts in orange (left axis) and percent change from the previous year in blue (right axis).

5 CONCLUSIONS

5.1 Post-harvest Loss Due to Fungal Decay

Fungal decay of fruits and vegetables accounts for a significant portion of post-harvest losses worldwide (Tripathi and Dubey, 2004; Parfitt et al., 2010). Although the degree to which post-harvest disease and spoilage by microorganisms contribute to global food waste has been difficult to accurately quantify, it is largely agreed that reducing these losses and increasing shelf-life is essential to preserving our food supplies for current and future generations (Parfitt et al., 2010).

The use of chemical fungicides is currently the most common method for controlling post-harvest fungal disease and contamination. However, two major concerns exist with the use of these fungicides: residues that may negatively affect the environment and human health, and the development of resistance by the pathogen. These concerns have prompted many to seek alternatives to this method of treatment, with several areas of research emerging with alternative strategies for managing fungal contamination and disease.

The use of antagonistic microorganisms has shown great potential for controlling disease and spoilage (Wilson et al., 1991; Weiskopf, 2013). Another emerging treatment method has been to strengthen the host defense mechanisms with the use of chemical compounds that induce or stimulate disease resistance in the host (Yao and Tian, 2005; Weiskopf, 2013). The use of these biologically-active natural products has begun to receive attention as a viable alternative to current synthetic fungicides because of their low toxicity (Wilson et al., 1991; Tripathi and Dubey, 2004; Weiskopf, 2013). These methods are very promising for enhancing food preservation and the more we understand about these complex interactions, the better we will be to develop solutions to disease, spoilage, and contamination.

5.2 Antifungal Volatile Organic Compounds

The use of biologically-derived VOCs has been shown to have great potential for both controlling microbial growth and stimulating natural plant defense mechanisms. The coevolution of soil microbiota, plant-associated endophytes, and fungal pathogens have produced mechanisms ideally suited for the complex ecology of their environments. The long-term efficacy of low quantities of VOCs suggests the potential of these compounds for *in situ* application in the treatment and suppression of fungal food spoilage and disease (Cornelison et

al., 2013). Additionally, the development of synergistic formulations supports a theory of soil-based fungistasis as a source of potential control agents, as VOC mixtures are likely responsible for the observed fungistatic activity of many suppressive soils. The evaluation of microbially-derived VOCs has expanded the pool of potential control agents and has led to the production of several patentable VOC formulations with significant anti-*P. destructans* activity (Cornelison et al., 2013, Gabriel and Cornelison, 2014). The availability of volatile formulations for control of *P. destructans* growth could prove to be a powerful tool for wildlife management agencies, if effective application methods can be established.

The typical low level of antimicrobial VOCs produced in natural hosts and the significant antagonistic activity observed at these low levels is promising. The contact-independent activity of antagonistic VOCs has several advantages over topical and oral, contact-dependent, treatment options that have been shown to be effective at inhibiting the growth of pathogens. Contact-independent antagonism allows for the potential treatment of many individuals with a single application and facilitates uniform exposure, reducing the potential for unaffected microbial refugia on the host that may facilitate re-colonization once the inhibitory compound has been removed or degraded.

Interestingly, several compounds that stimulated *P. destructans* growth when exposed singly were found to synergistically inhibit growth when used as a component of a formulation, avowing to the unpredictability of VOC formulation development. Also worth noting, is as more compounds are added to the testing pool, the number of possible combinations to produce a formulation increase dramatically (Table 5.1). Furthermore, there are several challenges to developing antimicrobial susceptibility assays when moving from traditional media-based methods to gaseous headspace methods. Therefore, formulation development is often both

laborious and unpredictable, requiring extended periods of time to set up each assay and necessitating the testing of every possible combination to discover synergistic inhibitory formulations. It may be beneficial for future investigations to seek to streamline the methodologies of these assays in order to increase the speed of the formulation screening process.

Table 5.1 Combinations of several compounds in formulations of two and three compounds

# of compounds	Formulations with 2 compounds	Formulations with 3 compounds
4	12	24
6	30	120
8	56	336
10	90	720
12	132	1320
14	182	2184
16	240	3360

The contact-independent activity of antagonistic VOCs has several advantages over topical and oral, contact-dependent, treatment options that have been shown to be effective at inhibiting the growth of *P. destructans* in previous studies (Hoyt et al. 2015). The typical low level of antimicrobial VOCs produced in natural hosts and the significant antagonistic activity observed at these low levels is promising.

5.3 Novel Fungal Management Strategies

In order to develop an effective disease management strategy, concurrent development of both a treatment formulation and a dispersal system was pursued. Several microbially-produced

VOCs were identified from the scientific literature for their antifungal activities, and tested singly and in combinations at various ratios and concentrations. Two *in vitro* methods were used to assess the degree of inhibition caused by gaseous VOCs. The first entailed pipetting aliquots of a VOC or formulation on an absorbent disc, then sealing the disc in a Petri dish with freshly-inoculated spores or mycelial plugs. The second entailed using a sealed glove box to raise the headspace concentration by evaporating the VOC or formulation on a hot plate, then sealing a glass jar with Petri dishes of freshly-inoculated spores or mycelial plugs from within the glove box. This first method was unable to verify the exact gaseous concentration of the exposure, as the degree of evaporation was unknown without quantitative analysis. However, the second method permitted the exact gaseous concentration to be established at the time of exposure and is thought to better represent an exposure typical of a field treatment trial.

An international PCT patent application was submitted by Georgia State University in 2014, detailing three effective anti-*P. destructans* VOC formulations and a VOC dispersal system for eliciting microbial control (Gabriel and Cornelison, 2014).

5.4 Wildlife Disease Management

The most effective VOC formulation from the *in vitro* studies was used in an *ex situ* study with a prototype dispersal device and live bats to determine any negative toxicological effects the VOCs may elicit at concentrations likely to be used during treatment. This trial yielded no significant toxicological effects and led the way to begin an *ex situ* infectivity and treatment trial with live bats. However, this trial was prematurely canceled due to a lack of adequate animal facility management, invalidating all data obtained during the trial.

Although several VOC formulations demonstrated significant synergistic inhibitory activity, the potential mammalian toxicity and non-GRAS status of several VOCs was a significant factor in the decision to pursue experimental treatment with the use of the B-23 formulation as a treatment agent. This permitted bypassing toxicological evaluations because mammalian safety was already established. To this end, the B-23 formulation was tested against *P. destructans* to determine the minimum inhibitory concentration and effective dose. Significant inhibition was observed with as little as 24-hour exposure of B-23 at 300 ppmv. Various treatment regimens and potential toxicological effects were then explored for this dose. As it cannot be assumed that 100% volatilization would occur following aerosolization from the treatment device, the evaporative efficiency and environmental fate of B-23 was assessed by analyzing air and water samples obtained during field trials at Black Diamond Tunnel, during the winter treatment trials of 2016/17.

5.5 Treatment at Black Diamond Tunnel

Although there are not enough data to make any strong conclusions as to whether the three treatments during the winter of 2016/17 at Black Diamond Tunnel were effective at reducing bat mortality, there were several observations that appear promising. During all three treatments, there were no bats observed arousing and flying or leaving the tunnel, indicating the dispersal of the treatment formulation, the operation of the L-30, or the use of the capstan winch were not significantly disruptive to cause bats to arouse or fly from the tunnel. Furthermore, the second bat survey, 1 month after the first treatment, yielded 216 bats. Observing 10 more bats than were present preceding the first treatment further strengthens the theory that the bats at this site were

not demonstrating an aversion to the B-23 formulation or the methods employed to conduct treatment.

No compounds of the B-23 formulation were detectible from any 1-week post-treatment water or air samples. Air samples obtained 1-hour post-treatment yielded detectible compounds of the B-23 formulation, with several chromatographic peaks having indicated similar, higher, and lower concentrations of specific compounds, when compared to a 300 ppmv gas standard. This indicated environmental factors at Black Diamond Tunnel might affect air movement dynamics, volatility, and gaseous homogeneity, among other factors. Additionally, only having one air sample inlet and placing that inlet near the water level likely contributed to the variability of concentrations observed. Future sampling may benefit from including air samples from multiple heights within the tunnel, in order to gain a broader understanding of the gaseous dynamics in this environment following treatment.

On February 28, 2017, a bat survey was conducted at Black Diamond Tunnel, yielding 152 individuals. When the data becomes available, this population count will be compared to surveys from other hibernacula in the area to determine if there were any significant differences in population dynamics and survivorship that may be attributed to treatment initiatives. Pending no significant negative results, treatments will continue be conducted up to the next three years in order to strengthen the statistical power of results and conclusions that may be drawn from this study.

5.6 Beyond White-Nose Syndrome

This investigation sought to develop safe and efficacious treatment options for bats afflicted with WNS, in order to increase fitness and survivorship. However, these treatment

methodologies may also aid in managing other wildlife and crop diseases. Other uses being investigated include, but are not limited to, treating snake fungal disease (SFD) of snakes infected with *Ophidiomyces ophiodiicola* (Cornelison et al., 2016; Kane et al., 2017), treating nosemosis or chalkbrood disease of honey bees (*Apis mellifera*) infected with *Nosema apis* or *Ascospaera apis*, respectively, treating noble rot of crops infected with *Botrytis cinerea*, treating grain contamination by *Aspergillus flavus*, and treating citrus black spot of citrus (*Citrus* spp.) leaves and fruit infected with *Phyllosticta citricarpa*. The methods and technologies developed during this investigation also have the potential to be used for purposes beyond disease management, in many systems where microbial control may be desired.

Biomimicry has opened the doors to exploring exciting new approaches to solving difficult microbial control challenges. By harnessing novel microorganisms and their natural antagonistic compounds, technology has allowed us to not only develop a new set of tools and techniques for controlling microorganisms but the potential to yield a great number of natural, safe, and patentable formulations that enhance both effectiveness and safety of what can be found in nature.

REFERENCES

- Adams RA, Pedersen SC.** 2000. Ontogeny, Functional Ecology, and Evolution of Bats. Cambridge University Press. 139-140.
- Alamri A, El-Newehy MH, Al-Deyab SS.** 2012. Biocidal polymers: synthesis and antimicrobial properties of benzaldehyde derivatives immobilized onto amine-terminated polyacrylonitrile. Chemistry Central Journal **6**:111.
- Balis C, Kouyeas V.** 1968. Volatile inhibitors involved in soil mycostasis. Annales de Z'Institut phyto-pathologique Benaki NS **8**:145-149.
- Ballman A, Benedict L, Britzke E, Castle K, Cottrell W, Cryan P, DeLiberto T, Elliot A, Ewing R, Hicks A, Reynolds R, Rubado J, Slack B, Williams L, Coleman J.** 2011. A national plan for assisting states, federal agencies, and tribes in managing white-nose syndrome in bats. Retrieved 2016-05-06. <<http://digitalcommons.unl.edu/usfwspubs/454/>>
- Blehert DS, Hicks AC, Behr M, Meteyer CU, Berlowski-Zier BM, Buckles EL, Coleman JTH, Darling SR, Gargas A, Niver R, Okoniewski JC, Rudd RJ, Stone WB.** 2009. Bat White-Nose Syndrome: An Emerging Fungal Pathogen? Science **323**:227-227.
- Boyles JG, Cryan PM, McCracken GF, Kunz TH.** 2011. Economic Importance of Bats in Agriculture. Science **332**:41 –42.
- Calabrese EJ, Baldwin LA.** 2003. HORMESIS: The Dose-Response Revolution. Annual Review of Pharmacology and Toxicology **43**:175–197.
- Chuankun X, Minghe M, Leming Z, Keqin Z.** 2004. Soil volatile fungistasis and volatile fungistatic compounds. Soil Biology and Biochemistry **36**:1997-2004.

Cornelison CT, Gabriel KT, Barlament C, Crow SA. 2014. Inhibition of *Pseudogymnoascus destructans* Growth from Conidia and Mycelial Extension by Bacterially Produced Volatile Organic Compounds. *Mycopathologia* **177**:1–10.

Cornelison CT, Keel MK, Gabriel KT, Barlament CK, Tucker TA, Pierce GE, Crow SA. 2014. A preliminary report on the contact-independent antagonism of *Pseudogymnoascus destructans* by *Rhodococcus rhodochrous* strain DAP96253. *BMC Microbiology* **14**:246.

Cornelison CT, Cherney B, Gabriel KT, Barlament CK, Crow SA. 2016. Contact-Independent Antagonism of *Ophidiomyces ophiodiicola*, the Causative Agent of Snake Fungal Disease by *Rhodococcus rhodochrous* DAP 96253 and Select Volatile Organic Compounds. *Journal of Veterinary Science & Technology* **7**.

Cryan PM, Meteyer CU, Boyles JG, Blehert DS. 2010. Wing pathology of white-nose syndrome in bats suggests life-threatening disruption of physiology. *BMC Biology* **8**:135.

Dobbs CG, Hinson WH. 1953. A Widespread Fungistasis in Soils. *Nature* **172**:197-199.

Ezra D, Strobel GA. 2003. Effect of substrate on the bioactivity of volatile antimicrobials produced by *Muscodor albus*. *Plant Science* **165**:1229-1238.

Fernando WGD, Ramarathnam R, Krishnamoorthy AS, Savchuk SC. 2005. Identification and use of potential bacterial organic antifungal volatiles in biocontrol. *Soil Biology and Biochemistry* **37**:955–964.

Fisher MC, Henk DA, Briggs CJ, Brownstein JS, Madoff LC, McCraw SL, Gurr SJ. 2012. Emerging fungal threats to animal, plant and ecosystem health. *Nature* **484**:186–194.

Fleming A. 1929. On the Antibacterial Action of Cultures of a *Penicillium*, with Special Reference to their Use in the Isolation of *B. influenzae*. *Br J Exp Pathol* **10**:226-236.

- Frick WF, Pollock JF, Hicks AC, Langwig KE, Reynolds DS, Turner GG, Butchkoski CM, Kunz TH.** 2010. An Emerging Disease Causes Regional Population Collapse of a Common North American Bat Species. *Science* **329**:679-682.
- Froschauer A, Coleman J.** 2012. North American bat death toll exceeds 5.5 million from white-nose syndrome. U.S. Fish & Wildlife Service. Retrieved 2016-05-06.
<http://www.fws.gov/news/ShowNews.cfm?_ID=31254>
- Gabriel KT, Cornelison CT.** February 18, 2016. Volatile Organic Compounds for Inhibiting Fungal Growth. International PCT application WO 2016/025572 A1.
- Garbeva P, Hol WHG, Termorshuizen AJ, Kowalchuk GA, de Boer W.** 2011. Fungistasis and general soil biostasis - A new synthesis. *Soil Biology and Biochemistry* **43**:469-477.
- Gause GF.** 1934. Experimental Analysis of Vito Volterra's Mathematical Theory of the Struggle for Existence. *Science* **79**:16-17.
- Ghannoum MA, Rice LB.** 1999. Antifungal Agents: Mode of Action, Mechanisms of Resistance, and Correlation of These Mechanisms with Bacterial Resistance. *Clin Microbiol Rev* **12**:501-517.
- Hoyt JR, Cheng TL, Langwig KE, Hee MM, Frick WF, Kilpatrick AM.** 2015. Bacteria Isolated from Bats Inhibit the Growth of *Pseudogymnoascus destructans*, the Causative Agent of White-Nose Syndrome. *PLoS ONE* **10**(4): e0121329.
- Kai M, Effmert U, Berg G, Piechulla B.** 2007. Volatiles of bacterial antagonists inhibit mycelial growth of the plant pathogen *Rhizoctonia solani*. *Archives of Microbiology* **187**:351-360.

- Kane LP, Allender MC, Archer G, Leister K, Rzadkowska M, Boers K, Souza M, Cox S.** 2017. Pharmacokinetics of nebulized and subcutaneously implanted terbinafine in cottonmouths (*Agkistrodon piscivorus*). *J Vet Pharmacol Ther.*
- Kerr JR.** 1999. Bacterial inhibition of fungal growth and pathogenicity. *Microbial Ecology in Health & Disease* **11**:129-142.
- Lorch JM, Meteyer CU, Behr MJ, Boyles JG, Cryan PM, Hicks AC, Ballmann AE, Coleman JTH, Redell DN, Reeder DM, Blehert DS.** 2011. Experimental infection of bats with *Geomyces destructans* causes white-nose syndrome. *Nature* **480**:376-378.
- Maslo B, Fefferman NH.** 2015. A case study of bats and white-nose syndrome demonstrating how to model population viability with evolutionary effects. *Conservation Biology* **29**:1176-1185.
- Mitchell A, Strobel G, Hess W, Vargas P, Ezra D.** 2008. *Muscodor crispans*, a novel endophyte from *Ananas ananassoides* in the Bolivian Amazon. *Fungal Diversity* **31**:37–43.
- Mitchell AM, Strobel GA, Moore E, Robison R, Sears J.** 2010. Volatile antimicrobials from *Muscodor crispans*, a novel endophytic fungus. *Microbiology* **156**:270–277.
- Muller LK, Lorch JM, Lindner DL, O'Connor M, Gargas A, Blehert DS.** 2013. Bat white-nose syndrome: A real-time TaqMan polymerase chain reaction test targeting the intergenic spacer region of *Geomyces destructans*. *Mycologia* **105**:253-259.
- Parfitt J, Barthel M, Macnaughton S.** 2010. Food waste within food supply chains: quantification and potential for change to 2050. *Philosophical Transactions of the Royal Society of London B: Biological Sciences* **365**:3065–3081.

Pierce GE, Drago GK, Ganguly S, Tucker TA, Hooker JW, Jones S, Crow SA. 2011.

Preliminary report on a catalyst derived from induced cells of *Rhodococcus rhodochrous* strain DAP 96253 that delays the ripening of selected climacteric fruit: bananas, avocados, and peaches. *J Ind Microbiol Biotechnol* **38**:1567–1573.

Rastetter EB, Gren GI. 2002. Changes in Individual Allometry Can Lead to Species

Coexistence without Niche Separation. *Ecosystems* **5**:0789-0801.

Schalchli H, Hormazabal E, Becerra J, Birkett M, Alvear M, Vidal J, Quiroz A. 2011.

Antifungal activity of volatile metabolites emitted by mycelial cultures of saprophytic fungi. *Chemistry & Ecology* **27**:503–513.

Southam C, Ehrlich J. 1943. Effects of Extract of Western Red-cedar Heartwood on Certain

Wood-decaying Fungi in Culture. *Phytopathology* **33**:5517–5524.

Strobel GA, Gandhi NR, Skebba VP. March 2012. Antimicrobial compositions and related

methods of use. EP2424372 A2.

Taborda CP, Da Silva MB, Nosanchuk JD, Travassos LR. 2008. Melanin as a virulence

factor of *Paracoccidioides brasiliensis* and other dimorphic pathogenic fungi: a minireview.

Mycopathologia **165**:331-9.

Tripathi P, Dubey NK. 2004. Exploitation of natural products as an alternative strategy to

control postharvest fungal rotting of fruit and vegetables. *Postharvest Biology and*

Technology **32**:235–245.

Turner GG, Meteyer CU, Barton H, Gumbs JF, Reeder DM, Overton B, Bandouchova H,

Bartonička T, Martínková N, Pikula J, Zukal J, Blehert DS. 2014. Nonlethal screening of

bat-wing skin with the use of ultraviolet fluorescence to detect lesions indicative of white-nose syndrome. *Journal of Wildlife Diseases* **50**:566-573.

Vecellio L. 2006. The mesh nebuliser: a recent technical innovation for aerosol delivery. *Breathe* **2**:253-260.

Verant ML, Meteyer CU, Speakman JR, Cryan PM, Lorch JM, Blehert DS. 2014. White-nose syndrome initiates a cascade of physiologic disturbances in the hibernating bat host. *BMC Physiology* **14**:10.

Voisard C, Keel C, Haas D, Dèfago G. 1989. Cyanide production by *Pseudomonas fluorescens* helps suppress black root rot of tobacco under gnotobiotic conditions. *EMBO J* **8**:351-358.

Wang C, Wang Z, Qiao X, Li Z, Li F, Chen M, Wang Y, Huang Y, Cui H. 2013. Antifungal activity of volatile organic compounds from *Streptomyces alboflavus* TD-1. *FEMS Microbiology Letters* **341**:45–51.

Watve MG, Tickoo R, Jog MM, Bhole BD. 2001. How many antibiotics are produced by the genus *Streptomyces*? *Archives Of Microbiology* **176**:386-390.

Weisskopf L. 2013. The potential of bacterial volatiles for crop protection against phytopathogenic fungi, p. 1352-1363. In Méndez-Vilas, A (ed.), *Microbial Pathogens and Strategies for Combating Them: Science, Technology and Education*. Formatex Research Center.

White-Nose Syndrome Map. 2017. Retrieved 2017-04-21.

<<https://www.whitenosesyndrome.org/resources/map>>

- Wilson CL, Wisniewski ME, Biles CL, McLaughlin R, Chalutz E, Droby S.** 1991. Biological control of post-harvest diseases of fruits and vegetables: alternatives to synthetic fungicides. *Crop Protection* **10**:172–177.
- Yao H, Tian S.** 2005. Effects of pre- and post-harvest application of salicylic acid or methyl jasmonate on inducing disease resistance of sweet cherry fruit in storage. *Postharvest Biology and Technology* **35**:253–262.
- Yuan J, Raza W, Shen Q, Huang Q.** 2012. Antifungal Activity of *Bacillus amyloliquefaciens* NJN-6 Volatile Compounds against *Fusarium oxysporum* f. sp. cubense. *Appl Environ Microbiol* **78**:5942–5944.
- Zou C-S, Mo M-H, Gu Y-Q, Zhou J-P, Zhang K-Q.** 2007. Possible contributions of volatile-producing bacteria to soil fungistasis. *Soil Biology and Biochemistry* **39**:2371-2379.

APPENDICES

APPENDIX A

List of compounds produced by microorganisms that have demonstrated antimicrobial activity.

Citation	Volatile Organic Compound	Source Organism
Wang 2013	Dimethyl sulfide	<i>Streptomyces</i> sp. TD-1
	3-carene-10-al	<i>Streptomyces</i> sp. TD-2
	Humulene-(v1)	<i>Streptomyces</i> sp. TD-3
	Isoledene	<i>Streptomyces</i> sp. TD-4
	2-Methylisoborneol	<i>Streptomyces</i> sp. TD-1
	Benzene, 1,2,3-trimethyl	<i>Streptomyces</i> sp. TD-4
Yuan 2012	Toluene	<i>Bacillus amyloliquefaciens</i> NJN-6
	Ethylbenzene	<i>Bacillus amyloliquefaciens</i> NJN-7
	1,2,4-trimethylbenzene	<i>Bacillus amyloliquefaciens</i> NJN-8
	P-xylene	<i>Bacillus amyloliquefaciens</i> NJN-9
	Styrene	<i>Bacillus amyloliquefaciens</i> NJN-10
	Benzene	<i>Bacillus amyloliquefaciens</i> NJN-11
	2-Undecanol	<i>Bacillus amyloliquefaciens</i> NJN-12
	2-nonanone	<i>Bacillus amyloliquefaciens</i> NJN-13
	2-decanone	<i>Bacillus amyloliquefaciens</i> NJN-14
	2-Undecanone	<i>Bacillus amyloliquefaciens</i> NJN-15
	Naphthalene	<i>Bacillus amyloliquefaciens</i> NJN-16
	Naphthalene, 1-methyl-	<i>Bacillus amyloliquefaciens</i> NJN-17
Naphthalene, 2-methyl-	<i>Bacillus amyloliquefaciens</i> NJN-18	
Schalchli 2011	6-Pentyl- α -pyrone	<i>Trichoderma viride</i>
	Ethanol	<i>Schizophyllum commune</i> (Shi-1)
	Ethanol	<i>Schizophyllum commune</i> (Shi-2)
	β -Bisabolol	<i>Trametes versicolor</i>
	β -Bisabolol	<i>Schizophyllum commune</i> (Shi-1)
	β -Bisabolol	<i>Schizophyllum commune</i> (Shi-2)
	Spathulenol	<i>Trametes versicolor</i>
	Ethyl 2-methylbutanoate	<i>Schizophyllum commune</i> (Shi-1)
	Ethyl 2-methylbutanoate	<i>Schizophyllum commune</i> (Shi-2)
	2-Methylbutyl acetate	<i>Schizophyllum commune</i> (Shi-1)
	2-Methylbutyl acetate	<i>Schizophyllum commune</i> (Shi-2)
	Cadinene	<i>Trichoderma viride</i>
β -Bisabolene	<i>Trichoderma viride</i>	

	β -Bisabolene	<i>Schizophyllum commune</i> (Shi-1)
	β -Bisabolene	<i>Schizophyllum commune</i> (Shi-2)
Kai 2006	Dodecanal	<i>Stenotrophomonas rhizophila</i> P69
	β -Phenylethanol	<i>Stenotrophomonas rhizophila</i> P70
	Dodecanal	<i>Staphylococcus epidermidis</i>
	β -Phenylethanol	<i>Staphylococcus epidermidis</i>
	Benzyl nitrile	<i>Serratia plymuthica</i>
	β -Phenylethanol	<i>Serratia plymuthica</i>
	Trans-9-hexadecene-1-ol	<i>Serratia plymuthica</i>
	β -Phenylethanol	<i>Serratia plymuthica</i>
	Dimethyl trisulside	<i>Serratia odorifera</i>
	β -Phenylethanol	<i>Serratia odorifera</i>
	Undecadiene	<i>Pseudomonas trivialis</i>
	Undecene	<i>Pseudomonas trivialis</i>
	Benzyl oxybenz nitrile	<i>Pseudomonas trivialis</i>
	Undecene	<i>Pseudomonas fluorescens</i>
Fernando 2005	2-ethyl-1-hexanol	<i>Pseudomonas spp.</i>
	Benzaldehyde	<i>Pseudomonas spp.</i>
	Benzothiazole	<i>Pseudomonas spp.</i>
	Decanal	<i>Pseudomonas spp.</i>
	N,N-Dimethyloctylamine	<i>Pseudomonas spp.</i>
	Nonanal	<i>Pseudomonas spp.</i>

APPENDIX B

Phosphate Buffered Saline (PBS) Solution Composition

Component	Quantity (per 1 L deionized water)
NaCl	8 g
KCl	0.2 g
Na ₂ PO ₄	1.44 g
KH ₄ PO ₄	0.24 g

Adjust to pH 7.4, then autoclave or filter-sterilize.

APPENDIX C

Conidia Harvesting Solution Composition

Component	Quantity (per L of deionized water)
Tween80	500 ml
NaCl	4.5 g

Mix until homogeneous, then autoclave.

APPENDIX D

Version 1.4.4 source code for the version 1.4 dispersal system controller

```
1  /*
2  * Title:   Automated Dispersal Controller
3  * Author:  Kyle T. Gabriel
4  * Date:    2013-2016
5  * Version: 1.4.4
6  * Type:    Arduino Source Code
7  * Chip:    ATMEGA328P-PU
8  * Board:   version 1.4
9  * PHP:     version 1.7 (generates SETTINGS.TXT)
10 *
11 * Compiler: Arduino IDE 1.0.6
12 * Libraries: EEPROMAnything, DS1337, SdFat
13 *
14 * Prior work that was used and modified:
15 * SD Card read/write by Alex Shubovich,
16 *   http://overskill.alexshu.com/?p=107
17 * DS1337 RTC Library by Tim,
18 *   Gipsonhttps://code.google.com/p/mosquino/wiki/DS1337
19 * Based on xSmurf's RTC,
20 *   http://www.arduino.cc/cgi-bin/yabb2/YaBB.pl?num=1191209057/0
21 */
22
23 #include <EEPROM.h>           // Store variables in EEPROM
24 #include <EEPROMAnything.h>  // Store whole arrays in EEPROM
25 #include <SdFat.h>           // Read/Write SD Card
26 #include <DS1337.h>          // Real Time Clock
27 #include <Wire.h>            // Real Time Clock
28 #include <avr/power.h>       // Real Time Clock
29 #include <avr/sleep.h>       // Real Time Clock
30 #include <math.h>            // Calculations for thermistor
31
32 // Enable (1) or disable (0) debug mode (print status to serial)
33 #define DEBUG 0
34
35 #define int2Pin 2           // Real Time Clock interrupt (pin 2, INT0)
36 #define ledPin 4           // LED for indicating status
37 #define mosfetPin 6        // MOSFET to switch power to dispersal device
38 #define vflowPin 9         // N- and P-MOSFETs, switch battery to voltage divider
39 #define vreadPin 14        // Read 12v battery voltage through voltage divider
40 #define tempPin 17         // Read voltage of 10k thermistor
41 #define SDcardPin 15       // card select of SD card reader (D3 of breakout board)
42 #define SDcardInsPin 16    // SD-card (CD) (not inserted = 3.3v, inserted = gnd)
43
44 // Filenames written/read from the SD card
45 #define LOCKFILE "LOCK.TXT"
46 #define SETTINGS "SETTINGS.TXT"
47 #define LOG "LOG.TXT"
48
49 // SD card connections
50 // D3 - cardSelect (pin 15, ADC1)
51 // CMD - MOSI
52 // CD - cardDetect (pin 16, ADC2)
53 // CLK - SCK
```

```

54 // D0 - MISO
55 // VDD - Power: Positive 3.3-volt
56 // GND - Power: Ground
57 SdFat sd;
58 SdFile myFile;
59
60 // Real time clock (RTC) for timekeeping and timers
61 DS1337 RTC = DS1337();
62 long timers[3]; // Stores how many seconds until each timer ends
63 long startTime; // The epoch time when the device turns on
64 long timeTotal; // The epoch time every time the device wakes
65 long offTimer; // The epoch time when the device turns off
66 long logTimer; // Determines batteryCheck() run interval
67 long minTimer; // Stores lowest timer duration time remaining
68
69 int ArrayCount = 0;
70 int DurArrayCount = 0;
71 int FirstCusRun = 1;
72
73 // Variables read from SETTINGS.TXT on SD card
74 char fileID[14]; // Unique ID of generated configuration file
75 long TotalRun = -1; // All operation will cease after this duration
76 long Delay = -1; // Delay after powering on until the first dispersal begins
77 int DurOn = 0; // Duration to distribute compound
78 long DurOff = 0; // Seconds between distributions
79 long DurLog = 360; // Time between appending log
80 long ArrayDurOff[5]; // Store Off Durations for custom program
81 int ArrayDurOn[5]; // Store On Durations for custom program (seconds=x/10)
82 int Arrayppmv[5]; // Store ppmv for custom program
83 int MolW = -1; // Molecular weight of compound dispersed (g/mol) (actual=x/10)
84 int CpndSlp = -1; // Compound dispersal rate (g/sec) (actual=x/10000)
85 int Atm = -1; // Atmospheric pressure (atm) (actual=x/10)
86 int Vol = -1; // Volume to treat (m^3) (actual=x/10)
87 int ppmv = -1; // Parts per million (volume/volume)
88 int Cus_Num = 0; // Store the custom number of on/off/ppmv
89 boolean Custom = false; // Basic or custom program?
90 boolean Cus_Rep = false; // Repeat after the last off duration?
91 boolean IntTemp = false; // Use internal temperature sensor?
92 int lowVoltage = 0; // Minimum voltage to trigger low voltage warning (actual=x/10)
93
94 struct config_t { // Variables to store in EEPROM
95     boolean BatLow; // Battery voltage low
96 } progvar;
97
98 void setup() {
99     Serial.begin(9600);
100     delay(10);
101
102     pinMode(ledPin, OUTPUT);
103     pinMode(mosfetPin, OUTPUT);
104
105     space(); dash(); dot(); dot(); dash(); // Flash LED: Setup begins
106
107     pinMode(vflowPin, OUTPUT); // Opens 12-volt flow to voltage divider
108     pinMode(SDcardInsPin, INPUT); // SD card insert detection
109     pinMode(SDcardPin, OUTPUT); // SD card
110     pinMode(int2Pin, INPUT); // Interrupt pin for DS1337 alarm
111     digitalWrite(int2Pin, HIGH); // Pull-up resistor enabled for RTC interrupt
112
113     if (digitalRead(SDcardInsPin) == HIGH) { // No SD card inserted
114         while(1) {

```

```

115         space(); dash(); dash(); dash(); dot();
116         delay(5000);
117     }
118 }
119
120     if (!sd.begin(SDcardInsPin, SPI_HALF_SPEED)) { // SD card init failed
121         while(1) {
122             space(); dash(); dash(); dot(); dot();
123             delay(5000);
124         }
125     } else readSDSettings(); // Read variables from the SD card
126
127 // If the LOCKFILE is present, the program has previously ended.
128 // The user must delete LOCKFILE from the SD card to permit the
129 // program to run again.
130 if (myFile.open(LOCKFILE, O_READ)) {
131     while(1) {
132         space(); dash(); dot(); dash(); dot();
133         delay(2000);
134     }
135 }
136
137 EEPROM_readAnything(0, progvar);
138 progvar.BatLow = false;
139 EEPROM_writeAnything(0, progvar);
140
141 // Initialize Real Time Clock (RTC)
142 RTC.start();
143
144 // If RTC not set, set time to epoch
145 if (!RTC.time_is_set()) {
146     Serial.println(F("Clock unset, set to 1/1/2000 epoch (946684800 seconds)."));
147     RTC.setSeconds(0);
148     RTC.setMinutes(0);
149     RTC.setHours(0);
150     RTC.setDays(1);
151     RTC.setMonths(1);
152     RTC.setYears(2000);
153     RTC.writeTime();
154 }
155
156 // Read and record program start time from RTC
157 RTC.readTime();
158 startTime = RTC.date_to_epoch_seconds();
159
160 // Initial battery voltage check
161 if ((float)batteryVoltage() / 100.0 < lowVoltage / 10.0) {
162     writeErrorLog(4);
163     while(1) {
164         dash(); dot(); dot(); dash();
165         delay(5000);
166     }
167 }
168
169 updateOnDur(); // Initial duration update
170 writeLogInit(); // Initial log amendment
171
172 // Indicate pre-run setup executed without error
173 dot(); dash(); dash(); dot();
174
175 // Sleep for pre-run delay

```

```

176         RTC.snooze(Delay);
177
178         // Record time and set log timer, after delay
179         RTC.readTime();
180         timeTotal = RTC.date_to_epoch_seconds();
181         logTimer = timeTotal - DurLog;
182     }
183
184     void loop() {
185         // Set current time to compare to timers
186         RTC.readTime();
187         timeTotal = RTC.date_to_epoch_seconds();
188
189         // Permanently end program if TotalRun has elapsed
190         if ((Cus_Rep || !Custom) && timeTotal - startTime >= TotalRun) {
191             end_Program();
192         }
193
194         // Check temperature/voltage and update the On Duration
195         if (timeTotal - logTimer >= DurLog) {
196             readTemperature();
197             updateOnDur();
198             writeLogUpdate();
199             if ((float)batteryVoltage() / 100.0 < lowVoltage / 10.0) {
200                 if (!progvar.BatLow) {
201                     progvar.BatLow = true;
202                     EEPROM_writeAnything(0, progvar);
203                     writeErrorLog(4);
204                 }
205             } else if (progvar.BatLow) {
206                 progvar.BatLow = false;
207                 EEPROM_writeAnything(0, progvar);
208             }
209             logTimer = timeTotal; // Reset timer
210         }
211
212         // Turn dispersal device on for appropriate duration of time
213         power_On();
214
215         // Calculate the lowest remaining off time of all timers
216         calc_minTimer();
217
218         // Print debug information to serial
219         if (DEBUG) debug_Log();
220
221         // Sleep until timer has expired
222         if (minTimer > 0) RTC.snooze(minTimer);
223     }
224
225     // Send status messages to serial
226     void debug_Log() {
227         Serial.println();
228         Serial.print(millis());
229         Serial.print(F(" "));
230         Serial.print(timeTotal - startTime);
231         Serial.print(F(" "));
232         Serial.print(readTemperature());
233         Serial.print(F(" "));
234         Serial.print(minTimer);
235         //Serial.print(" ");
236         //for (byte mask = 0x80; mask; mask >>= 1) { // Print the 8 bits of a byte

```

```

237 // if (mask & progvar.errorSav) Serial.print('1');
238 // else Serial.print('0');
239 //}
240 Serial.println();
241 Serial.flush();
242 }
243
244 // Indicate the program has ended and create LOCKFILE to prevent restarting
245 void end_Program() {
246     writeLogEnd();
247
248     myFile.open(LOCKFILE, O_RDWR | O_CREAT | O_AT_END);
249     myFile.println(F("This file was created by a finished dispersal regimen."));
250     myFile.println(F("Delete this file to permit a new regimen to run."));
251     myFile.close();
252
253     while(1) {
254         digitalWrite(ledPin, HIGH);
255         delay(10);
256         digitalWrite(ledPin, LOW);
257         RTC.snooze(10); // Sleep 10 seconds
258     }
259 }
260
261 // Calculate new on duration (milliseconds) based on measured temperature and user input
262 void updateOnDur() {
263     if (IntTemp) {
264         float Conc_g_per_V;
265         if (Custom) {
266             for (int i = 0; i < Cus_Num; i++) {
267                 Conc_g_per_V = (((12.187 * Arrayppmv[i] * ((float)MolW / 10.0)) /
268 (273.15 + readTemperature())) * ((float)Atm / 10.0)) * ((float)Vol / 10.0);
269                 ArrayDurOn[i] = Conc_g_per_V / CpndSlp * 100;
270             }
271         } else {
272             Conc_g_per_V = ((12.187 * ppmv * ((float)MolW / 10.0)) / (273.15 +
273 readTemperature())) * ((float)Atm / 10.0) * ((float)Vol / 10.0);
274             DurOn = Conc_g_per_V / CpndSlp * 100;
275         }
276     }
277 }
278
279 // Turn the distribution device on for a calculated or specified duration of time
280 void power_On() {
281     if (FirstCusRun) {
282         writeLogOn();
283         digitalWrite(ledPin, HIGH);
284         digitalWrite(mosfetPin, HIGH);
285         if (Custom) {
286             delay((long)ArrayDurOn[DurArrayCount] * 100);
287             timeTotal = timeTotal + (ArrayDurOn[DurArrayCount] / 10);
288         } else {
289             delay(DurOn * 100);
290             timeTotal = timeTotal + (DurOn / 10);
291         }
292         digitalWrite(ledPin, LOW);
293         digitalWrite(mosfetPin, LOW);
294         offTimer = timeTotal;
295         FirstCusRun = 0;
296     } else if (!Custom && timeTotal - offTimer >= DurOff) {
297         writeLogOn();

```

```

298     digitalWrite(ledPin, HIGH);
299     digitalWrite(mosfetPin, HIGH);
300     delay((long)DurOn * 100);
301     digitalWrite(ledPin, LOW);
302     digitalWrite(mosfetPin, LOW);
303     timeTotal = timeTotal + (DurOn / 10);
304     offTimer = timeTotal;
305 } else if (Custom && timeTotal - offTimer >= ArrayDurOff[DurArrayCount]) {
306     if (Cus_Rep && DurArrayCount >= Cus_Num - 1) {
307         DurArrayCount = 0;
308     } else DurArrayCount++;
309     writeLogOn();
310     digitalWrite(ledPin, HIGH);
311     digitalWrite(mosfetPin, HIGH);
312     delay((long)ArrayDurOn[DurArrayCount] * 100);
313     digitalWrite(ledPin, LOW);
314     digitalWrite(mosfetPin, LOW);
315     timeTotal = timeTotal + (ArrayDurOn[DurArrayCount] / 10);
316     offTimer = timeTotal;
317     if (!Cus_Rep && DurArrayCount >= Cus_Num - 1) end_Program();
318 }
319 }
320
321 // Determine the lowest time remaining from all timers
322 // This is how long the processor will sleep for
323 long calc_minTimer() {
324     if (!Cus_Rep) timers[0] = 31536000;
325     else {
326         if (TotalRun - (timeTotal - startTime) <= 0) timers[0] = 0;
327         else timers[0] = TotalRun - (timeTotal - startTime); // total time remaining
328     }
329     if (Custom) timers[1] = ArrayDurOff[DurArrayCount] - (timeTotal - offTimer);
330     else timers[1] = DurOff - (timeTotal - offTimer); // remaining time off
331     timers[2] = DurLog - (timeTotal - logTimer); // remaining time until log
332
333     // Determine which timer has the lowest time remaining
334     minTimer = timers[0];
335     for (int i = 1; i < 3; i++) {
336         if (minTimer > timers[i] && timers[i] > 0) minTimer = timers[i];
337     }
338 }
339
340 // Write an initial log entry for the current dispersal regimen
341 void writeLogInit() {
342     myFile.open(LOG, O_RDWR | O_CREAT | O_AT_END);
343     myFile.println();
344     myFile.print(F("Seconds,FileID,Delay"));
345     if (Cus_Rep || !Custom) myFile.print(F(",Total"));
346     if (IntTemp) myFile.print(F(",Temp,MW,Atm,Vol,Rate"));
347     if (Custom) {
348         for (int i = 0; i < Cus_Num; i++) {
349             if (IntTemp) {
350                 myFile.print(F(",ppm"));
351                 myFile.print(i);
352             }
353             myFile.print(F(",On"));
354             myFile.print(i);
355             if (i == Cus_Num - 1 && !Cus_Rep) {
356                 } else {
357                 myFile.print(F(",Off"));
358                 myFile.print(i);

```

```

359         }
360     }
361 } else {
362     if (IntTemp) myFile.print(F(",ppm"));
363     myFile.print(F(",On,Off"));
364 }
365
366 myFile.println();
367 myFile.print(F("0,"));
368 myFile.print(fileID);
369 myFile.print(Delay);
370 if (Cus_Rep || !Custom) {
371     myFile.print(F(","));
372     myFile.print(TotalRun);
373 }
374 if (IntTemp) {
375     myFile.print(F(","));
376     myFile.print(readTemperature());
377     myFile.print(F(","));
378     myFile.print((float)MolW/ 10.0, 1);
379     myFile.print(F(","));
380     myFile.print((float)Atm / 10.0, 1);
381     myFile.print(F(","));
382     myFile.print((float)Vol / 10.0, 1);
383     myFile.print(F(","));
384     myFile.print((float)CpndSlp / 10000.0, 4);
385 }
386 if (Custom) {
387     for (int i = 0; i < Cus_Num; i++) {
388         if (IntTemp) {
389             myFile.print(F(","));
390             myFile.print(Arrayppmv[i]);
391         }
392         myFile.print(F(","));
393         myFile.print((float)ArrayDurOn[i] / 10.0, 1);
394         if (i == Cus_Num - 1 && !Cus_Rep) {
395             } else {
396                 myFile.print(F(","));
397                 myFile.print(ArrayDurOff[i]);
398             }
399         }
400     } else {
401         if (IntTemp) {
402             myFile.print(F(","));
403             myFile.print(ppmv);
404         }
405         myFile.print(F(","));
406         myFile.print((float)DurOn / 10.0, 1);
407         myFile.print(F(","));
408         myFile.print(DurOff);
409     }
410 myFile.println();
411 myFile.print(F("Seconds, Type, On, Temp, Volts"));
412 if (IntTemp) {
413     if (Custom) {
414         for (int i = 0; i < Cus_Num; i++) {
415             myFile.print(F(",On("));
416             myFile.print(i);
417             myFile.print(F(")"));
418         }
419     } else myFile.print(F(",On"));

```

```

420     }
421     myFile.println();
422     myFile.close();
423 }
424
425 // Write the duration to the log file when the distribution device turns on
426 void writeLogOn() {
427     myFile.open(LOG, O_RDWR | O_CREAT | O_AT_END);
428     myFile.print(timeTotal - startTime);
429     myFile.print(F(",On"));
430     if (Custom) {
431         myFile.print(DurArrayCount);
432         myFile.print(F(","));
433         myFile.print((float)ArrayDurOn[DurArrayCount] / 10.0, 1);
434     } else {
435         myFile.print(F(","));
436         myFile.print((float)DurOn / 10.0, 1);
437     }
438     myFile.println();
439     myFile.close();
440 }
441
442 // Write periodic updates of battery voltage and temperature to the log
443 void writeLogUpdate() {
444     myFile.open(LOG, O_RDWR | O_CREAT | O_AT_END);
445     myFile.print(timeTotal - startTime);
446     myFile.print(F(",UPDATE,"));
447     myFile.print(readTemperature());
448     myFile.print(F(","));
449     myFile.print((float)batteryVoltage() / 100.0);
450     if (IntTemp) {
451         if (Custom) {
452             for (int i = 0; i < Cus_Num; i++) {
453                 myFile.print(F(","));
454                 myFile.print((float)ArrayDurOn[i] / 10.0,1);
455             }
456         } else {
457             myFile.print(F(","));
458             myFile.print((float)DurOn / 10.0,1);
459         }
460     }
461     myFile.println();
462     myFile.close();
463 }
464
465 // Write the last log line of the dispersal regimen
466 void writeLogEnd() {
467     myFile.open(LOG, O_RDWR | O_CREAT | O_AT_END);
468     myFile.print(timeTotal - startTime); // Seconds since the device began running
469     myFile.print(F(",The device has reached the scheduled end."));
470     myFile.println();
471     myFile.close();
472 }
473
474 // Write error description to the log
475 void writeErrorLog(int i) {
476     myFile.open(LOG, O_RDWR | O_CREAT | O_AT_END);
477     myFile.print(timeTotal - startTime);
478     myFile.print(F(",ERROR,"));
479     switch (i) {
480         case 1:

```

```

481         myFile.print(F(""));
482         break;
483     case 2:
484         myFile.print(F(""));
485         break;
486     case 3:
487         myFile.print(F("SETTINGS.TXT improperly configured."));
488         break;
489     case 4:
490         myFile.print(F("Battery charge too low."));
491         break;
492     default:
493         myFile.print(F("UNKNOWN ERROR."));
494         break;
495     }
496     myFile.println();
497     myFile.close();
498 }
499
500 // Reads SETTINGS.TXT for operational parameters
501 void readSDSettings() {
502     char character;
503     String settingName;
504     String settingValue;
505     myFile.open(SETTINGS, O_READ);
506     while ((character = myFile.read()) >= 0) {
507         while(character != '='){
508             settingName = settingName + character;
509             character = myFile.read();
510         }
511         character = myFile.read();
512         while(character != '\n'){
513             settingValue = settingValue + character;
514             character = myFile.read();
515             if (character == '\n' || character == ','){
516                 //Debugging Printing
517                 Serial.print(settingName);
518                 Serial.print(F("="));
519                 Serial.println(settingValue);
520                 // Apply the value to the parameter
521                 applySetting(settingName,settingValue);
522                 // Reset Strings
523                 settingValue = "";
524                 if (character == ',') {
525                     ArrayCount++;
526                     character = myFile.read();
527                 } else settingName = "";
528             }
529         }
530         ArrayCount = 0;
531     }
532     // close the file:
533     myFile.close();
534 }
535
536 // Apply the value to the parameter by searching for the parameter name
537 // Using settingValue.toInt(); for Integers
538 // toFloat(settingValue); for Float
539 // toBoolean(settingValue); for Boolean
540 void applySetting(String settingName, String settingValue) {
541     if (settingName == "FILEID") settingValue.toCharArray(fileID, 14);

```

```

542     if (settingName == "TotalRun") TotalRun = settingValue.toInt();
543     if (settingName == "Delay") Delay = settingValue.toInt();
544     if (settingName == "IntTemp") IntTemp = toBoolean(settingValue);
545     if (settingName == "Custom") Custom = toBoolean(settingValue);
546     if (settingName == "Cus_Rep") Cus_Rep = toBoolean(settingValue);
547     if (settingName == "Cus_Num") Cus_Num = settingValue.toInt();
548     if (settingName == "DurOn") DurOn = settingValue.toInt();
549     if (settingName == "DurOff") DurOff = settingValue.toInt();
550     if (settingName == "DurLog") DurLog = settingValue.toInt();
551     if (settingName == "MolW") MolW = settingValue.toInt();
552     if (settingName == "CpndSlp") CpndSlp = settingValue.toInt();
553     if (settingName == "Atm") Atm = settingValue.toInt();
554     if (settingName == "Vol") Vol = settingValue.toInt();
555     if (settingName == "ppmv") ppmv = settingValue.toInt();
556     if (settingName == "ZDurOn") ArrayDurOn[ArrayCount] = settingValue.toInt();
557     if (settingName == "ZDurOff") ArrayDurOff[ArrayCount] = settingValue.toInt();
558     if (settingName == "ZOnppmv") Arrayppmv[ArrayCount] = settingValue.toInt();
559     if (settingName == "lowVoltage") lowVoltage = settingValue.toInt();
560 }
561
562 // Convert string to float
563 float toFloat(String settingValue) {
564     char floatbuf[settingValue.length()];
565     settingValue.toCharArray(floatbuf, sizeof(floatbuf));
566     float f = atof(floatbuf);
567     return f;
568 }
569
570 // Convert string to integer and then to boolean (1=true, 0=false)
571 boolean toBoolean(String settingValue) {
572     if (settingValue.toInt() == 1) return true;
573     else return false;
574 }
575
576 // Read temperature from thermistor
577 float readTemperature() {
578     int RawADC = 0;
579     for (int i = 0; i < 3; i++) {
580         RawADC = RawADC + analogRead(tempPin);
581     }
582     RawADC = RawADC / 3;
583     // a1, b1, c1, d1 constants for calculating temperature with NTC thermistor
584     float abcd[] = { 3.354016E-03, 2.569850E-04, 2.620131E-06, 6.383091E-08 };
585     // Rref = the reference temp of 25degC; in c, log is natural log
586     // Rfixed = 9999.5 ohms, fixed resistor (lower half of voltage divider)
587     float lnR = log (((9999.5/(RawADC*3.3/1023.0))*3.3 - 9999.5)/10000.0);
588     float invT = abcd[0] + abcd[1]*lnR + abcd[2]*lnR*lnR + abcd[3]*lnR*lnR*lnR;
589     float Temp_C = (1/invT) - 273.15;
590     return Temp_C;
591 }
592
593 // Read battery voltage
594 int batteryVoltage() {
595     digitalWrite(vflowPin, HIGH);
596     delay(100);
597     int rawValue = analogRead(vreadPin);
598     digitalWrite(vflowPin, LOW);
599     int batteryVoltage = (rawValue * 12.64 / 1023.0) * 100;
600     return batteryVoltage;
601 }
602

```

```

603 // Alternate method to read battery voltage
604 uint16_t readBat(uint8_t ch) { // Circuit: GND---[R10k]---A0---[R5k]---12V
605     ADMUX = (1<<REFS0); // For Aref=AVcc;
606     ADCSRA = (1<<ADEN) | (1<<ADPS2) | (1<<ADPS1) | (1<<ADPS0); //Rrescalar
607     ch = ch & 0b00000111; //Select ADC Channel ch must be 0-7
608     ADMUX |= ch;
609     ADCSRA |= (1<<ADSC); //Start Single conversion
610     while(ADCSRA & (1<<ADSC)); //Wait for conversion to complete
611     return(ADC);
612 }
613
614 // LED communication modeled after Morse code: dot, dash, space
615 void dot() {
616     digitalWrite(ledPin, HIGH);
617     delay(300);
618     digitalWrite(ledPin, LOW);
619     delay(300);
620 }
621 void dash() {
622     digitalWrite(ledPin, HIGH);
623     delay(900);
624     digitalWrite(ledPin, LOW);
625     delay(300);
626 }
627 void space() {
628     delay(600);
629 }

```